Volume 67C
Number 3
July–Sept. 1963

Engineering and Instrumentation

U.S. DEPARTMENT OF COMMERCE

SECTION C

JOURNAL OF RESEARCH
NATIONAL BUREAU OF STANDARDS

Journal of Research
of the
National Bureau of Standards

C. Engineering and Instrumentation

JULY–SEPT. • 1963

VOLUME • 67C

NUMBER • 3

Editor: Martin Greenspan

Associate Editors: G. F. Montgomery, R. B. Jacobs

Publication dates:
Feb. 15, May 15, Aug. 15, Nov. 15, 1963

JOURNAL OF RESEARCH

The National Bureau of Standards Journal of Research reports research and development in the fields of activity shown at right. Also included from time to time are survey articles on topics closely related to the Bureau's scientific and technical program.

The Journal is published in four separate sections as follows:

A. Physics and Chemistry

Contains papers of interest primarily to scientists working in these fields. Issued six times a year. Annual subscription: domestic, $4.00; foreign, $4.75.

B. Mathematics and Mathematical Physics

Presents studies and compilations designed mainly for the mathematician and the theoretical physicist. Issued quarterly. Annual subscription: domestic, $2.25; foreign, $2.75.

C. Engineering and Instrumentation

Reports research and development results of interest chiefly to the engineer and the applied scientist. Issued quarterly. Annual subscription: domestic, $2.25; foreign, $2.75.

D. Radio Propagation

Reports work in radio propagation physics and upper atmospheric research. Issued six times a year. Annual subscription: domestic, $4.00; foreign, $4.75.

U.S. DEPARTMENT OF COMMERCE
Luther H. Hodges, Secretary

NATIONAL BUREAU OF STANDARDS
A. V. Astin, Director

Functions and Activities

The functions of the National Bureau of Standards are set forth in the Act of Congress, March 3, 1901, as amended. These include the development and maintenance of the national standards of measurement and the provision of means and methods for making measurements consistent with these standards; the determination of physical constants and properties of materials, the development of methods and instruments for testing materials devices, and structures; advisory services to government agencies on scientific and technical problems; invention and development of devices to serve special needs of the Government; and the development of standard practices, codes, and specifications. The work includes basic and applied research development, engineering, instrumentation, testing, evaluation, calibration services, and various consultation and information services. The Bureau also serves as the Federal technical research center in a number of specialized fields. The scope of activities of the National Bureau of Standards is suggested in the following listing of the divisions and sections engaged in technical work.

Washington, D.C.

Electricity. Resistance and Reactance. Electrochemistry. Electrical Instruments. Magnetic Measurements. Dielectrics. High Voltage.
Metrology. Photometry and Colorimetry. Refractometry. Photographic Research. Length. Engineering Metrology. Mass and Scale. Volumetry and Densimetry.
Heat. Temperature Physics. Heat Measurements. Cryogenic Physics. Equation of State. Statistical Physics.
Radiation Physics. X-Ray. Radioactivity. Radiation Theory. High Energy Radiation. Radiological Equipment. Nucleonic Instrumentation. Neutron Physics.
Analytical and Inorganic Chemistry. Pure Substances. Spectrochemistry. Solution Chemistry. Standard Reference Materials. Applied Analytical Research. Crystal Chemistry.
Mechanics. Sound. Pressure and Vacuum. Fluid Mechanics. Engineering Mechanics. Rheology. Combustion Controls.
Polymers. Macromolecules: Synthesis and Structure. Polymer Chemistry. Polymer Physics. Polymer Characterization. Polymer Evaluation and Testing. Applied Polymer Standards and Research. Dental Research.
Metallurgy. Engineering Metallurgy. Microscopy and Diffraction. Metal Reactions. Metal Physics. Electrolysis and Metal Deposition.
Inorganic Solids. Engineering Ceramics. Glass. Solid State Chemistry. Crystal Growth. Physical Properties. Crystallography.
Building Research. Structural Engineering. Fire Research. Mechanical Systems. Organic Building Materials. Codes and Safety Standards. Heat Transfer. Inorganic Building Materials. Metallic Building Materials.
Applied Mathematics. Numerical Analysis. Computation. Statistical Engineering. Mathematical Physics. Operations Research.
Data Processing Systems. Components and Techniques. Computer Technology. Measurements Automation. Engineering Applications. Systems Analysis.
Atomic Physics. Spectroscopy. Infrared Spectroscopy. Solid State Physics. Electron Physics. Atomic Physics.
Instrumentation. Engineering Electronics. Electron Devices. Electronic Instrumentation. Mechanical Instruments. Basic Instrumentation.
Physical Chemistry. Thermochemistry. Surface Chemistry. Organic Chemistry. Molecular Spectroscopy. Molecular Kinetics. Mass Spectrometry.

Office of Weights and Measures.
Boulder, Colo.

Cryogenic Engineering Laboratory. Cryogenic Equipment. Cryogenic Processes. Properties of Materials. Cryogenic Technical Services.

Central Radio Propagation Laboratory

Ionosphere Research and Propagation. Low Frequency and Very Low Frequency Research. Ionosphere Research. Prediction Services. Sun-Earth Relationships. Field Engineering. Radio Warning Services. Vertical Soundings Research.
Radio Propagation Engineering. Data Reduction Instrumentation. Radio Noise. Tropospheric Measurements. Tropospheric Analysis. Propagation-Terrain Effects. Radio-Meteorology. Lower Atmosphere Physics.
Radio Systems. Applied Electromagnetic Theory. High Frequency and Very High Frequency Research. Modulation Research. Antenna Research. Navigation Systems.
Upper Atmosphere and Space Physics. Upper Atmosphere and Plasma Physics. Ionosphere and Exosphere Scatter. Airglow and Aurora. Ionospheric Radio Astronomy.

Radio Standards Laboratory

Radio Physics. Radio Broadcast Service. Radio and Microwave Materials. Atomic-Frequency and Time-Interval Standards. Millimeter-Wave Research.
Circuit Standards. High Frequency Electrical Standards. Microwave Circuit Standards. Electronic Calibration Center.

Order all publications from the Superintendent of Documents
U.S. Government Printing Office, Washington, D.C., 20402

Use of funds for printing this publication approved by the Director of the Bureau of the Budget (June 19, 1961).

JOURNAL OF RESEARCH of the National Bureau of Standards—C. Engineering and Instrumentation
Vol. 67C, No. 3, July–September 1963

Apparatus for the Detection of Piezoelectric Coupling

Lothar Frenkel

(February 1, 1963)

An apparatus for the investigation of the piezoelectric coupling in granular powders is described. The apparatus is based on the method of Giebe and Scheibe but employs the sensitive detection and recording methods commonly employed in the study of nuclear quadrupole resonances. Some sample recorder traces are shown. The traces indicate that the apparatus is a workable qualitative tool with at least the possibility of some quantitative usefulness.

1. Apparatus for the Detection of Piezoelectric Coupling

The standard method used for the qualitative determination of the presence of piezoelectric coupling in small crystals is that of Giebe and Scheibe [1, 2, 3].[1] In this method a sensitive oscillator is tuned over a frequency range in the short wave band. A small test capacitor is filled with the sample and put in parallel with the tuning condenser.

When the oscillator frequency passes the mechanical resonance frequency of a grain of the material under test the grain is momentarily excited by piezoelectric coupling to the oscillating field and energy is absorbed by the grain from the oscillator. The oscillator output is monitored by a detector and a pair of earphones which register the resonances as clicks. This method of detecting is rather cumbersome, of limited sensitivity and inherently difficult to use quantitatively.

In recent years interest in radiofrequency spectroscopy has led to a number of simple and sensitive instruments for the detection and measurement of minute absorptions of radiofrequency energies which could very well be used for the study of weakly piezoelectric substances.

Livingston [4] noted that the apparatus used by him to study the pure nuclear quadrupole resonance of Cl in sodium chlorate registered spurious signals at various frequencies which he interpreted as piezoelectric responses of grains of the substance under study in the coil of the oscillator. The stray electric fields across the coil of his oscillator presumably caused the response of the grains.

Having observed this effect independently during a study of nuclear quadrupole resonances, we proceeded to investigate the response of our equipment to grains placed, as in the method of Giebe and Scheibe, in a small capacitor. We found that this combination of the Giebe and Scheibe method with techniques commonly employed in nuclear resonance studies does indeed result in a very sensitive detector for piezoelectric coupling.

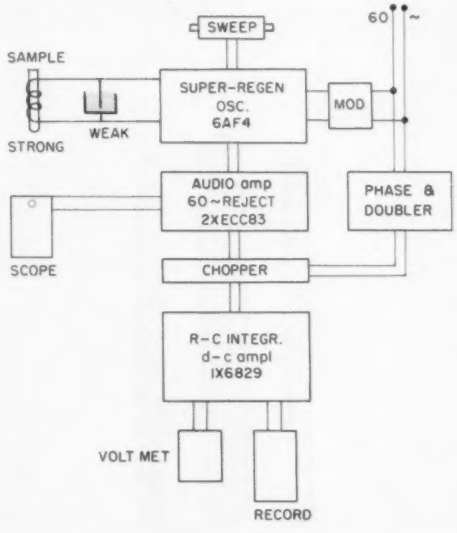

FIGURE 1. *Block diagram of apparatus.*

[1] Figures in brackets indicate the literature references at the end of this paper.

2. Descriptions of Apparatus

A block diagram of our apparatus is given in figure 1. The oscillator, a 6AF4 triode, is arranged as a superregenerative detector with a quench frequency of approximately 30 kc/s. Three individual capacitors make up the capacitance in the tank circuit. Their functions are as follows:

(1) A variable tuning capacitor driven by a small clock motor allows the center frequency to be swept slowly over a range of about 1 Mc/s in the vicinity of 25 Mc/s; (2) a vibrating capacitor made out of a small loudspeaker modulates the frequency of the oscillator by a maximum of about 10 kc/s from the instantaneous center frequency. The modulating frequency is 60 c/s.; (3) finally, a small test capacitor (shown in fig. 2) holds the sample under test.

If the center frequency of the oscillator coincides with the mechanical resonance frequency of a grain the oscillator will be loaded twice in every complete cycle of modulation; i.e., each time the modulation amplitude is zero. This results in a signal of twice the modulation frequency at the oscillator plate. This signal is filtered and amplified in a four-stage low noise audio amplifier. To minimize noise the signal is then chopped at twice the modulation frequency and the chopped signal is integrated in an RC network with a long time constant. The output from the integrating capacitor may be displayed on a recorder after suitable amplification.

We have made no attempt to analyze the recorder responses theoretically. Clearly the signal seen on the recorder as the frequency of the oscillator is slowly swept depends on a large number of variables such as the quench frequency of the superregenerative detector, the modulation amplitude, the chopper phase as well as on the number and shape of the grains in the sample. It should be noted that the response in this device does not result from individual grains as in the methods of Giebe and Scheibe, but rather from the random number of grains having their mechanical resonances near the instantaneous center frequency. This is because the modulation frequency is much larger than the width of each grain's mechanical resonance response. The signal to sample size relationship therefore is that of random fluctuations.

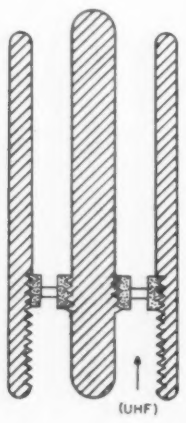

FIGURE 2. *Sample holder.*

3. Results

To test the apparatus, a number of substances listed in reference 2 as having weak or very weak coupling were tried and the resulting tracks are shown in figure 3. Substances for which the cou-

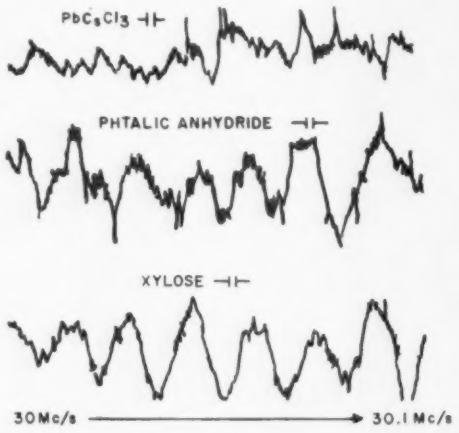

FIGURE 3a. *Recorder responses versus frequency for substances placed in the test capacitor.*

The top trace in figure 3b shows the background.

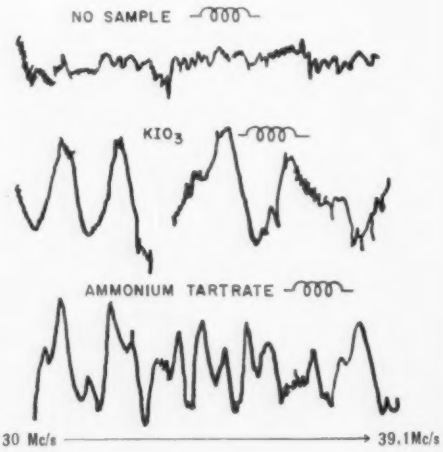

FIGURE 3b. *Recorder response versus frequency with material in the coil of the oscillator.*

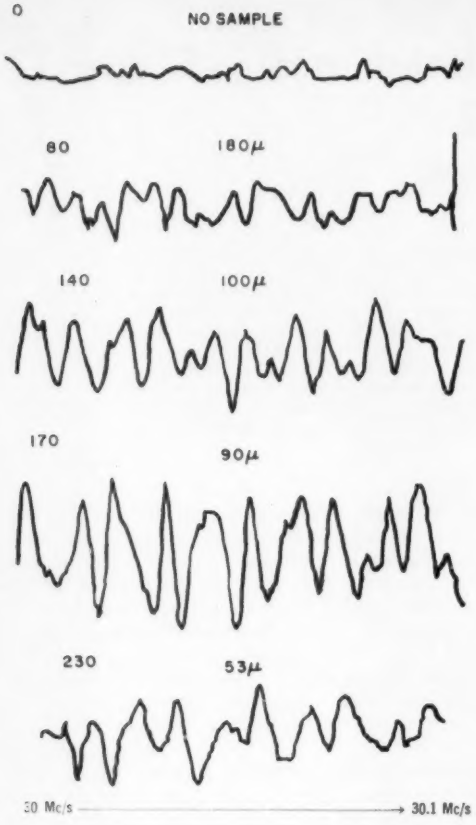

FIGURE 4. *Recorder response versus frequency as a function of grain size for* $NaClO_3$.

The numbers on the right are sieve numbers.

pling is very strong as seen by this device are best tested in the coil since the strong signals otherwise saturate the amplifier. The traces for potassium iodate and ammonium tartrate in figure 3 were obtained in this way.

For other materials, in particular barium nitrate and dibasic ammonium citrate, no tracks were seen.

Potassium iodate is listed by Mason as having no coupling. In this material phase changes were first discovered by Hettich, [5] using the method of Giebe and Scheibe, and, more recently, both the piezoelectric and nuclear quadrupole characteristics of this material were investigated by Herlach, [6] who also discovered its ferro-electric properties.

For such work the method described here would seem ideal, first, because nuclear quadrupole equipment is available and can be used with minor changes for the investigation of piezoelectric coupling and secondly because the recorder traces may be evaluated in a semiquantitative way as regards the strength of the coupling. Figure 4, for instance, shows the effect of selecting grain size at equal settings.

The author is indebted to M. Greenspan and L. Bennett for advice, and to Van Johnson for suggestions concerning the electronics.

4. References

[1] E. Giebe and A. Scheibe, ZS f. Phys. **33,** 760 (1925).
[2] Mason, Piezoelectric crystals and their applications to Ultrasonics, pp. 47–58 (D. van Nostrand, 1950).
[3] S. B. Elings and P. Terpstra, Z. Krist. **67,** 279 (1928).
[4] Livingston Ann. N.Y. Acad. of Sciences **55,** 800 (1952).
[5] A. Hettich, ZS fur Phys. **65,** 506 (1930).
[6] F. Herlach, Helv. Phys. Acta **34,** 305–330 (1961).

(Paper 67C3–129)

JOURNAL OF RESEARCH of the National Bureau of Standards—C. Engineering and Instrumentation
Vol. 67C, No. 3, July–September 1963

Large Aperture Interferometers With Small Beam Dividers

James B. Saunders

(April 3, 1963)

This paper shows some practical interferometers for testing very large and very small specimens. This is accomplished by using a particular type of beam divider that operates near the vertex of a convergent or divergent beam of light that permits almost unlimited size fields of view. Thus very large or very small specimens can be tested. Also, the wave front reversing properties of this beam divider permit tests to be made without the necessity of using standards of reference, thus eliminating the requirement for large standards that are usually expensive and require large working areas. The principles of these interferometers are so closely related to previously described instruments that very little additional explanation is required for an understanding of their operation. Several variations of the Kösters prism type of interferometer are shown schematically.

The testing of large specimens such as massive optical elements has previously required large aperture interferometers. The sizes of interferometers, such as the Mach-Zehnder [1] [1] for wind tunnel work and the Twyman-Green [2] for testing large optical elements, have been limited primarily by the size of precision beam dividers that could be made. Large beam dividers require high grade optical glass and high precision surfaces. The distortion of large beam divider elements by gravity is also a significant factor.

The application of divergent [3] and convergent beam interferometers permits the realization of much larger working spaces than can be obtained in the above-mentioned forms. The limit in aperture size is equal to the aperture of the largest lenses and/or mirrors that can be produced. This paper illustrates a method for producing very large aperture interferometers, with small beam dividers, that do not require reference standards.

One example of a large field (or aperture) interferometer for wind tunnel work is that described by Williams [4]. The beam divider of this instrument is a modified Kösters double-image prism. This prism can be quite small and the end mirror can be quite large.

The Kösters double-image prism and other modifications [5] of it provide small beam dividers for a variety of large aperture interferometers. This prism has been used as the beam divider for a variety of interferometers whose aperture equals that of the prism. Figure 1a shows one of the earliest applications [6] of this prism.

The difficulty of producing accurate prisms of large size and the difficulty of making optical glass sufficiently homogeneous in large pieces limits the size of this prism for precision interferometers. However, large prisms are no longer required. They may be replaced by a small prism and large lens or mirror. The small size Kösters prisms may be constructed and adjusted to a high degree of precision. Figure 1b shows the arrangement of a prism-lens combination that may replace the arrangement of figure 1a. The aperture of this interferometer (fig. 1b) is limited only by the size of the lens and optical flat. Chromatic aberration in the lens does not affect the fringe pattern if monochromatic light is used. Spherical aberration does not affect the fringes or observed results if the indicated rays (in the zone that includes the reference point) are collimated. Chromatic and astigmatic aberrations are negligible if the lens has axial symmetry and the source is located on the axis. Consequently, axial symmetry (assuming the axis to lie in the dividing plane) is the only critical requirement for the lens. Any accurately centered, machine-polished lens, made of good glass, will meet the required specifications.

A large interferometer for wind tunnel tests is shown in figure 2. This interferometer, with a different form of prism, was described by Williams [4].

The principal difference between the methods of analysis of data with a divergent beam interferometer such as that shown in figure 2 and conventional (parallel beam) interferometers for wind tunnel and other tests, is that spherical coordinate geometry is used for the former and rectangular coordinate geometry is used for the latter.

Since the Kösters double-image prism is so well compensated, most interferometers in which it is applied may be used with white light. Also, when the optical path difference is near zero and the light beams suffer both division and recombination in one or two prisms, extended sources may be used. These two features permit high intensity and high visibility both of which are favorable for instantaneous photography of results. When beam division or recombination occurs only once in a prism, as in the alinement interferometers [7] of figure 3, the size of the source must be limited in one direction to a narrow slit or point.

[1] Figures in brackets indicate the literature references at the end of this paper.

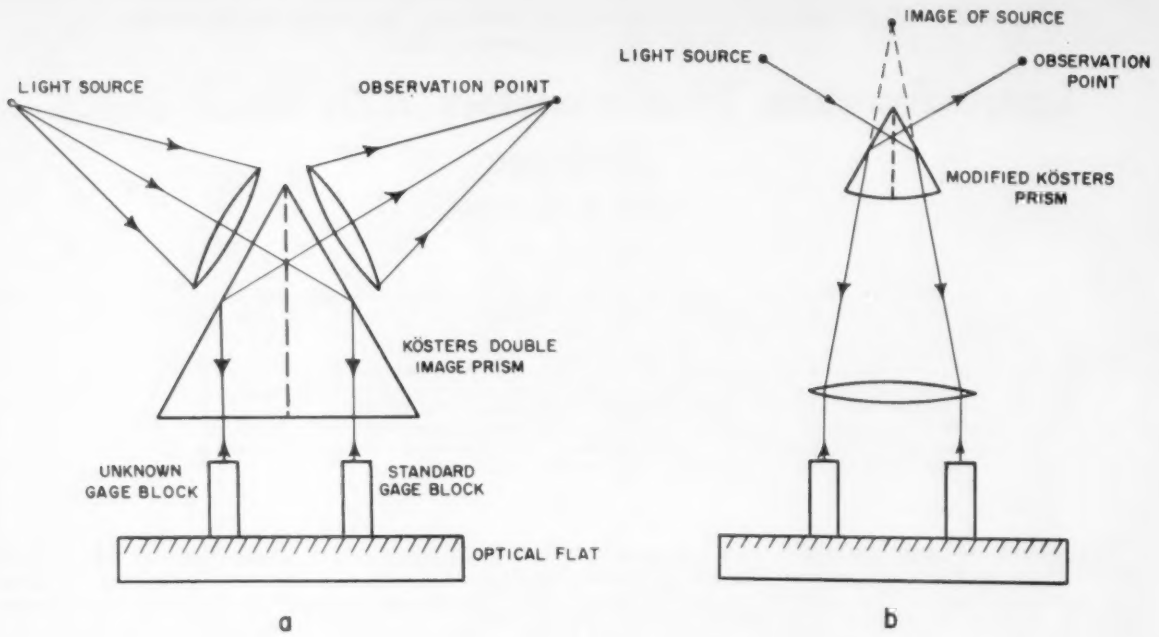

FIGURE 1. a. *An interferometer for measuring the parallelism of gage blocks.*
b. *Same as a, but modified to permit larger apertures.*

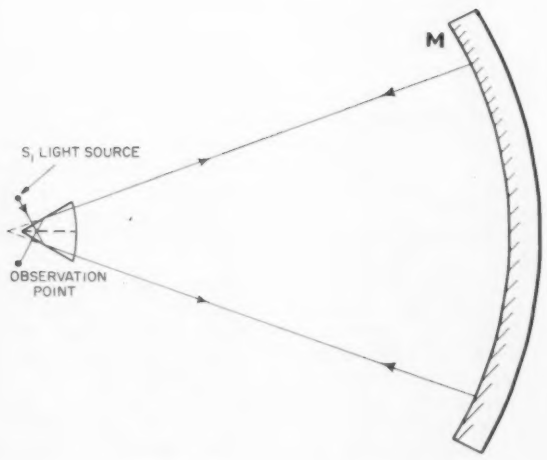

FIGURE 2. *Interferometer for wind tunnel measurement of density gradients.*

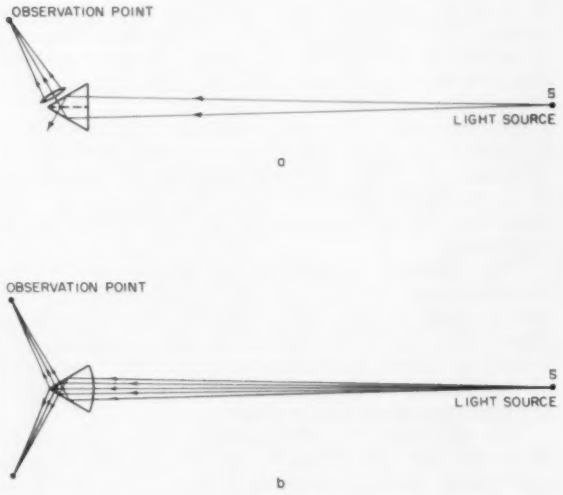

FIGURE 3. *An alinement interferometer.*
a. Conventional type Kösters double-image prism.
b. Modified (spherical base) prism.

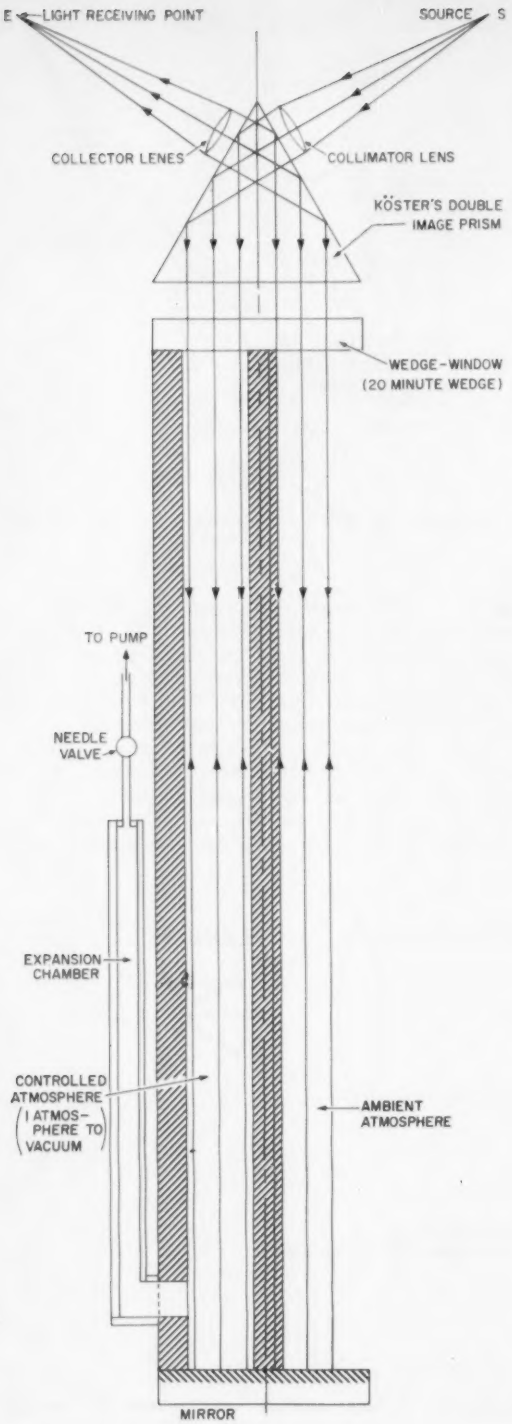

FIGURE 4. *An interferometer for measuring the refraction of gases.*

Figure 4 shows the arrangements of optical elements of a refraction interferometer that was designed for measuring the wavelength of light under ambient conditions. It is also quite practical for measuring the refractive indices of gases. The two coherent and parallel beams of light from the Kösters prism are affected differently by having one traverse a 1-m path that is controlled (either evacuated or filled with standard air) and the other traverse the same geometrical distance in ambient air. If the standard air space is evacuated the order of interference is a measure of the wavelength of light in the ambient air.

A simple procedure for obtaining a column of air having an optical density equivalent to that of standard air in the controlled space, is to start with the controlled space evacuated and the ambient space controlled to some desired temperature. Air is slowly introduced into the controlled space. This causes a change in the optical path difference and consequently the order of interference. The geometrical path in the controlled space and its change with temperature are known from previous measurements. Consequently, the difference in optical path, between vacuum and standard air in this space is known. The corresponding change in order of interference is obtained by adjusting the density in the controlled space to that of standard atmosphere. The space is then sealed by closing the inlet valve. The measured order of interference is then a measure of the difference in optical path between standard and ambient air.

The aperture of this interferometer may be increased by using a spherical base prism with a lens or mirror in the same manner as that illustrated in figure 1.

Figure 5a represents the optics of an interferometer [8] for testing long gage blocks. Lenses or mirrors may also be used to increase the aperture of this interferometer, as is shown in figure 5b for use in wind tunnel optics, and for measuring the parallelism of faces on bodies of large cross section. Figure 6 shows the same instrument formed with parabolic mirrors replacing the lenses of figure 5b.

Figures 2 and 7 indicate the range in size of spherical surfaces that may be tested interferometrically for departure from true spheres. The spherical surface, M, in figure 2 can be as large as the largest mirror ever made. The size of the ball, B, in figure 7 may have a diameter of only a fraction of a millimeter.

The aperture of the surface plate interferometer [11], as previously described, is limited to approximately 2 in. For testing large surface plates of 12 to 20 ft in length a larger aperture is desirable. The method of increasing apertures, described here, is equally applicable to that of the surface plate interferometer.

The usual functions of the interferometers described above (and also that of most other interferometers) are either to compare a standard length or surface with an unknown, or the variation of density of fluids in one space with a homogenous space, or the difference in optical path between the

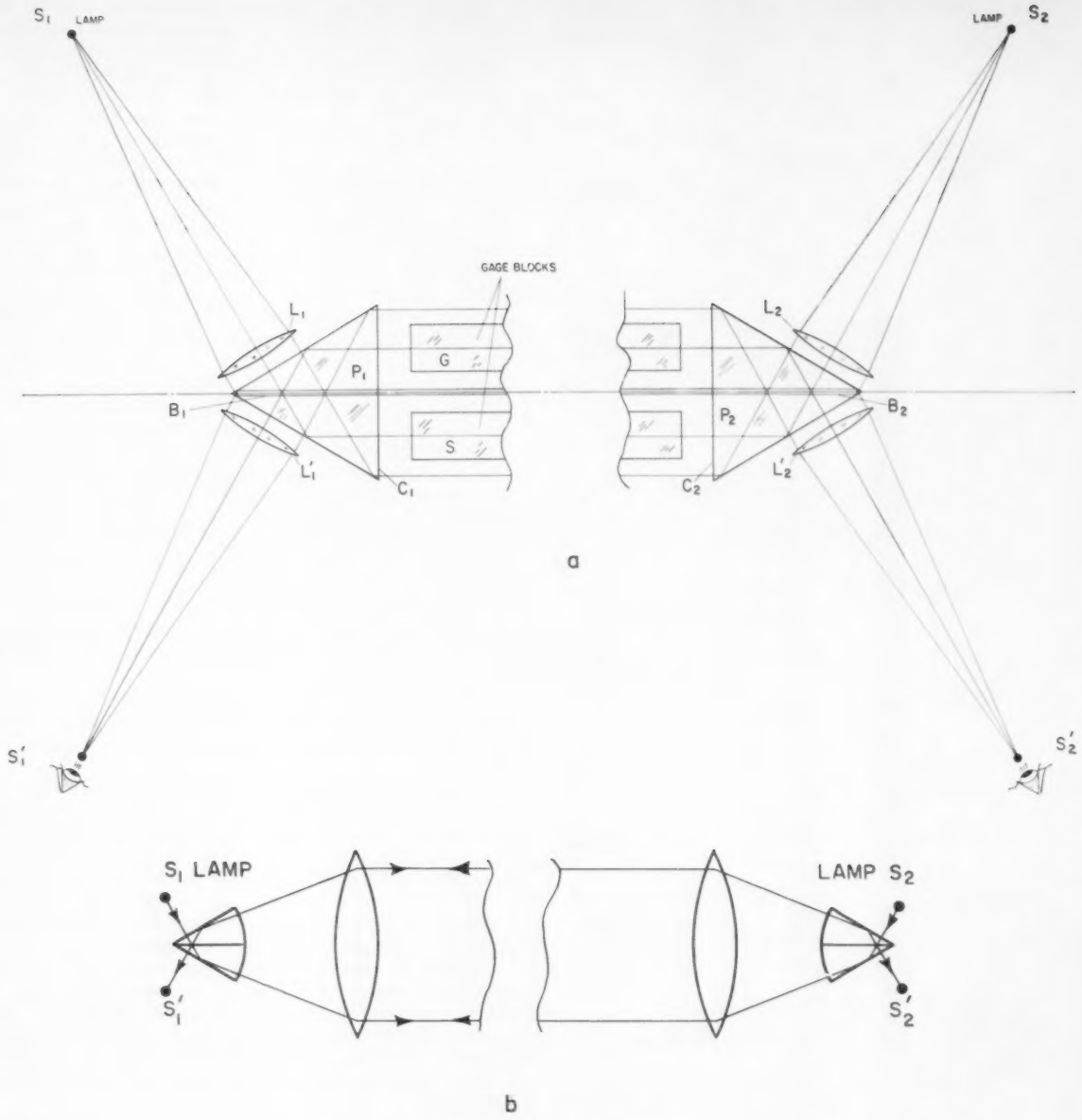

FIGURE 5. a. *A parallelism testing interferometer.*
b. *Same as a, but modified to permit larger apertures.*

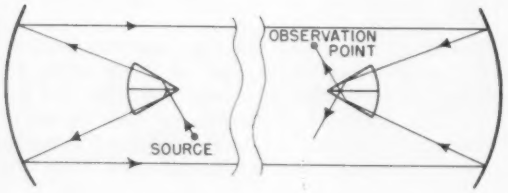

FIGURE 6. *A large aperture interferometer for parallelism testing, wind tunnel optics, etc.*
Mirrors M_1 and M_2 are parabolas.

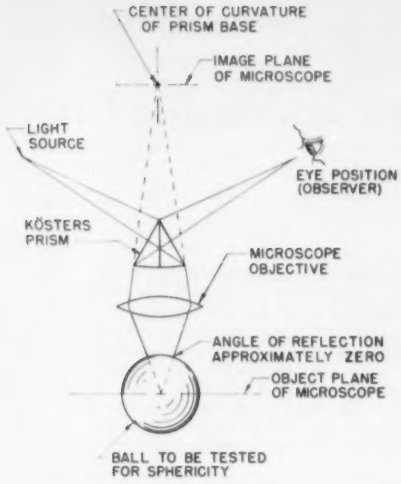

FIGURE 7. *An interferometer for testing the sphericity of small balls.*

two component beams. The wave front reversing [5] properties of these interferometers permit measurements to be made without reference standards. This author [9] has described methods of obtaining many results without the use of standards for reference. The aberrations of lenses and mirrors [10], the homogeneity of optical mediums, etc., may be obtained without reference standards. Consequently, very small prisms can be used with large lenses or mirrors to provide interferometers for testing specimens of all sizes without the use of reference standards.

References

[1] Candler, C., Modern interferometers, p. 487, (Hilger & Watts, Ltd., Hilger Div., London, England, 1951).
[2] Ibid., chap. VII.
[3] Ibid., p. 170.
[4] Williams, W. E., Interferometer apparatus for quantitatively determining fluid pressures in wind tunnels, U.S. Patent No. 2,434,029. (1948.)
[5] Saunders, James B., The wavefront reversing interferometer, reprinted from Optics in Metrology (Pergamon Press, London, England, 1960).
[6] Engelhard, E., Precise interferometric measurement of gage blocks, NBS Circ. 581, p. 4. (1957.)
[7] Saunders, J. B., An alinement interferometer, p. 541. Appl. Opt. **2,** No. 5 (May 1963).
[8] Saunders, J. B., A new method of measuring gage blocks, J. Research NBS, **64C** (Eng. and Instr.), No. 3, 173. (1960.)
[9] Saunders, J. B., Measurement of wave front without a reference standard, J. Research NBS **65B** (Math. and Math. Phys.) No. 4, 239 (1961); **66B** (Math. and Math. Phys.) No. 1, 26 (1962).
[10] Saunders, J. B., The Kösters double-image prism, Appendix C. p. 2, 393, of Concepts of Classical Optics, by J. Strong (W. H. Freeman & Co., San Francisco, Calif., 1958).
[11] Saunders, J. B., Interferometer for large surfaces, J. Research NBS **62,** p. 137 (1959) RP2943.

(Paper 67C3–130)

JOURNAL OF RESEARCH of the National Bureau of Standards—C. Engineering and Instrumentation
Vol. 67C, No. 3, July–September 1963

A Far-Infrared Vacuum Grating Spectrometer

L. R. Blaine [1]

(March 4, 1963)

A far-infrared vacuum grating spectrometer has been designed, built and tested at the National Bureau of Standards. This instrument has been in operation and under constant improvement for the past two years. Its useful range of operation is from 30 to 400 cm^{-1}. The detecting and dispersing elements are a Golay pneumatic detector and a series of 2¼×3 in. plane gratings. A spectral resolution of from 0.5 to 1.0 cm^{-1} has been attained in the region between 30 and 200 cm^{-1}.

The far-infrared absorptions of several halogenated ethanes in the liquid state have been observed and measured. The absorptions observed were: pentachloroethane, 175.5 cm^{-1}, 164.5 cm^{-1}, and 85 cm^{-1}; symmetric-tetrachloroethane, 172.0 cm^{-1} and 87 cm^{-1}; 1 bromo-2-chloroethane, 202.0 cm^{-1} and 123 cm^{-1}.

1. Introduction

In recent years a renewed and enlarged interest has been aroused in the direct measurement of spectra below 200 cm^{-1}. It is in this low frequency region that one observes absorption bands arising from the bending and twisting modes of complex molecules.

This work is primarily concerned with the construction of an instrument of medium resolution that would be capable of observing and measuring these low lying frequencies.

2. Equipment

In order to design a vacuum instrument that would possess the convenience and adaptability necessary for the numerous phases of infrared research, four basic aims were used as guides: (1) the maintaining of a maximum level of source energy, (2) the use of window mounts that could easily be adapted to many situations, (3) the accessibility of optical components for convenient adjustment and interchange, and (4) the allowance for subsequent improvements on the instrument, both in size and quality.

2.1. Instrument Housing

The instrument housing as shown in figures 1 and 2 is divided into four separate chambers, each of which is accessible through one or more cover plates. These chambers are interconnected by three focal plane windows. Each window and cover plate is O-ring sealed and has its mounting holes indexed for rapid interchange and adaptation.

The main section, composed of chambers C2 and C3, was fabricated from 5/16-in. aluminum plate. The plate was rolled into a cylinder 72 in. long ×22 in. in diameter. All of the joints were heli-arc welded. Chambers C1 and C4 were fabricated from the same material and can be detached from the main housing.

Chamber C1 houses the source and source optics (fig. 2). It may be flushed with a dry inert gas or evacuated as the research allows. Liquid or gas absorption cells up to 10 cm in length may be placed in the path between M2 and W1.

Chamber C2 is essentially a variable path gas absorption cell. The path length may be varied from 2 to 6 m. The reflector, MR, is a six-position turret that is controlled from cover A3. On this turret plane reflectors are mounted and selected as needed.

The monochromator chamber C3 is of sufficient size to house a spectrometer having a focal length of 60 cm. At present a modified monochromator section of a Perkin-Elmer Model 12 single-beam spectrometer is being used. The grating turntable is driven by an externally located synchronous motor. An O-ring sealed shaft transmits the power through the vacuum wall at cover A8. The monochromator slits are driven by an electric motor located within the vacuum chamber. Slit motor and detector leads are brought outside through the Kovar seals in cover A7. Cover A6 provides for access to the grating and contains a glass window for observation purposes. Between C2 and C3 there is a separating window W2, which can be removed or installed as the research demands. This allows one to make use of the added path length of the monochromator whenever noncorrosive gases are being studied.

Chamber C4 is used specifically to house the Golay pneumatic detector and may be flushed with dry nitrogen or evacuated. The cover of this chamber is hinged and is fitted with Kovar seals for signal and power connections. In this chamber liquid and gas absorption cells up to 15 cm in length may be introduced into the optical path at window W3.

The vacuum system is composed of a forepump, oil diffusion pump, and strategically located cold traps (fig. 1). Chambers C2 and C3 are evacuated through 4-in. copper tubing beginning at covers A2 and A5 and joining at the cold trap T1. Preceding the cold trap T1, there is a 4-in. 300 liter/sec oil diffusion pump P1. Preceding P1 is a packless

[1] This work was done in partial fulfillment of the requirements for the degree of Master of Science for the Graduate School of the University of Maryland.

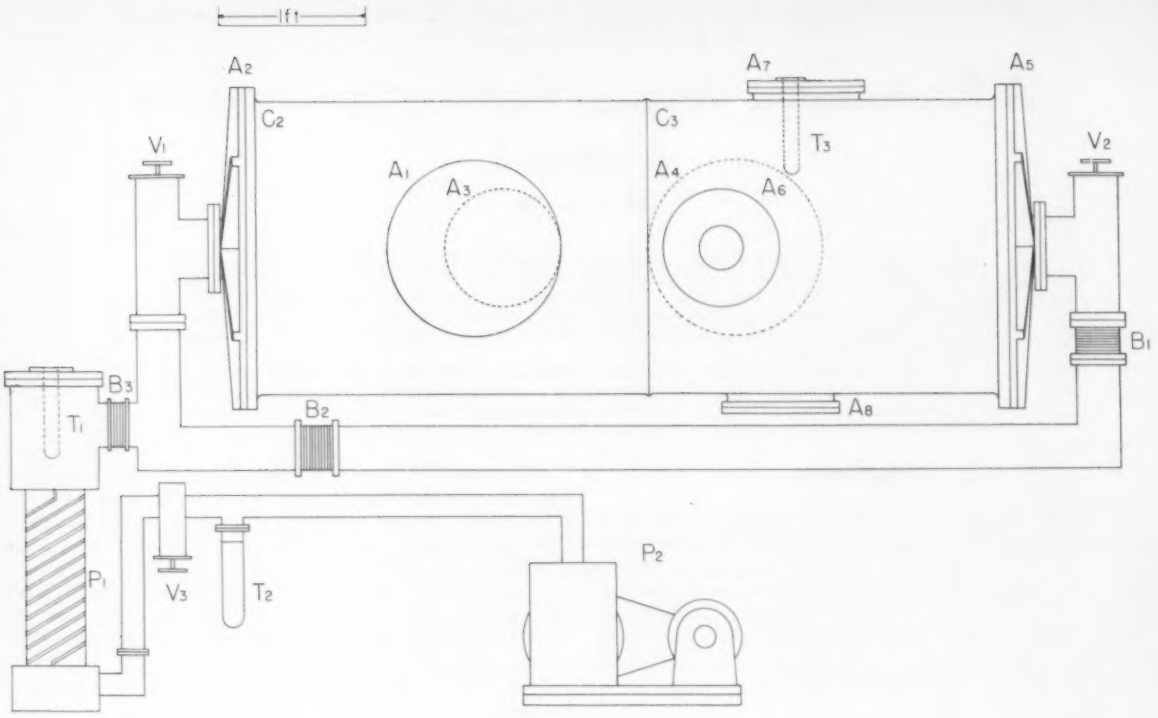

FIGURE 1. *Instrument housing and vacuum system. (side view)*

valve V3, a cold trap T2, and a forepump P2. An additional cold trap in the form of a cold finger, T3, is suspended in the monochromator chamber, C3, at cover plate A7.

This vacuum system has been found adequate for the removal of atmospheric absorption with respect to the present path length and resolution of the instrument.

2.2. Optical System

The optical system is divided into four sections: source optics, absorption cell optics, monochromator optics, and detector optics (fig. 2).

a. Light Path

The light is first modulated at 10 c/s at the source S by the chopper C, passes to reflector M1, to spherical mirror MS1, to plane mirror M2 and is then focused on the plane of window W1.

On entering chamber C2 it is reflected from plane mirror M3 to spherical mirror MS2 and then to one of the six plane reflectors on the turret MR. From this point it is reflected into the spherical mirror MS3 and into the mirror system of the multipass absorption cell. This is composed of several small plane mirrors, M4, M5, M6, M7, and one spherical mirror MS4, having a 50-cm radius of curvature. A path length of up to 6 m is available by changing the arrangement of the multipass mirrors. These are prepositioned on a plate that can be changed as a unit. This operation can be performed through cover plate A3. After leaving the multipass cell, the light passes to plane mirror M8, spherical mirror MS5, plane mirror M9, and through the exit window W2.

From the window W2, the light is brought to a focus on the monochromator entrance slit S1. It then passes through a standard Littrow-type f/4.5 grating monochromator. The monochromator exit slit, S2, is then focused on the window W3 by the plane mirrors M11 and M12 and the spherical mirror MS6.

After entering chamber C4 the light may pass either to toroidal mirror MT, or to a 90-deg-off-axis ellipsoidal mirror ME, and then be focused into the Golay receiver D. The toroidal mirror with its short focal length leaves space only for short liquid and gas absorption cells up to 2 cm in thickness. The ellipsoidal mirror, however, has conjugate focal distances of 3 and 21 cm and will allow absorption cells up to 15 cm in length to be placed between window W3 and the ellipsoid ME.

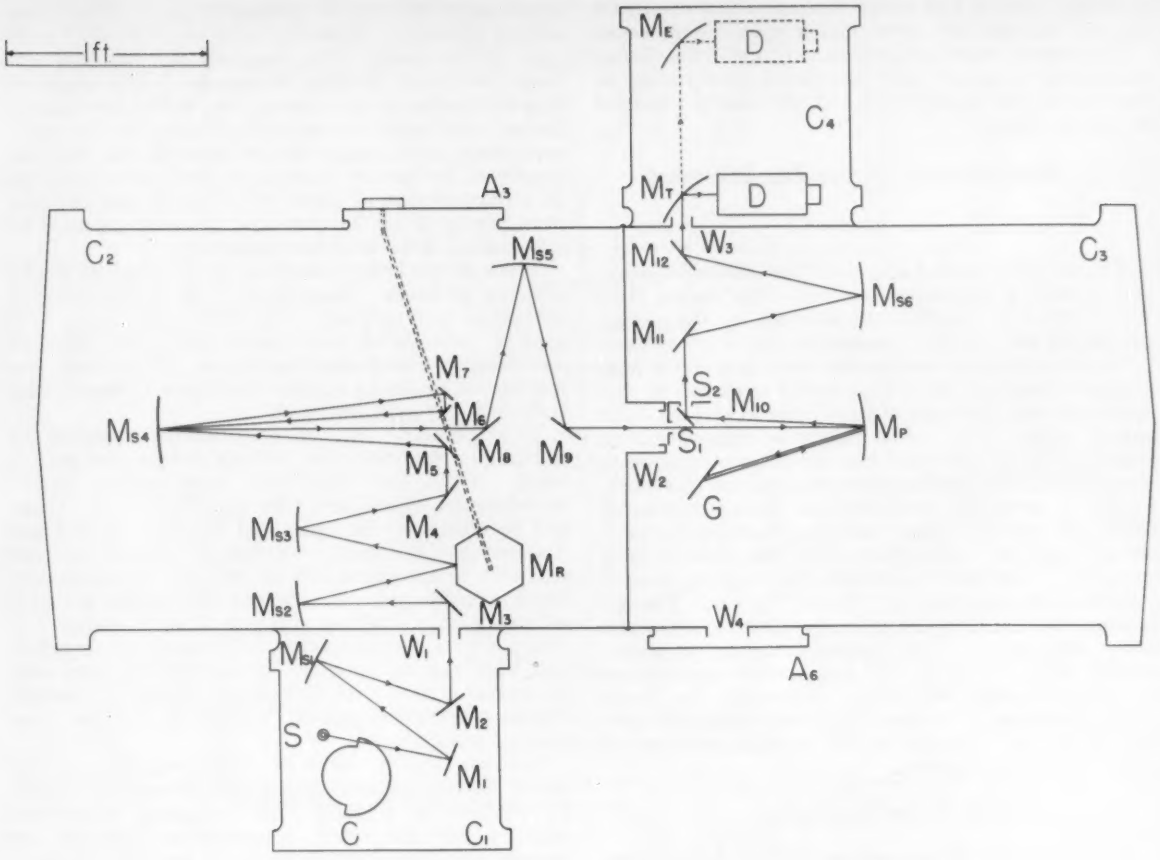

FIGURE 2. *Optical system.*

b. Monochromator and Modifications

(1) *Grating drive.* The P.E. 12 is a prism instrument and its Littrow mirror is rotated by a sine bar which allows only 10 deg of angular rotation. In order to eliminate this inconvenience and obtain 360 deg of rotational freedom the sine bar was removed and a precision worm gear substituted. Connection was then made to the power shaft at A8. The prism table was removed and a suitable grating mount was substituted for the standard Littrow mirror mount.

The grating turntable driving system consists of a synchronous motor, standard three-speed transmission, several precision worm gears, a rotation counter, an O-ring sealed drive shaft, and an independent rapid traverse drive motor. The synchronous motor having a variable speed-reducer gives a range of scanning speeds from 1.2 to 0.16 deg of arc per minute of time. This provides scanning speeds compatible with the time constants of the detector system.

The rapid traverse drive is specifically designed for rapid positioning of the grating and gives a scanning rate of 31.4 deg/min of time.

(2) *Slits.* The bilateral slits are geared to an electric motor which is located within the vacuum chamber C3, and controlled from an outside switch panel. A Veeder-Root rotation counter located in the gear train enables one to determine the slit width to within a few microns. This counter is readily observed through the window in cover A6.

(3) *Optical modification.* In order that the Golay detector could be placed in chamber C4, under atmospheric pressure, the standard optical system behind the monochromator exit slit, S2, had to be rearranged so as to focus the image of S2 on the window W3. This was accomplished by installing the plane mirrors M11 and M12 and the spherical mirror MS6.

(4) *Electrical system.* Controls for the slit drive, grating drives and vacuum gages are mounted on a control panel which is located on the instrument support frame. The electric motors that power these components are single phase ratio-motors [2] having a rating of approximately 1/100 hp. Power or signal

[2] Electric motors equipped with a built-in speed reducer.

leads that pass in and out of the individual chambers are fed through the cover plates with Kovar seals.

The signal detection system [3] consists of a Golay pneumatic detector and associated equipment so that the signal is amplified and ultimately recorded on a strip chart.

3. Spectroscopy in the Far Infrared

3.1. Sources

The choice of a good source for far infrared absorption studies is somewhat limited. The region from 400 to 100 cm^{-1} is efficiently covered by the globar. Below 100 cm^{-1} a high pressure mercury arc is used.

The source being used in this work is a 100 w high pressure mercury arc. This arc is enclosed in two envelopes, an inner one of fused quartz and an outer one of glass. The fused quartz is transparent to radiation below 100 cm^{-1} but the glass is opaque to this radiation and is therefore removed for this work. Figure 3 gives the transmission characteristics of fused and crystal quartz and the emission curve of excited mercury vapor filtered by the fused quartz envelope. The curve 3d shows the relative level of a globar continuum in the 100 cm^{-1} region. The arc is unique in that it has an intense emission continuum below 100 cm^{-1}. This emission covers a region roughly from 100 to 10 cm^{-1} and reaches a maximum at approximately 80 cm^{-1}. Although the fused quartz envelope is transmitting only about 15 percent at 90 cm^{-1}, the arc is still emitting a factor of 3 over a standard globar.

3.2. Order Separation

As one works at successively lower frequencies, the problem of obtaining spectra free of overlapping orders becomes very severe. The root of this problem is seen in an examination of the Planck radiation law for an ideal blackbody. Consider, as an illustrative example, a blackbody at a temperature of about 1,500 °K. The radiation curve for this source has a peak at about 3,000 cm^{-1}. We are interested in the region around 30 cm^{-1}. The intensity at 30 cm^{-1} is down by a factor of 5×10^{-4} from that at the peak. This suggests the required efficiency of one's filtering techniques. The emission characteristics of the mercury arc would lead one to believe that such a source would simplify the order separation problems in the far infrared, but the heat produced by the arc maintains the quartz envelope at a temperature of about 900 °C, and the emission then produced by the envelope, not being filtered by the quartz, must still be eliminated.

Black polyethylene has been quite effective in this filtering problem. Essentially, it is a dispersion of carbon in polyethylene. As shown by figure 5, it greatly attenuates the visible and near infrared wavelengths and passes the longer. Previously, one was forced to smoke a piece of window material with turpentine or camphor soot.

This difficulty can be considerably lessened by working in the first order, well away from the grating blaze. Thus the relatively short (high order) wavelengths, which are very sensitive to the blaze, will be efficiently concentrated in other regions and the longer (first order) wavelengths which are not sensitive to the blaze will be left less contaminated. Good quality gratings used as zero order selective reflectors offer another efficient filtering device [1].[4] When several are properly used in series their reflection edge can be as sharp as the transmission edge of crystal quartz with the added feature of control. Figure 4 gives the reflectivity curves of three good quality gratings.

Another widely used filtering technique makes use of the transmission properties of various crystals. In addition to a sharp high frequency absorption edge, a low frequency transmission edge is also present in these crystals which is usually not sharp enough to serve as an efficient filter. Only crystal quartz seems to fulfill this requirement. This transmission edge, however, can be sharpened and controlled by impregnating polyethylene with one or more of these crystals in powdered form [2].

Probably the most efficient filtering technique is that of using the reststrahlen of various crystals.

[3] Manufactured by Eppley Laboratory Inc., Newport, R.I.

[4] Figures in brackets indicate the literature references at the end of this paper.

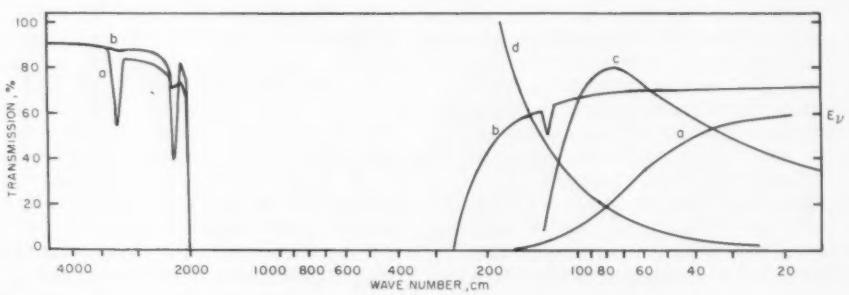

FIGURE 3. *Properties of quartz and the mercury arc.*

(a) Transmission of fused quartz. (b) Transmission of crystal quartz. (c) Spectral output of a high pressure mercury arc filtered by 1 mm of fused quartz. (d) Spectral output of a globar.

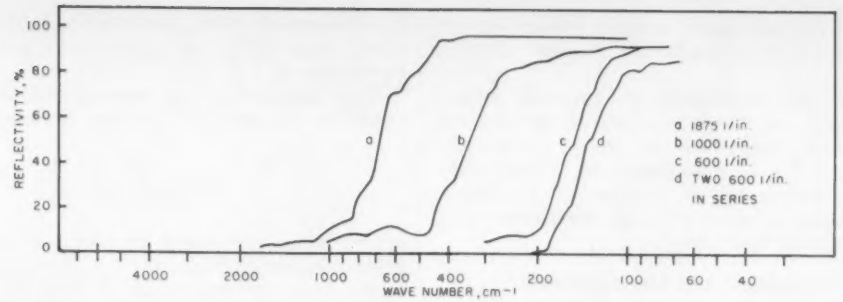

FIGURE 4. *Regular reflection of three gratings.*

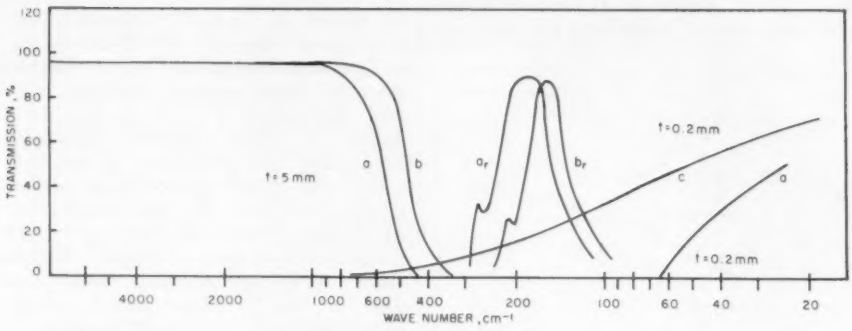

FIGURE 5. *Transmission and reflection properties.*
(a) NaCl, (b) KCl, (c) black polyethylene.

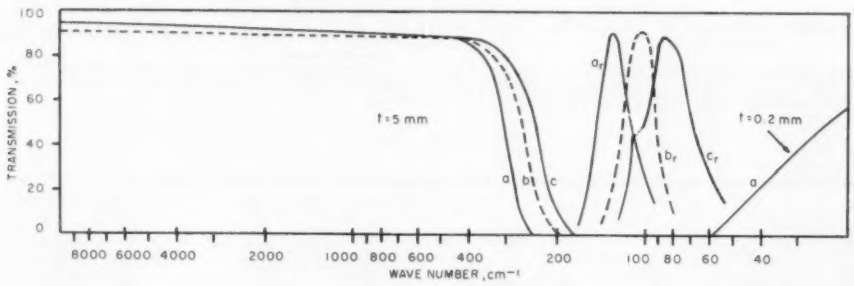

FIGURE 6. *Transmission and reflection properties.*
(a) KBr, (b) RbBr, (c) CsBr.

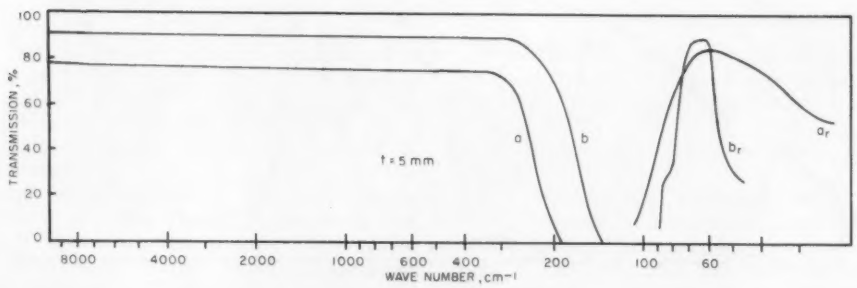

FIGURE 7. *Transmission and reflection properties.*
(a) KRS-5, (b) CsI.

Many of these crystals have a peak reflectivity of 90 percent and cover a reasonably narrow spectral interval.

In all cases the separation of spectral orders requires strategic use of the reflective, scattering, and transmissive properties of many materials. Figures 5, 6, and 7 give a sequence of transmission and reflection curves for a number of materials. They are arranged in order of their usefulness with respect to decreasing frequency.

3.3. Calibration and Measurement

Calibration is accomplished by measuring the pure rotation absorption spectrum of water vapor or other gases. Water vapor lines are obtained by reducing the flush rate of chambers C1 and C4.

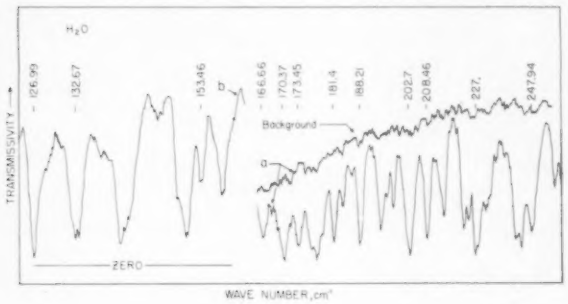

FIGURE 8. *Absorption spectrum of water vapor from 248 to 126 cm⁻¹.*

Conditions: (a) 600 1/in. dispersion grating, 0.05 mm black polyethylene, one NaCl reflection, one 1,800 1/in. scatter plate. (b) 320 1/in. dispersion grating, 0.1 mm black polyethylene, 0.5 mm crystal quartz, two 1,200 1/in. scatter plates.

In the case of other gases (NH_3, HCl, HCN) a 5-cm absorption cell at the appropriate pressure is placed in the beam.

First approximation measurements are made by applying the standard grating formula

$$\nu = \frac{n}{2d \cos \frac{1}{2}\alpha} \frac{1}{\sin \theta},$$

where ν is the wave number, d is the grating groove separation in cm, n is spectral order, and θ is the angular separation of the central image and the spectral line in question. The angle α is that angle subtended by the two slits at the center of the collimating mirror. The angle θ is determined by means of a rotation counter that is mounted in the gear train. A microswitch automatically activates a fiducial marker on the recorder every 500 counts. This system, without special calibration, will determine a relative frequency to 1 part in 1,000. A more accurate calibration is made by measuring the positions of several standard lines and from them determining an average central image position. By this procedure, and variations of it, frequencies of sharp symmetric lines can be measured to 1 part in 4,000. Figures 8 through 13 show recordings of the water lines between 200 and 30 cm^{-1}. Their latest accepted frequencies are indicated.[5] Figure 16 illustrates a case where the band to be measured has been bracketed by the calibrating lines. In this case a short air path was left unflushed before and after the band was recorded.

The task of measuring the center frequencies of the broad bands that are found in liquids and solids

[5] Frequencies of pure rotational water lines were kindly supplied by Dr. W. S. Benedict. These are calculated values derived from the best available energy levels.

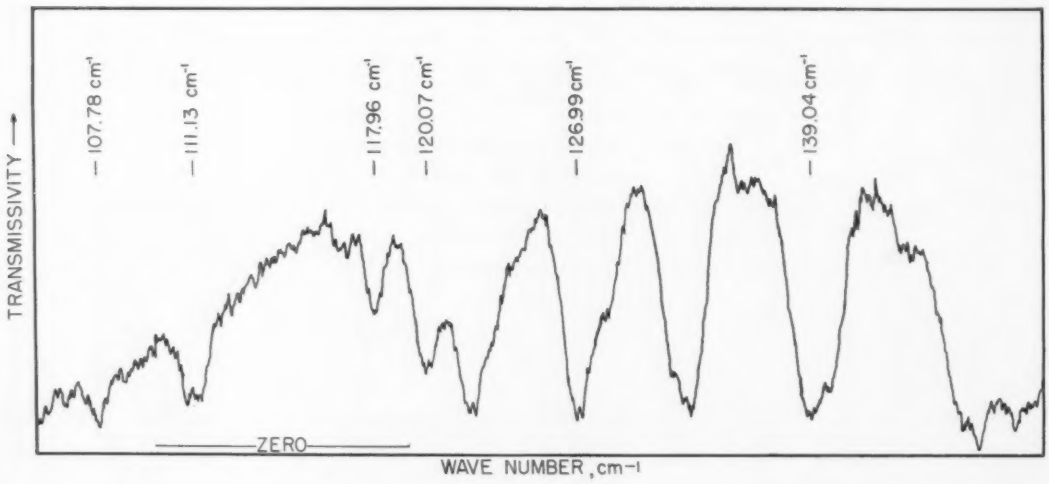

FIGURE 9. *Absorption spectrum of water vapor from 150 to 105 cm⁻¹.*

Conditions: 320 1/in. dispersion grating, 0.1 mm black polyethylene, 0.5 mm crystal quartz, one KBr reflection, one 600 1/in. scatter plate.

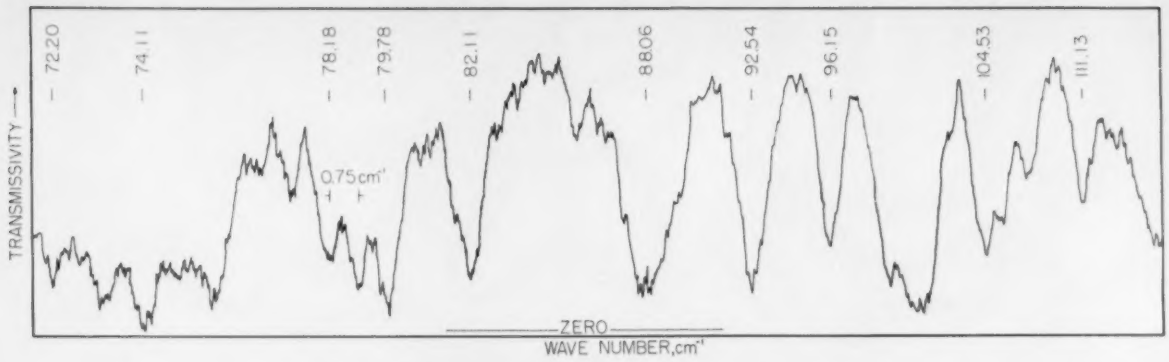

FIGURE 10. *Absorption spectrum of water vapor from 115 to 70 cm⁻¹.*

Conditions: 320 1/in. dispersion grating, 0.1 mm black polyethylene, 1.0 mm crystal quartz, one CsBr reflection, two 600 1/in. scatter plates.

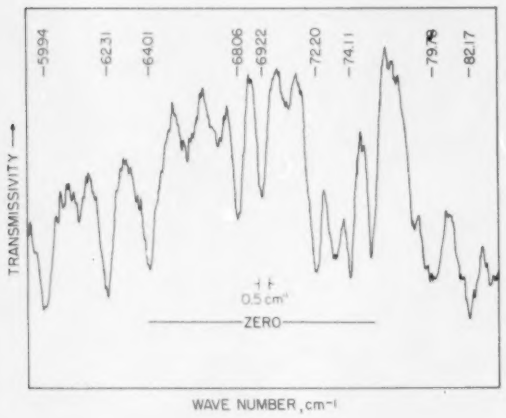

FIGURE 11. *Absorption spectrum of water vapor from 92 to 59 cm⁻¹.*

Conditions: 180 1/in. dispersion grating, 0.2 mm black polyethylene, 1.0 mm crystal quartz, one KRS-5 reflection, two 320 1/in. scatter plates.

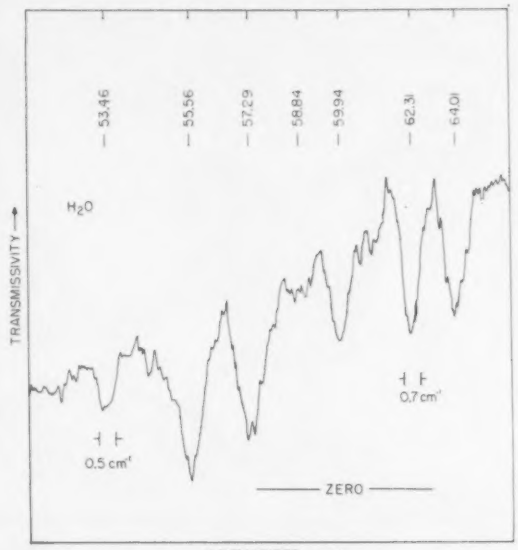

FIGURE 12. *Absorption spectrum of water vapor from 64 to 50 cm⁻¹.*

Conditions: 180 1/in. dispersion grating, 0.2 mm black polyethylene, 1.0 mm crystal quartz, 0.5 mm LiF, one KRS-5 reflection, two 320 1/in. scatter plates.

presents a difficulty which greatly reduces the precision and accuracy of measurement. Those bands having widths [6] between 5 and 20 cm^{-1} are in general no problem except in that their width makes it impossible to determine their centers precisely. A special problem is presented by those bands having widths greater than 20 cm^{-1}. This is due to the fact that in regions where the reststrahlen of a crystal are a necessary part of the filtering technique, the energy contour is usually no wider than the absorption band to be measured. In many cases the band contour is never directly observed, but must be obtained by subtracting out the reststrahlen background. The band center is then measured from a plotted contour. This greatly reduces the attainable precision and accuracy.

[6] Line widths = full line width at half intensity.

4. Observations and Measurements

In addition to the spectra of water vapor, the low lying absorptions of some haloethanes were observed. The compounds (Eastman Kodak) examined were of high purity. The high purity was affirmed by an examination of their infrared spectrum from 4,000 to 150 cm^{-1}.

The compounds observed were: pentachloroethane, 1-bromo-2-chloroethane, and symmetric-tetrachloroethane. The bands observed are listed in table 1. Those bands that were directly observable are shown in figures 14, 15, and 16 and are given to ± 0.5 cm^{-1}. The lower frequency bands, however, were extremely broad (25 to 50 cm^{-1}) and are correspondingly less precise.

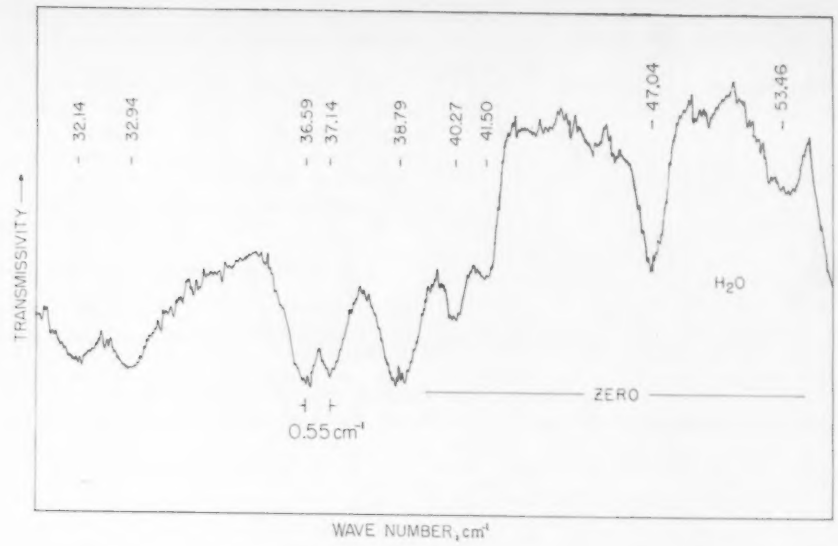

FIGURE 13. *Absorption spectrum of water vapor from 54 to 31 cm⁻¹.*

Conditions: 100 l/in. dispersion grating, 0.2 mm black polyethylene, 1.0 mm crystal quartz, 0.2 mm NaF-TlCl-polyethylene filter, one KRS-5 reflection, two 240 l/in. scatter plates. (This filter was kindly furnished by Hiroshi Yoshinaga of Osaka University in Japan.)

TABLE 1. *Observed bands of halogenated ethanes*

Compound	cm⁻¹
$Cl_3C-CHCl_2$	85. ±1.5 164.5±0.5 175.5±0.5
ClH_2C-CH_2Br	123. ±1.0 202.0±0.5
$Cl_2HC-CHCl_2$	87. ±1.0 172.0±0.5

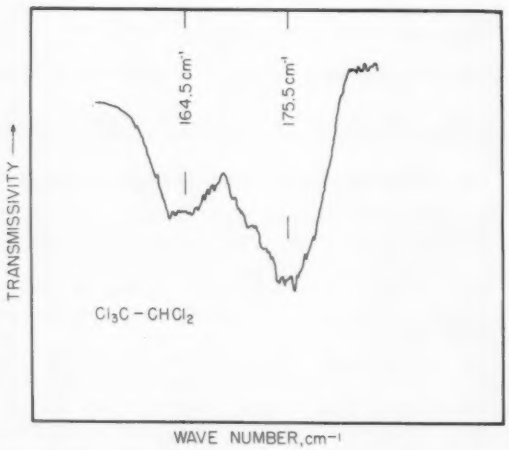

FIGURE 14. *Absorption of $Cl_3C-CHCl_2$ at 164.5 and 175.5 cm⁻¹.*

Cell thickness = 1.5 mm; Concentration = 1:3 (by volume) of compound in CCl_4.

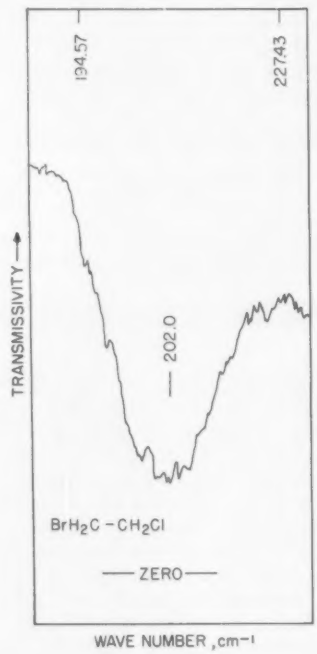

FIGURE 15. *Absorption of BrH_2C-CH_2Cl at 202 cm⁻¹.*

Cell thickness = 1.5 mm; Concentration = 1:30 (by volume) of compound in CCl_4.

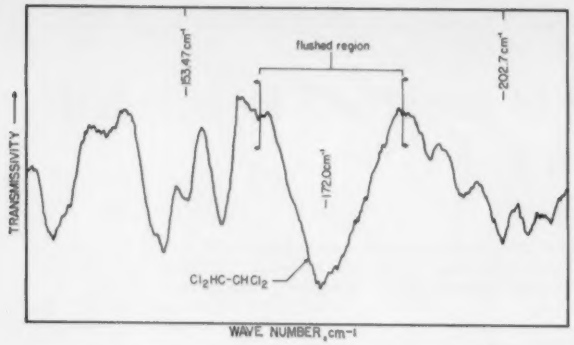

FIGURE 16. *Calibration of the 172.0 cm⁻¹ absorption band of $Cl_2HC-CHCl_2$.*

Cell thickness = 1.5 mm; Concentration = 1:10 (by volume) of compound in CCl_4.

5. Discussion

The far infrared offers many challenging problems that must be solved before high quality data will be available from this spectral region.

Quality is judged first in spectral resolution and second in accuracy and precision of measurement. Using the high quality work produced in the near infrared as a guide, the goal would be a spectral resolution of 0.03 cm^{-1} and a precision of approximately 0.005 cm^{-1}. By using the scanning techniques presently used in the near infrared, it is feasible that the goal of precision could be attained. The goal of resolution however is more challenging.

Considering first an f/4.0 single pass optical system, using 12×8 in. high quality grating and a high quality collimating mirror, one would have a system capable of attaining the 0.03 cm^{-1} spectral resolution. Thus it is seen that the optical system does not represent the major obstacle. The highest resolution attained with grating spectrometers by recent workers is of the order of 0.25 cm^{-1}, which is a factor of about 8 less than that expected. In order to reduce the spectral width to the 0.03 cm^{-1} mentioned above, one would have to accept a loss by a factor of 64 in detector output. This deficiency must be made up by more powerful sources, more efficient filtering techniques, and more sensitive detectors.

A study of the high pressure mercury arc to determine the origin of its long wavelength emission could possibly lead to more efficient sources. Also research in plasmas, high temperature blackbodies, and emissivities should be profitable.

A small factor may possibly be realized in more efficient filtering methods. The use of the reststrahlen of crystals still remains the most dependable method at present. These, teamed with good gratings as scatter plates, should be highly efficient in eliminating stray radiant energy. The development of an automatic crystal and grating changer may prove to be not only the most convenient but also the most efficient solution.

By far, the greater effort will have to be applied to detector development. Presently work is being done on supercooled bolometers and related devices [3]. Indications are that factors of 40 could be expected in this area.

The problem of maintaining spectral purity in the far infrared coupled with that of measuring the centers of the very broad bands of many liquids could be solved by the construction of a large high vacuum double-beam–single-beam spectrometer having an automatic crystal and grating changer. An instrument built along these lines would serve as a valuable tool in far infrared research.

The author expresses thanks to E. K. Plyler for his cooperation and helpful discussions, and to W. Koepper and M. Myers for the machining and welding done on this instrument.

6. References

[1] John U. White, J. Opt. Soc. Am. **37,** 713 (1947).
[2] Yahiko Yamada, Akiyoshi Mitsuishi, and Hiroshi Yoshinaga, J. Opt. Soc. Am. **52,** 17 (1962).
[3] Frank J. Low, J. Opt. Soc. Am. **51,** 1300 (1961).

(Paper 67C3–131)

JOURNAL OF RESEARCH of the National Bureau of Standards—C. Engineering and Instrumentation
Vol. 67C, No. 3, July–September 1963

Relation of Emittance to Other Optical Properties *

J. C. Richmond

(March 4, 1963)

An equation was derived relating the normal spectral emittance of an optically inhomogeneous, partially transmitting coating applied over an opaque substrate to the thickness and optical properties of the coating and the reflectance of the substrate at the coating-substrate interface.

1. Introduction

The 45° to 0° luminous daylight reflectance of a composite specimen comprising a partially transparent, spectrally nonselective, light-scattering coating applied to a completely opaque (nontransmitting) substrate, can be computed from the reflectance of the substrate, the thickness of the coating and the reflectivity and coefficient of scatter of the coating material. The equations derived for these conditions have been found by experience [1, 2][1] to be of considerable practical usefulness, even though several factors are known to exist in real materials that were not considered in the derivation. For instance, porcelain enamels and glossy paints have significant specular reflectance at the coating-air interface, and no real coating is truly spectrally nonselective.

The optical properties of a material vary with wavelength, but in the derivation of the equations referred to above, they are considered to be independent of wavelength over the rather narrow wavelength band encompassing visible light. The condition of spectral nonselectivity is met sufficiently well by a number of materials to permit use of the pertinent equations with but a single set of optical properties for visible light. Over the enormously wider range of wavelengths within which the emission and absorption of radiant energy are important, few if any materials are sufficiently nonselective to permit use of the pertinent equations with a single set of optical properties applicable to all wavelengths. Hence the optical properties as a function of wavelength are required for computation of wide-range spectral reflectance or emittance of such composite specimens.

The present study was undertaken to derive an equation relating the spectral reflectance (or emittance) of a composite specimen comprised of a partially transmitting, light-scattering coating applied to a completely opaque (nontransmitting) substrate, from the thickness of the coating and the spectral optical properties of the coating and substrate.

2. Review of the Literature

The relationship between the thickness and reflectance of a layer of light-scattering materials as a function of the optical constants of the material was developed by Kubelka and Munk [3]. Judd [1] developed graphical methods for the solution of the Kubelka-Munk equation, and demonstrated that it was useful in studying real materials which departed somewhat from the ideal material postulated in development of the equation. Kubelka [4] derived more exact equations in a form that was capable of relatively easy solution. In all of these cases, the materials considered were assumed to be spectrally nonselective, so that a single value of each optical constant could be used throughout the visible range of wavelengths.

Gardon [5] considered the case of an optically homogeneous material with a three-dimensional analysis. Hamaker [6] and Klein [7] worked with powders, which may be considered as a special case of optically inhomogeneous (light-scattering) materials, and derived equations for computing heat transfer by radiation in powders. In these cases a single value applicable to total blackbody radiation was used for each optical property.

* This work was sponsored and financed by the George C. Marshall Space Flight Center of NASA.

[1] Figures in brackets indicate the literature references at the end of this paper.

Saunderson [9] worked with partially transmitting plastics, and used equations for transmittance and reflectance derived by Kubelka and Munk [3], that are similar but not identical to those of Klein [7]. However, he did incorporate a correction for the specular reflection at the plastic-air interface.

3. Derivation of Equation

Because of the relationships

$$A+T+R=1, \tag{1}$$

in which A=absorptance, T=transmittance, and R=reflectance, and Kirchoff's law,

$$A=E, \tag{2}$$

in which E is emittance,[2] it is possible to compute emittance from reflectance for completely opaque specimens. This method will therefore be used, because of its simplicity as compared to the approach used by Gardon [5].

Consider a flux of completely diffuse radiant energy, incident in uniform geometric distribution over the entire area of an optically flat layer of inhomogeneous isotropic dielectric material having infinite area and uniform thickness. Upon attainment of a steady state condition, the incident flux that is not reflected at the surface will penetrate into the material, diminishing with the depth of penetration, the amount of diminution at any internal plane parallel to the surface being a function only of the distance of the plane from the surface.

Attenuation of the inward-bound diffuse flux will result from absorption of radiant energy within the specimen, and from backscattering by the dispersed particles in the material. The backscattered flux will proceed as completely diffuse flux propagated in a direction normal to the surface outward through the coating. In both cases, the radiant flux lost by lateral scattering will be compensated by an equal gain through similar scattering from adjoining portions of the specimen. The outward-bound flux will also be attenuated by absorption and backscattering. This backscattered flux will reinforce the incoming flux.

Under the postulated conditions, a one-dimensional mathematical analysis can describe the variation in diffuse radiant flux density along a line normal to the surface, due to absorption and scattering within the material, as a function of distance from the coating-substrate interface.

In using the one-dimensional analysis, the diffuse radiant flux traversing unit area normal to the direction of propagation is considered as being made up of two directionally opposed portions, one I, outward from the interior of the specimen and normal to the flat surface, and the other J, in the opposite inward direction. A spectral absorption coefficient, K, is defined by equating $KIdx$ to the reduction in I by absorption within a layer of infinitesimal thickness, dx. A scattering coefficient, S, is similarly defined by equating $SIdx$ to the flux scattered backwards from I in the unidirectional beam (and therefore included in J) within a layer of infinitesimal thickness, dx.

Within the distance dx the flux, I, will be not only diminished by absorption and scattering, but also augmented by the backscattering from J. Hence we can write

$$dI/dx=-(K+S)I+SJ \tag{3}$$

$$dJ/dx=(K+S)J-SI. \tag{4}$$

These are the general differential equations first used by Kubelka and Munk [3] as a starting point, and subsequently by many other investigators.

---

[2] Emittance, as used in this paper, is defined as follows: Emittance is a property of a specimen; it is the ratio of its emissive power to that of a blackbody radiator at the same temperature and under the same spectral and geometric conditions of viewing.

Emissive power is the rate of thermal emission expressed as radiant flux per unit surface area.

Hamaker's [6] solutions for eqs (3) and (4), considering both absorption and scattering, are

$$I=L_1(1-\beta)e^{\sigma x}+L_2(1+\beta)e^{-\sigma x} \tag{5}$$

$$J=L_1(1+\beta)e^{\sigma x}+L_2(1-\beta)e^{-\sigma x} \tag{6}$$

where L_1 and L_2 are constants determined by the boundary conditions, and where

$$\sigma=\sqrt{K(K+2S)} \tag{7}$$[3]

and

$$\beta=\sqrt{K/(K+2S)}. \tag{8}$$[3]

3.1. Equations Applicable to Coatings

Most coatings, such as paint, porcelain enamel, and ceramic coatings, unlike the materials postulated by Kubelka [4] and dealt with by Hamaker [6] and Klein [7], have a disperse medium other than air, usually of a glassy nature, in which the scattering particles are distributed. Hence specular reflectance at the coating-air and coating-substrate interfaces must be considered. This structural difference will give different boundary conditions than were considered by previous authors.

In the systems under consideration, the reflectance at the interfaces will be considered, as follows:

ρ_e=specular reflectance at the coating-air interface for externally incident, completely diffuse radiant flux (J_e).

ρ_s=reflectance of the substrate for completely diffuse radiant flux (J_0) incident upon the substrate from the coating.

ρ_i=specular reflectance of the coating-air interface for completely diffuse radiant flux (I_D) incident from within the coating.

Let x be the perpendicular distance from the coating-substrate interface to a point in the coating, and D be the thickness of the coating.

If only the disposition of incident flux be considered, and if radiant energy emitted by the specimen be ignored, the boundary conditions for substitution in eqs (5) and (6) are

$$I=J_o\rho_s \text{ at } x=0 \tag{9}$$

$$J=J_e(1-\rho_e)+I_D\rho_i \text{ at } x=D \tag{10}$$

when $x=0$, $e^{\sigma x}=e^{-\sigma x}=1$, hence from eqs (5), (6), and (9)

$$L_1(1-\beta)+L_2(1+\beta)=\rho_s[L_1(1+\beta)+L_2(1-\beta)], \tag{11}$$

and from eqs (5), (6), and (10),

$$L_1(1+\beta)e^{\sigma D}+L_2(1-\beta)e^{-\sigma D}=J_e(1-\rho_e)+\rho_i[L_1(1-\beta)e^{\sigma D}+L_2(1+\beta)e^{-\sigma D}]. \tag{12}$$

---

[3] It may be worth while to mention the physical significance of σ and β. As can be seen in eq (7), σ is a type of extinction coefficient. If $S=0$, $\sigma=K$; if $K=0$, $\sigma=0$. The combination σx is a dimensionless optical thickness; all layers having the same σx product will produce the same attenuation in a beam of radiant energy. σ is determined by the absolute values of S and K. β, on the other hand, is a function of the relative magnitudes of S and K. If $S=0$, $\beta=1$, and if $K=0$, $\beta=0$. β is shown by Klein [7] to be related to emissivity, E_∞, and reflectivity, R_∞, by the equations

$$E_\infty=\frac{2\beta}{1+\beta} \text{ and } R_\infty=\frac{1-\beta}{1+\beta},$$

provided there is no specular reflection at the surface. For glossy materials, these relationships are modified by specular reflection at the surface.

Solving eqs (11) and (12) for L_1 and L_2, we get:

$$L_1=\frac{J_e(1-\rho_e)[(1+\beta)-\rho_s(1-\beta)]}{[(1+\beta)-\rho_i(1-\beta)][(1+\beta)-\rho_s(1-\beta)]e^{\sigma D}-[(1-\beta)-\rho_i(1+\beta)][(1-\beta)-\rho_s(1+\beta)]e^{-\sigma D}} \quad (13)$$

$$L_2=\frac{-J_e(1-\rho_e)[(1-\beta)-\rho_s(1+\beta)]}{[(1+\beta)-\rho_i(1-\beta)][(1+\beta)-\rho_s(1-\beta)]e^{\sigma D}-[(1-\beta)-\rho_i(1+\beta)][(1-\beta)-\rho_s(1+\beta)]e^{-\sigma D}}. \quad (14)$$

The equations can be simplified by making the following substitutions:

Let

$$M=(1+\beta)-\rho_s(1-\beta) \quad (15)$$
$$N=(1+\beta)-\rho_i(1-\beta) \quad (16)$$
$$O=(1-\beta)-\rho_s(1+\beta) \quad (17)$$
$$P=(1-\beta)-\rho_i(1+\beta). \quad (18)$$

Then eqs (13) and (14) become

$$L_1=\frac{J_e(1-\rho_e)M}{MNe^{\sigma D}-OPe^{-\sigma D}} \quad (19)$$

$$L_2=\frac{-J_e(1-\rho_e)O}{MNe^{\sigma D}-OPe^{-\sigma D}}. \quad (20)$$

The overall specular plus diffuse reflectance, R, of the specimen is defined as the reflected flux divided by the incident flux. The reflected flux will include the fraction of J_e that is specularly reflected at the coating-air interface. That is

$$R=\frac{J_e\rho_e+(1-\rho_i)I_D}{J_e}. \quad (21)$$

From eqs (5), (19), and (20),

$$I_D=\frac{J_e(1-\rho_e)[(1-\beta)Me^{\sigma D}-(1+\beta)Oe^{-\sigma D}]}{MNe^{\sigma D}-OPe^{-\sigma D}}, \quad (22)$$

hence

$$R=\rho_e+(1-\rho_e)(1-\rho_i)\frac{(1-\beta)Me^{\sigma D}-(1+\beta)Oe^{-\sigma D}}{MNe^{\sigma D}-OPe^{-\sigma D}}. \quad (23)$$

R in eq (23) is the reflectance of the composite specimen under conditions of completely diffuse illumination and hemispherical viewing. The equation has been written in terms of the coating parameters β, σ, ρ_e, ρ_i, ρ_s, and the thickness of the coating, D. The values of these parameters vary with wavelength. The equation applies only to spectral reflectance, R_λ, under the given geometric conditions, and spectral values of the coating and coating-substrate parameters, β_λ, σ_λ, $\rho_{e\lambda}$, $\rho_{i\lambda}$, and $\rho_{s\lambda}$ are required. The subscript λ indicates that the symbol applies to the spectral value at wavelength λ.

When transmittance is zero, as it is in the case of the coated specimens under consideration, the emittance is equal to one minus the reflectance, as is indicated by eqs (1) and (2), if consistent geometric conditions of incident, reflected, and emitted flux are used. R has been defined as the spectral reflectance under conditions of diffuse illumination and hemispherical viewing. The emittance corresponding to R is E_H, the hemispherical spectral emittance. Hence we can write

$$E_H=1-\left\{\rho_e+(1-\rho_e)(1-\rho_i)\frac{(1-\beta)Me^{\sigma D}-(1+\beta)Oe^{-\sigma D}}{MNe^{\sigma D}-OPe^{-\sigma D}}\right\}. \quad (24)$$

It is legitimate also to apply eqs (1) and (2) to evaluate the normal spectral emittance, E_N, if, and only if, the geometric conditions of irradiation and viewing under which the external reflectance, ρ_e, is measured are (1) normal incidence and hemispherical viewing or (2) perfectly diffuse incidence and normal viewing.

If we consider that the internal reflectance of the coating plus substrate, neglecting the effect of specular reflectance at the coating-air interface, is R_t, then with diffuse illumination and hemispherical viewing

$$R=\rho_e+(1-\rho_e)R_t(1-\rho_t). \tag{25}$$

Equation (25) is another way of writing eq (24), with R_t replacing the fraction containing exponential terms.

$$R_t=\frac{(1-\beta)Me^{\sigma D}+(1+\beta)Oe^{-\sigma D}}{MNe^{\sigma D}-OPe^{-\sigma D}}. \tag{26}$$

For normal illumination and hemispherical viewing, the equation becomes

$$R_N=\rho_N+(1-\rho_N)R_t(1-\rho_t) \tag{27}$$

in which R_t is again the internal reflectance, neglecting the effect of specular reflectance at the coating-air interface, of the coating plus substrate. If R_t is the same for normal and diffuse incident flux,[4] we can write

$$E_N=1-\left\{\rho_N+(1-\rho_N)(1-\rho_t)\frac{(1-\beta)Me^{\sigma D}-(1+\beta)Oe^{-\sigma D}}{MNe^{\sigma D}-OPe^{-\sigma D}}\right\} \tag{28}$$

which is the desired equation.

Substituting for M, N, O, and P from eqs (15), (16), (17), and (18), and making use of the relationship

$$2\sinh x=e^x-e^{-x} \tag{29}$$

and

$$2\cosh x=e^x+e^{-x} \tag{30}$$

eq (28) reduces to

$$E_N=(1-\rho_N)\left\{1-(1-\rho_t)\frac{[(1-\rho_s)-\beta^2(1+\rho_s)]\sinh\sigma D+2\rho_s\beta\cosh\sigma D}{[(1+\beta^2)(1+\rho_t\rho_s)-(1-\beta^2)(\rho_t+\rho_s)]\sinh\sigma D+2\beta(1-\rho_t\rho_s)\cosh\sigma D}\right\}. \tag{31}$$

The specular reflectances at the coating-air interface, ρ_e and ρ_t, are for diffuse illumination and hemispherical viewing. The value to be used for ρ_s must be determined experimentally, because the coating-substrate interface is normally rough, and the reflectance may be affected by interaction between coating and substrate at the interface. For an optically smooth interface, which may be approximated by the coating-air interface for some coatings at some wavelengths, ρ_e and ρ_t can be computed from the index of refraction of the coating[5] by integration of the Fresnel equation over a hemisphere. In its general form, the equation for dielectrics can be written

$$2\rho_d=\frac{\sin^2(\varphi-\theta)}{\sin^2(\varphi+\theta)}+\frac{\tan^2(\varphi-\theta)}{\tan^2(\varphi+\theta)}, \tag{32}$$

in which ρ_d is the directional specular reflectance for unpolarized parallel flux, ϕ is the angle of incidence, and θ is the angle of refraction, both angles measured from the normal to the interface. The angles ϕ and θ are related to index of refraction, n, by Snell's law. In its most general form, this is $n_1\sin\phi=n_2\sin\theta$, in which n_1 is the index of refraction of the medium on the

[4] This condition will be approximated if the incident flux is completely diffused after traversing a small thickness of the coating.

[5] Most optically inhomogeneous coatings consist of opacifying particles dispersed in a continuous medium or vehicle. The scattering is due to the difference in indices of refraction of the opacifier and vehicle. For glossy coatings, the opacifying particles are not usually exposed at the surface of the coating, and the effective index of refraction for specular reflection is that of the vehicle.

side of the interface from which the flux is incident, and n_2 is that on the opposite side of the interface. In the case of flux incident from vacuum, $n_1=1$. In the case of air, no serious error is introduced by considering $n_1=1$ ($n_1=1.0003$, approximately, for air under normal conditions).

The reflectance of an optically smooth surface of index of refraction n, for completely diffuse flux incident from vacuum (or air) can be expressed as

$$\rho_e=\frac{\int_0^{\pi/2}\sin\varphi\cos\varphi\left\{\frac{\sin^2(\varphi-\theta)}{\sin^2(\varphi+\theta)}+\frac{\tan^2(\varphi-\theta)}{\tan^2(\varphi+\theta)}\right\}d\varphi}{2\int_0^{\pi/2}\sin\varphi\cos\varphi\,d\varphi} \tag{33}$$

This expression has been integrated by Walsh [8] to give

$$\rho_e=\frac{1}{2}+\frac{(n-1)(3n-1)}{6(n+1)^2}+\left\{\frac{n^2(n^2-1)^2}{(n^2+1)^3}\right\}\ln\frac{(n-1)}{(n+1)} -2n^3\frac{(n^2+2n-1)}{(n^2+1)(n^4-1)}+\left\{\frac{8n^4(n^4+1)}{(n^2+1)(n^4-1)^2}\right\}\ln n. \tag{34}$$

For completely diffuse flux incident on the interface from within the material of index n, all of the radiant energy that is incident at angles greater than the critical angle, φ_c, will be totally reflected. The critical angle is that at which $\theta=\pi/2$, or $\sin\varphi_c=\frac{1}{n}$. The fraction of flux incident at angles from $\sin^{-1}\frac{1}{n}$ to $\pi/2$ can be obtained by integration and divided by the total flux to give the fraction $1-\frac{1}{n^2}$ of the incident flux that is totally reflected. Hence only $\frac{1}{n^2}$ of the total flux will be incident at angles at which it is refracted, and a fraction ρ_e of that flux will be internally reflected, as indicated in eq (33). Hence we can write

$$\rho_i=1-\frac{1}{n^2}+\frac{\rho_e}{n^2} \quad \text{or} \quad n^2(1-\rho_i)=(1-\rho_e) \tag{35}$$

The expression for ρ_e given in eq (34) is somewhat complex. Judd [10] gives computed values of ρ_e and ρ_i for indices of refraction from 1.00 to 1.60 in increments of 0.01.

The geometric distribution of the emitted flux will be determined by the directional reflectance at the coating-air interface, and can be computed from the refractive index by means of the Fresnel equation. For normally incident parallel flux, the Fresnel equation reduces to

$$\rho_N=\left(\frac{n-1}{n+1}\right)^2 \tag{36}$$

and

$$1-\rho_N=\frac{4n}{(n+1)^2} \tag{37}$$

where ρ_N is specular reflectance for normally incident flux.

The normal spectral emittance, E_N, of any specimen can be computed from the hemispherical spectral emittance by use of the Fresnel equations for reflectance of internally incident normal and diffuse flux. This conversion is not affected by the coefficient of scatter of the coating.

4. Discussion

In the case of paper, layers of powder and unglazed porous ceramic materials, air may be considered the continuous phase, and there will be no specular reflection at the interfaces. If, in addition, there is no substrate, or if the reflectance of the substrate is zero, the conditions will

be identical to those postulated by Klein [7]. If zero is substituted for ρ_e, ρ_s, and ρ_t in eq (23), it reduces to

$$R=\frac{(1-\beta^2)\sinh \sigma D}{(1+\beta^2)\sinh \sigma D+2\beta \cosh \sigma D}, \tag{38}$$

which is identical to Klein's [7] eq (46).

4.1. Properties of Nonabsorbing, Nonscattering Layers

It may be of interest to consider how the emittance and reflectance of a coating will vary as S and K approach zero. Obviously, if both S and K are zero, the material will have perfect transmittance, and both reflectance and absorptance (or emittance) will be zero. This is true for a perfect vacuum, and is closely approximated by a gas at those wavelengths at which no absorption occurs.

a. Properties of Nonscattering Layers

If there is no scattering, $S=0$, and eqs (3) and (4) become

$$dI/dx=-KI \tag{39}$$

and

$$dJ/dx=KJ \tag{40}$$

hence

$$I_{(x+\Delta x)}=I_x e^{-K\Delta x}, \tag{41}$$

where I_x represents the flux density at a level x within the material, and $I_{(x+\Delta x)}$ represents the flux density after traversing a thickness Δx of the material. Equation (41) differs from the familiar Bouguer's law only in that the attenuation of completely diffuse flux is twice as rapid as that of unidirectional flux.

If the scattering coefficient, S, is zero, which will be approached by optically homogeneous materials, such as optical glass and many single crystals, then $\sigma=K$ and $\beta=1$, hence (24) reduces to

$$E_H=(1-\rho_e)\left\{1-\frac{(1-\rho_t)\rho_s e^{-KD}}{e^{KD}-\rho_t\rho_s e^{-KD}}\right\}. \tag{42}$$

However, when S becomes small, the internally reflected flux will not be rediffused, if reflected from optically smooth surfaces. Thus (42) is only valid if the coating-substrate interface is so rough that perfectly diffuse reflection occurs. For the more general case, where this interface approaches optical smoothness, a three-dimensional analysis of the type used by Gardon [5] is more nearly valid.

b. Properties of Nonabsorbing Layers

If the absorption coefficient, K, is zero, as will be approximated at some wavelengths by a freshly smoked layer of magnesium oxide or by freshly fallen snow, both σ and β become zero, and eq (24) becomes indeterminate, which would be expected for an opaque coating of the specified materials, but not for a composite specimen. However, under these conditions, eqs (3) and (4) become

$$dI/dx=-S(J-I)=dJ/dx. \tag{43}$$

This equation can be solved by a procedure similar to those used for eqs (3) and (4) to give

$$I=\frac{J_e[Sx(1-\rho_e)(1-\rho_s)+\rho_s(1-\rho_e)]}{SD(1-\rho_t)(1-\rho_s)+1-\rho_t\rho_s} \tag{44}$$

$$J=\frac{J_e[Sx(1-\rho_e)(1-\rho_s)+(1-\rho_e)]}{SD(1-\rho_t)(1-\rho_s)+1-\rho_t\rho_s}. \tag{45}$$

Substituting eq (44) in eq (21) we get

$$R=\rho_e+(1-\rho_i)(1-\rho_e)\frac{SD(1-\rho_s)+\rho_s}{SD(1-\rho_i)(1-\rho_s)+(1-\rho_i\rho_s)}. \tag{46}$$

If ρ_e, ρ_i, and ρ_s are zero, as they were under the conditions postulated by Klein [7], eq (46) reduces to

$$R=\frac{SD}{SD+1}, \tag{47}$$

which is identical to Klein's eq (48).

Under the conditions postulated for the derivation of eq (47), the emittance will approach zero and the reflectance will approach one as the coating approaches a thickness at which it is completely opaque, which will only occur at infinite thickness. Since $K=0$, the absorptance is zero by definition, and the transmittance is one minus the reflectance. Hence we can write

$$T=\frac{1}{SD+1}, \tag{48}$$

which is identical to Klein's eq (a7).

4.2. Example of Computed Emittance

Figure 1 is a plot of emittance, computed from eq (31), as a function of thickness for composite specimens with optically smooth surfaces comprised of a coating having an index of refraction of 1.40 (from which $\rho_e=0.028$, $\rho_i=0.53$), a value of β of 0.8, and values of σ of 40, 20, 13.3, and 10.0 mm^{-1}, respectively, applied over a mat substrate having a reflectance into the coating of 0.9. (The values of S and K corresponding to a β of 0.8 and σ of 40, 20, 13.3, and 10 mm^{-1} are as follows: $S=8.0$, 4.0, 2.65, and 2.0 mm^{-1} and $K=28.44$, 14.22, 9.42, and 7.11 mm^{-1}, respectively.) These conditions might be approximated at wavelengths in the visible by a glossy gray paint applied over a white backing. All of the coating materials have the same emissivity (about 0.918), but the coating with a σ value of 40 mm^{-1} reaches 99 percent of this value at a thickness of 0.05 mm, while the coating with a σ value of 10 mm^{-1} requires a thickness of 0.2 mm to reach the same value.

The plotted emittance at zero thickness of the coating is greater than the emittance (0.10) of the substrate because the coating has a lower index of refraction than the substrate, and hence reduces reflection at the interface. The plotted value is what would be obtained with a very thin, perfectly transparent glossy coating having an index of refraction of 1.40.

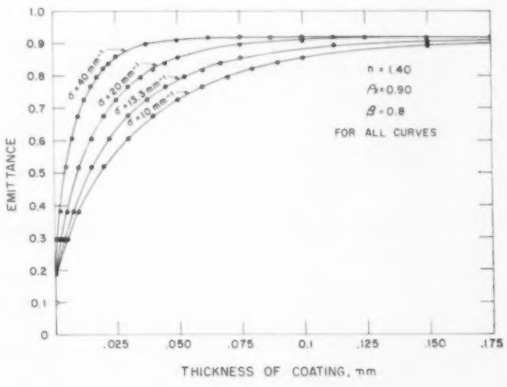

FIGURE 1. *Computed normal spectral emittance, plotted as a function of coating thickness, for a composite specimen comprised of partially transmitting coatings with optically smooth surfaces having an index of refraction of 1.40, β value of 0.80, and σ values of 40, 20, 13.3, and 10 mm^{-1}, respectively, applied over a substrate having a reflectance of 0.90, plotted as a function of coating thickness. These conditions would be approximated by a glossy gray paint applied over a polished metal or white substrate.*

Note that the emittance at zero coating thickness is not that of the substrate. It was assumed that even at zero thickness, there would be an effect of the index of refraction of the coating. Actually, such effect would be produced by a transparent coating of index of refraction of 1.40. The coating having a σ value of 40 mm^{-1} becomes essentially opaque at about 0.05 mm, and the other coatings at successively greater thicknesses.

4.3. Limitations to Equations

There are a number of conditions encountered in practice that deviate from the conditions postulated in the derivation of eq (24). There will always be a thermal gradient normal to the surface in any situation where a body is heated internally and is dissipating radiant energy, and the effect of such a gradient has been omitted in the derivation. In the case of thick ceramic coatings (typically 0.5 mm or more), significant errors may be introduced by ignoring the effect of thermal gradients, especially at high temperatures. The gradients will be negligibly small when the specimen and surroundings are at room temperature or below, and the effect of the gradients in thin coatings, typically less than 0.1 mm, is considered to be negligibly small even at high temperatures.

During firing of porcelain enamels and some other types of ceramic coatings, on some metals, there is appreciable chemical reaction at the coating-metal interface, and some of the reaction products diffuse into the coating for measurable distance. The reaction products may change the reflectance of the substrate into the coating, and the reaction products diffusing into the coating may significantly change its optical properties near the interface. The extent and importance of these effects depend upon the particular materials involved, their thicknesses, the firing, and the service conditions. When the total effect of these factors is large, appropriate adjustments in the values substituted into the equation are required for its useful application. Most types of organic and flame-sprayed ceramic coatings, however, will be essentially free from these effects.

In the case of some paints, there may be segregation of the pigment particles within the vehicle during drying, which will also tend to invalidate the equation. For mat coatings, where the coating-air interface is not optically smooth even on a micro scale, it may be necessary to measure ρ_e and ρ_i experimentally, instead of computing them from the index of refraction.

5. Summary

The thermal radiation properties of a composite specimen, comprised of a partially transmitting coating applied over an opaque substrate, usually vary significantly with the thickness of the coating. An equation was derived relating these properties to the thickness of the coating, the reflectance of the substrate, and the optical properties of the coating material. If the optical properties of a coating and the reflectance of the substrate are known as functions of wavelength, the equation can be used to compute (1) the normal spectral emittance (or reflectance) of any thickness of coating over the substrate or (2) the thickness of the coating over the substrate required to give any normal spectral emittance (or reflectance) within any given wavelength interval intermediate between the emittance of the substrate and of an infinitely thick coating.

The author gratefully acknowledges the assistance of Louis Joseph, of the Applied Mathematics Division, in checking the mathematics, and of Deane B. Judd, of the Optics and Metrology Division, for his advice and helpful suggestions.

6. List of Symbols

A=absorptance.
T=transmittance.
R=reflectance.
E=emittance.
I=diffuse radiant flux proceeding outward from the interior of a specimen.
J=diffuse radiant flux proceeding inward toward the interior of a specimen.
K=absorption coefficient.

S=backscattering coefficient.
x=distance from the coating-substrate interface to a point in the coating.
L=a constant that depends upon boundary conditions.
$\sigma=\sqrt{K(K+2S)}$.
$\beta=\sqrt{K/(K+2S)}$.
ρ_e=reflectance of the coating-air interface for externally-incident diffuse radiant flux.
ρ_s=reflectance of the substrate for diffuse radiant flux incident on the coating-substrate interface from within the coating.
ρ_i=reflectance of the coating-air interface for internally incident diffuse radiant flux.
J_e=externally incident diffuse radiant flux.
J_0=flux J at $x=0$ (at coating-substrate interface).
I_D=flux I at $x=D$ (at coating-air interface).
D=thickness of coating.
$M=(1+\beta)-\rho_s(1-\beta)$.
$N=(1+\beta)-\rho_i(1-\beta)$.
$O=(1-\beta)-\rho_s(1+\beta)$.
$P=(1-\beta)-\rho_i(1-\beta)$.
n=index of refraction.
n_1=index of refraction in medium from which flux is incident.
n_2=index of refraction in medium into which flux is refracted.
φ=angle of incidence, from the normal.
θ=angle of refraction, from the normal.
φ_c=critical angle of incidence for total internal reflectance.
E_H=hemispherical spectral emittance.
ρ_N=reflectance of the coating-air interface for normally incident parallel flux.
E_N=normal spectral emittance.
R_i=internal reflectance of a coating.

7. References

[1] Judd, D. B., Optical specification of light-scattering materials, J. Res. NBS **19,** 287 (1937) RP1026.
[2] ASTM Method C 347–57, Reflectivity and Coefficient of Scatter of White Porcelain Enamels, 1961 ASTM Book of Standards, pp. 612–615.
[3] Kubelka, P., and F. Munk, Ein Beitrag zur Optik der Farbanstriche, Z. tech. Physik, **12,** 593 (1931).
[4] Kubelka, P., New contributions to the optics of intensely light-scattering materials, Part I. J. Opt. Soc. Am. **38,** 448 (1948).
[5] Gardon, R., The emissivity of transparent materials, J. Am. Ceram. Soc. **39** [8], 278–285 (1956).
[6] Hamaker, H. C., Radiation and heat conduction in light-scattering material, Philips Res. Reports, 2, 55–67, 103–111, 112–125, 420–425 (1947).
[7] Klein, J. D., Heat transfer by radiation in powders, Doctor's Dissertation, Mass. Inst. of Technology (1960).
[8] Walsh, J. W. T., The reflection factor of a polished glass surface for diffused light, Dept. Sci. and Ind. Res. Illumination Research, Tech. Paper No. 2, p. 10 (1926).
[9] Saunderson, J. L., Calculation of the color of pigmented plastics, J. Opt. Soc. Am. **32** [12], 727–736.
[10] Judd, D. B., Fresnel reflection of diffusely incident light, J. Research NBS **29,** 329–332 (1942) RP1504.

(Paper 67C3–132)

JOURNAL OF RESEARCH of the National Bureau of Standards—C. Engineering and Instrumentation
Vol. 67C, No. 3, July–September 1963

Minimization of the Arrestment Error in One-Pan, Two-knife Balance Systems

H. A. Bowman and H. E. Almer

(May 1, 1963)

The arrestment error is defined as the error associated with the arrestment, unloading, reloading, and release cycle after correction for balance drift and changes in sensitivity with beam tilt. In a well-designed one-pan, two-knife, constant-load balance the observable arrestment error is caused by inconstancy of the perpendicular distance from the effective point of suspension of the hangdown to the effective axis of rotation of the center knife. Four causes for this distance to vary are recognized and their effective removal discussed. The requirements for two arrestment systems are then set out, one in which the balance bearings remain in contact indefinitely under nearly constant load, the other in which the bearings are uncoupled in such a way as to permit the bearings to be recoupled in a contact configuration as nearly identical to the previous configuration as possible.

A 1-kg test instrument is described with which many balance systems can be experimentally investigated including the two arrestment systems mentioned above (the "constant-load" and "rocking-beam" systems).

The arrestment error (expressed as a standard deviation) for the "rocking-beam" system can be reduced to 1.5×10^{-8} of the load; for the "constant-load" system to 3×10^{-9}. When slight external vibrational disturbances are not scrupulously excluded occasional unpredictable shifts in balance indication are observed. These exceed the normal arrestment errors by about an order of magnitude. The arrestment error does not vary greatly with beam-swing period over its normal range.

1. Introduction

This paper is in a series describing studies on sources and possible elimination of residual weighing errors on balances for weight calibrations operating near the highest attainable precision. Previous studies were concerned with humidity of the ambient air [1],[1] with oscillation of the pan assembly [2], and with the weighing series used [3]. The present paper describes studies on the arrestment error in one-pan, two-knife constant-load balances, whose suitability for weight calibration has been previously advocated by Peiser [4]. A general-purpose performance test for such balances has also been published [5].

The arrestment systems of high-precision balances usually involve complex parts, they are the most difficult to adjust, and have long been recognized as an important, if not always the dominating source of residual weighing errors.

In sections 2 and 3 we will describe and define terms relating to arrestment systems and errors which are brought into relation with the equilibrium conditions of a balance with fixed counterweight. In section 4 we discuss the principal residual sources of arrestment errors in balances of high precision operated expertly. For each of these errors one or more possible cures are suggested. In section 5 a test instrument is described on which several kinds of arrestments can be tried and evaluated. The experimental results are then given in section 6.

[1] Figures in brackets indicate the literature references at the end of this paper.

2. Conventional Arrestment and Release

Figure 1 shows schematically the essential parts of the oscillating structure of a simple one-pan, two-

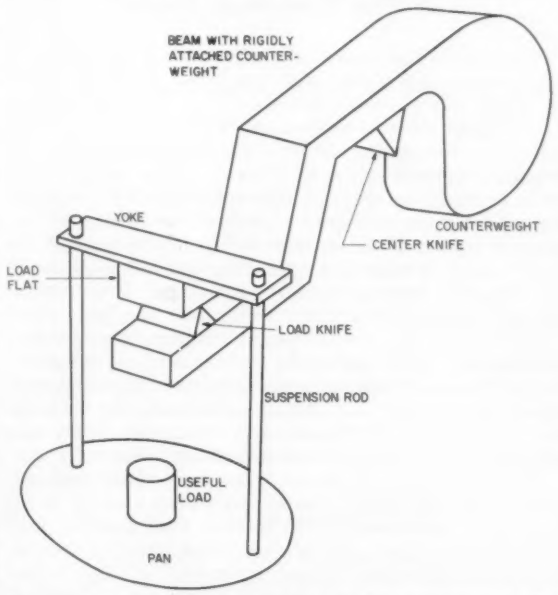

FIGURE 1. *Schematic sketch of the oscillating structure of the basic form of the one-pan, two-knife balance.*

The counterweight is made of such a mass and placed at such a distance that the balance is "on-scale" when the design load is placed on the pan.

knife substitution balance. Unloading and reloading of the pan is potentially the most damaging process in a weighing cycle. The suspension, for example, designed to accept vertical loads, may have horizontal forces impressed upon it. The arrestment system is designed to protect balances during this reloading process.

We define an arrested balance as one placed in a condition for unloading and reloading with minimum disturbance to the balance adjustment. We define a released balance as one in which the beam and hangdown can oscillate about the knife-bearings free from constraints other than those imposed by the gravitational field, the surrounding atmosphere, and—if used—a beam-swing damping system.

The arrestment system is designed to arrest as well as to release the balance with the minimum disturbance to that balance adjustment. Conventionally the system performs the following tasks:

1. It removes the freedom of swing from the beam.
2. It removes the freedom of swing from the pan and suspension assembly (hangdown).
3. It firmly supports the hangdown so that the load flat is no longer in contact with the load knife and so that loads can be placed on and/or removed from the pan.
4. It lifts the beam so that the center knife is out of contact with its flat.
5. It is able to reverse steps 1 to 4 recoupling both knives and flats in precisely the original contact configuration and releasing the pan without appreciable swing.

Steps 1 to 4 are called arrestment, step 5 release.

3. The Arrestment Error

Corwin [6] has previously presented a discussion of the arrestment error. Although our analysis differs in detail, our ideas are based on his. The arrestment error is here defined as the sum of all errors associated with the "operating cycle"—that is arrestment, unloading, reloading, and release. This arrestment error is readily measured experimentally by change of balance indication upon repeated reloadings of the same weight. Random variability of the mass of the test weight during the operating cycle would make the observed arrestment error too large. If the transfer mechanism offers one weight to the pan more reproducibly than two different weights, the observed arrestment error would be too small. We believe both of these effects are negligible in our experiments. Slow balance drift and changes of sensitivity with tilt are separately evaluated and excluded from the experimentally determined arrestment error.

The inclusion of errors from unloading and reloading in our definition of arrestment error is an important innovation. It is true that loading and unloading are not part of the arrestment operation. Experimental observations, however, of the errors due to arrestment and release alone give observed errors that are too low to be significant from the view point of a real weighing cycle. The significant test of an arrestment system is how well it protects the reproductibility of a balance during the unloading and reloading operation.

The idealized equilibrium conditions of a released one-pan two-knife balance is:

$$M\,r\cos\theta+M_B\,p\cos\phi=0,$$

where M is the total mass of the hangdown whose effective point of suspension is at a perpendicular distance r from the effective center-knife axis. The line parallel to the distance r is inclined by $90+\theta$ to the gravitational-field direction and M_B is the mass of the beam with its rigidly attached counterweight, the combined center of gravity of which is at a perpendicular distance p from the effective center-knife axis. The line parallel to the distance p is inclined by $90+\phi$ to the gravitational field.

$\theta+\phi$ is a constant of the balance related to the readout angle by another constant.

In a well-designed beam, to be discussed in a later paper, p and ϕ will remain constant during a weighing cycle to well within the weighing precision. The masses M and M_B will also remain constant to higher precision. Variability of θ before and after the arrestment cycle must be caused almost exclusively by changes in r. This realization simplifies the search for possible arrestment errors. One further consideration may also be useful. As has been previously pointed out [6] one source of variability in r arises from nonequality and nonuniformity of knife-edge radii. Whereas load-dependence of these imperfections are eliminated as possible sources of weighing error in constant-load balances, θ-dependent variations remain. Balances should therefore be used as zero-point instruments or calibrated for systematic variations with θ. Arrestment errors systematic with the observed quantity, θ, need not be investigated; it should be noted that they are excluded by the definition given in section 2.

4. Sources and Elimination of Arrestment Errors

4.1. Nonparallelism of Knives

The schematic diagrams (fig. 2) show how the arm length r, the perpendicular distance of the effective point of suspension (eps) from the effective axis of roatation of the center knife, is changed by nonparallel knives when associated with imperfect reproducibility of centering of load along a line parallel to the terminal knife.

The parallelism of knives is a most important balance adjustment which should always be carried out to the highest attainable perfection. Nevertheless the remaining nonparallelism in practice is a demonstrable source of weighing imprecision. Although all too often forgotten this error was recognized long ago by Thiessen [7] and corrected by insertion of an intermediate knife edge perpendicular and coplanar with the terminal knife as illustrated in figure 3. The finite curvature of the intermediate knife will permit a very small

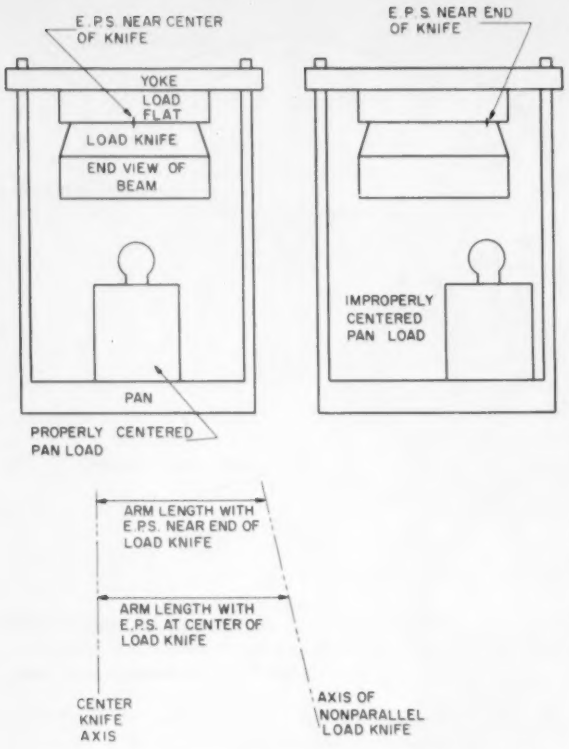
E.P.S. NEAR CENTER OF KNIFE
E.P.S. NEAR END OF KNIFE
YOKE
LOAD FLAT
LOAD KNIFE
END VIEW OF BEAM
IMPROPERLY CENTERED PAN LOAD
PAN
PROPERLY CENTERED PAN LOAD
ARM LENGTH WITH E.P.S. NEAR END OF LOAD KNIFE
ARM LENGTH WITH E.P.S. AT CENTER OF LOAD KNIFE
CENTER KNIFE AXIS
AXIS OF NONPARALLEL LOAD KNIFE

FIGURE 2. *The upper two diagrams indicate how the effective point of support (the eps) of the suspension by the beam is caused to migrate along the load knife edge due to failure to assure proper centering of the load on the pan.*

At the bottom is a sketch showing how the arm length, r, varies when the two knives are not parallel under conditions of eps migration.

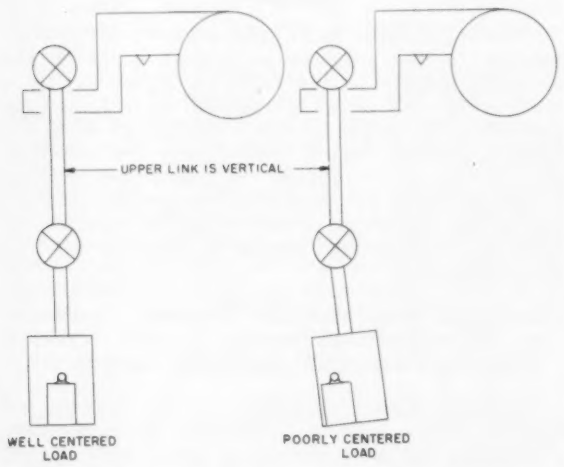

FIGURE 4. *This sketch illustrates the principle that the link connecting two universal couplings will hang at a constant angle with respect to vertical.*

The upper universal coupling is the knife-edge compensator and the lower is a ball bearing gimbal ring.

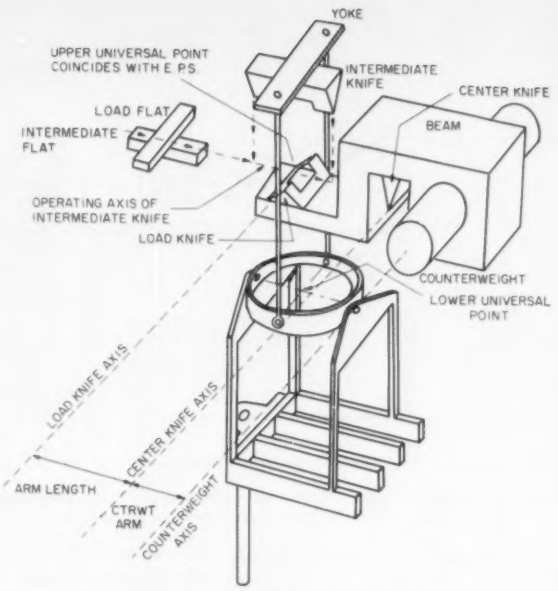

FIGURE 3. *An exploded sketch of the oscillating system of the apparatus used in the arrestment study.*

For simplicity, the mechanical structure which maintains the load and intermediate flats in their proper relative positions is not shown. At the top is an exploded view of the knife-edge compensator.

movement of the effective point of suspension arising from rotation of the intermediate knife. A universal coupling or gimbal has been described [2] by which the intermediate knife is always vertically alined (see fig. 4). The major error from nonparallelism of knives then remaining arises from failure of the arrestment system precisely to reengage the suspension with the beam.

4.2. Change in Inclination of the Terminal Flat

The exactly analogous error arising from lack of reproducibility of load centering along a line perpendicular to the terminal-knife is associated with the finite knife radius. The error δr is illustrated in figure 5 and is of the order of $\rho\delta\alpha$ where α in radians is the inclination of the terminal flat to the horizontal and ρ is the knife-edge radius. Even when ρ/r is less than 10^{-4}, $\delta\alpha$ should also be less than 10^{-4} in balances working near the highest attainable precision.

Again the universal coupling (fig. 4) assures a highly reproducible inclination of the terminal flat, to the precision required [2], and the major remaining error from inclination of the terminal flat again arises from failure of the arrestment system precisely to reengage the suspension.

4.3. Nonplanarity of Flats

Figure 6 will be readily understood as illustrating the effects of nonplanarity of either the center or the terminal flat in conjunction with any failure to reproduce the exact contact configuration between knives and flats.

686-132—63——3

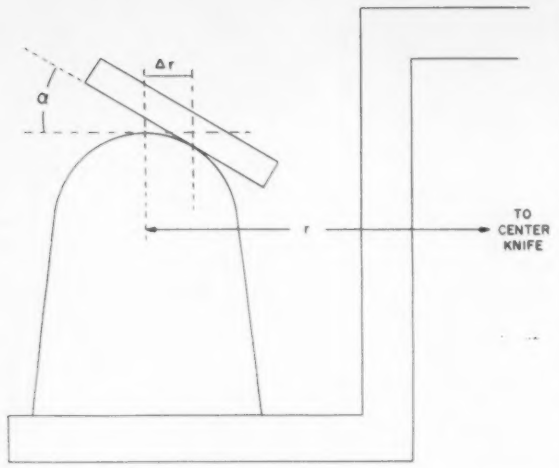

FIGURE 5. *If the load flat tilts through an angle δα, a variation in r results which is of approximate magnitude ρδα.*

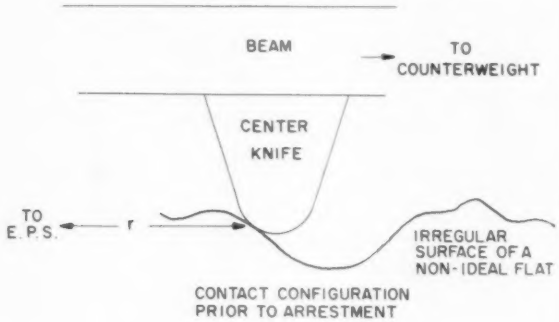

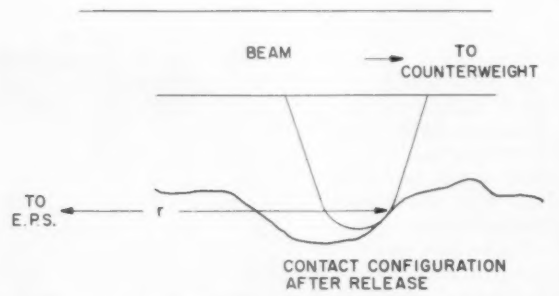

FIGURE 6. *This sketch illustrates the variability in r due to nonreproducible release on a non-ideal flat.*

Although the center knife is shown in this sketch, this source of error is present on all knife-flat pairs.

Of course highly sharp knives, and flats that are planar within a fraction of an optical wavelength will help to reduce this error, but it is quite clear that the only good way of eliminating this as well as the two previous errors is not to uncouple knives and flats.

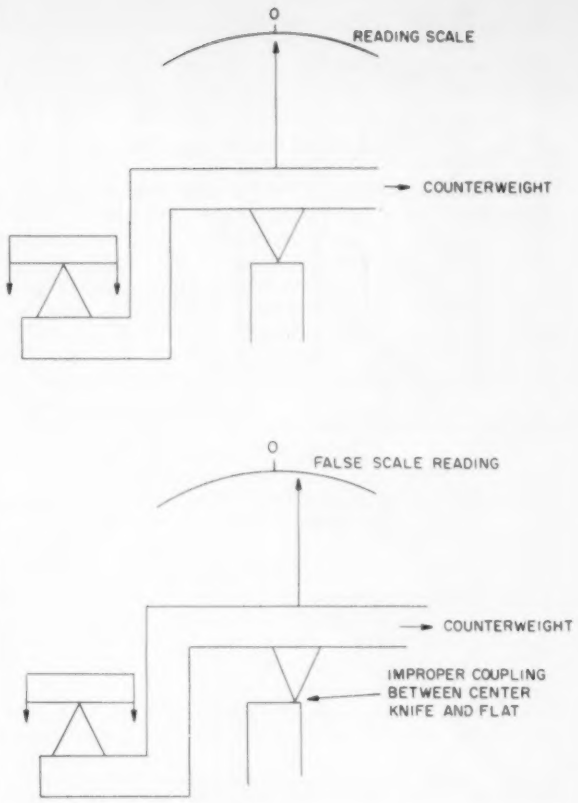

FIGURE 7. *This sketch shows a reading error which results from nonreproducible release.*

4.4. Dependence of Balance Indication on Beam Placement

The error arising from displacement of the pointer relative to the scale or equivalent parts of the read-out system is illustrated in figure 7. It is another of the errors associated with failure to reproduce the precise contact configuration of the balance bearings but it differs from the others in that it can be eliminated without resorting to a system in which knives are not removed from their flats. The observing system must be sensitive to beam angle alone such as can be attained with an autocollimator.

4.5. Special Requirement for Arrestment Systems in in Which Bearings Remain Coupled During a Weighing Cycle, "Constant-Load" Arrestment

Gould [8] after careful study of the one-kilogram balance of the National Physical Laboratory concluded that an improvement in performance would be achieved by retaining center-knife contact. This proved difficult experimentally.

With the simplification associated with a two-knife design we have stipulated not only that both bearings should remain in contact but that the

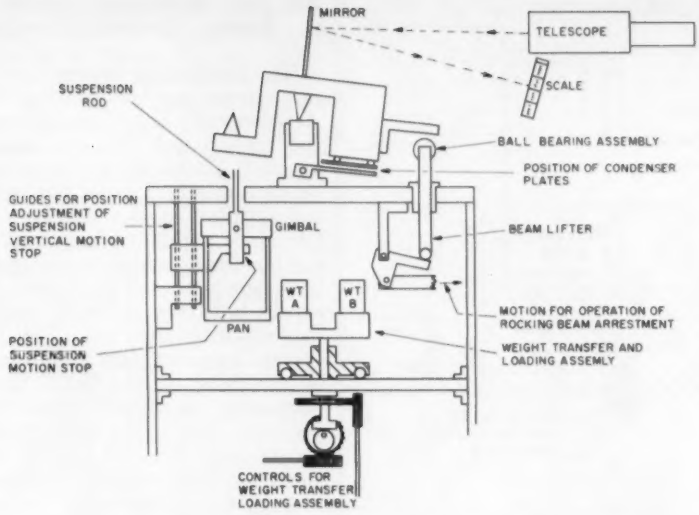

FIGURE 8. *Sketch of the apparatus used in the arrestment study.*
Instruments installed but not pertinent to this study are eliminated for clarity

knives should be kept loaded, indefinitely, to nearly constant load forces. Our design of constant-load arrestment is described in section 5.

4.6. Special Requirements for Arrestment Systems in Which Bearings Are Uncoupled

It is recognized that situations might exist where decoupling of balance bearings is necessary. Moreover, in our study of sources of arrestment errors an experimental distinction between those specifically connected with the uncoupling operation becomes desirable. It was incumbent upon us to set out the requirements and to design a near optimum arrestment system in which the bearings are uncoupled.

Corwin [6] has pointed out that in practice moving linkages necessarily introduce nonideal movements. We have therefore required an arrestment system to have no moving part responsible for the precision of alinement of the beam or suspension. The alinement should be accomplished by members rigidly and permanently attached to the balance frame.

A study of the history of high-precision balances and the experience of previous workers in the field emphasize the need for the arrestment system to be capable of adjustment by simple rapid procedures.

5. The Test Instrument

A flexible test instrument has been constructed. Through the incorporation of thermocouples, vibration pickups, strain gages, displacement gages, etc., it is too complex for routine use as a balance, but rather it is designed for the critical study of systems for—

a. arrestment
b. damping
c. operation in controlled atmospheres
d. readout of balance indication
e. vibration control
f. temperature control.

Only the first of these, that is the study of arrestment systems, is described in this paper.

Figure 3 is a sketch of salient members of the oscillating system of the test instrument. Figure 8 shows the external members necessary to the arrestment studies.

5.1. Bearings

The 1¾-in. long knives are of Tantung G. The center ½ in. of the terminal knife has been removed to accommodate the intermediate-flat structure. The knife mounting is illustrated in figure 9. The facets are flat to one fringe and this flatness extends to within 0.0005 in. of the edge as indicated by micro-interferometry.

The agate flats used are up to four fringes high in the center. Whenever electrical contact through the bearings is needed Tantung flats can be used without detectable change in performance.

These are not the best possible bearings. For the arrestment studies it may be an advantage to work with appreciably non-ideal bearings (for example to demonstrate the minimization of the error discussed in section 4.3).

5.2. The Beam and Suspension

Only a very few special features deserve mention. The beam [9] differs from the sketch in figure 1 by having a semicylindrical counterweight owing to a last minute decision to reduce the balance capacity to 1 kg. The arm length is 2 inches. In the gimbal [5] of the suspension miniature nonmagnetic ball bearings are used. In the weight-loading system each loading tray can be individually adjusted to match the aspect to the working surface of the pan.

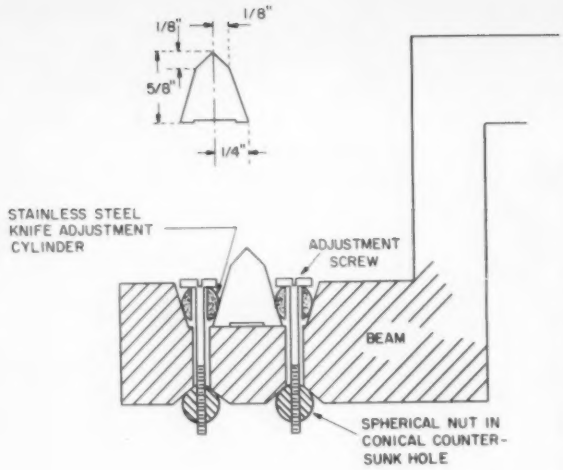

FIGURE 9. *The method of mounting and adjusting the knives on the beam.*

The center knife is mounted and adjusted in the same manner.

5.3. The Arrestment System in Which Bearings Remain Coupled ("Constant-Load" System)

The mechanical system used for load change without uncoupling the bearings is shown in figure 10. A spherically ended member is rigidly attached to the upper link of the suspension. Immediately above this member and attached to the frame of the balance is a horizontal flat surface. Both members are stainless steel. Arrestment is accomplished in two steps. First, a force is gradually applied to the system (comparable to the gradual removal of mass from the pan). This causes the suspension to rise slowly until the spherical surface comes into gentle contact with the flat. The force continues to increase; however, further upward suspension motion is prevented by the flat. The increase in force results only in driving these two surfaces into firm contact. When the force is comparable to a 30-mg weight removal, the second step of the process is started. This consists of raising the weight-transfer tray until the weight on the pan has been lifted free and clear. This condition is shown on the right in figure 10. When the pan is empty, the force of contact between the sphere and flat is about 1 kg.

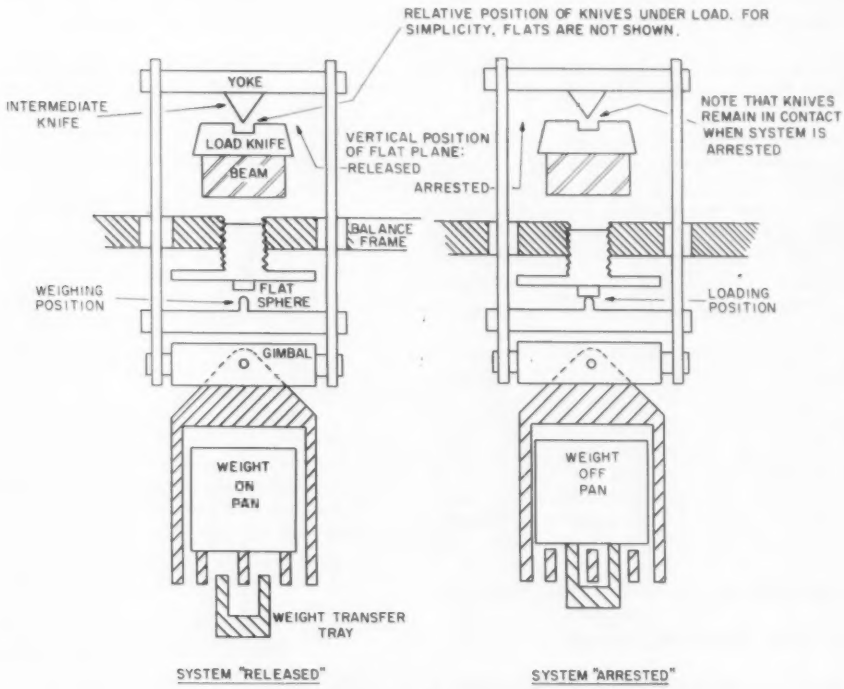

FIGURE 10. *The "constant-load" method of arrestment.*

For simplicity the assembly of flats between the load and intermediate knives is not shown—the important point is that these two knives remain in contact with their associated flats in both the "released" condition (on the left) an in the "arrested" condition (shown on the right). To operate the system the weight transfer tray is moved upward. When it comes into contact with the weight on the pan (thereby accepting part of the weight-load from the pan) the suspension moves upward indicating a smaller weight load. When the sphere (on the suspension) touches the flat (on the frame) the upward motion of the suspension is terminated, and continued upward motion of the tray results in lifting the load free and clear of the pan. Under these circumstances, the counterweight moment maintains all knives and flats in the system in contact and loaded at their operating load level.

The next weight is then lowered onto the pan which returns the contact force between the sphere and flat to its previous value of about 30 mg. This force is gradually removed which permits the sphere to fall gently away from the flat and oscillate around its new equilibrium position. The significant point is that during the entire process the contact forces between the knives and flats in the system have varied only slightly from their operating levels. Thus, by maintaining contact between knives and flats during loading, we have minimized knife-flat recoupling errors associated with faulty release. The variable force was applied to the system mechanically by the removal of small weights from hangers on the yoke. It might be mentioned here that we were able to apply a variable force to the beam electrostatically through a condenser arrangement shown in figure 8. This was done in connection with another study not pertinent to arrestment. The data presented in this report were taken when the beam was manipulated by the addition or removal of small weights. The beam can also be manipulated by merely raising the weight transfer tray as shown in figure 10.

5.4. The Arrestment System in Which Bearings Are Uncoupled ("Rocking-Beam" System)

Figure 11 illustrates the essential features of the arrestment system fulfilling the requirements stated in section 4.6. At the top, the balance is shown in its "weighing position." It is rotating about its center knife with the suspension load indicated by the load flat. In the second view the beam lifter has forced the counterweight end of the beam upward and the load end downward until the load flat is "just" in contact with three alinement pins, A, B, and B′. Pin B′ is on the opposite side of the beam and therefore not visible. These pins are rigidly attached to the bed plate as illustrated. As the beam lifter continues upward, the load flat load is surrendered by the load knife to the three alinement pins. For reasons which will be explained later, the beam lifter has not contributed to the system alinement in this operation. All guidance has been achieved by the regular contact characteristics between the center knife and flat; and, depending upon the geometric perfection of the center knife, the motion of the beam has been around the center knife axis. With the contact broken between the load knife and flat, the beam and suspension are decoupled and the balance is acceptably arrested. Release is accomplished by lowering the beam lifter and permitting the load knife and flat to recontact. If it is desired to break the center-knife contact, the beam is rotated beyond the "partial-arrest" position to the "complete-arrest" position shown at the bottom. The beam-lifter is prevented from placing a horizontal force on the system since it is fabricated from a ball bearing riding on a ball bushing. Thus, even though its vertical motion may be imperfect, any horizontal component is taken up by the ball members. This assembly is shown in figure 12.

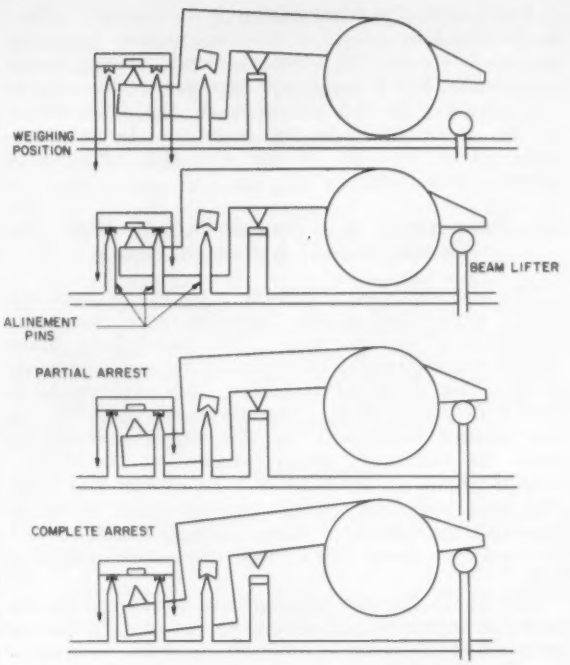

FIGURE 11. *The "rocking-beam" method of arrestment.*

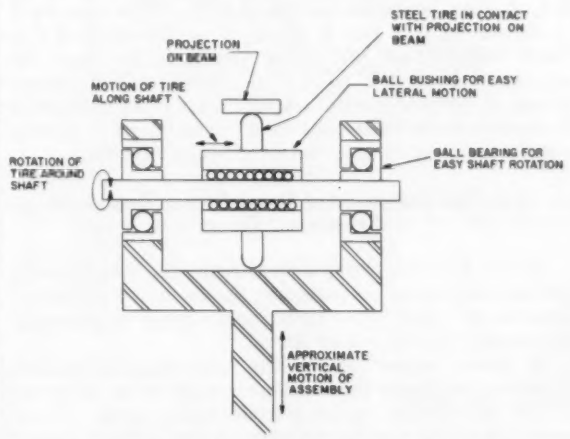
STEEL TIRE IN CONTACT WITH PROJECTION ON BEAM
PROJECTION ON BEAM
BALL BUSHING FOR EASY LATERAL MOTION
MOTION OF TIRE ALONG SHAFT
ROTATION OF TIRE AROUND SHAFT
BALL BEARING FOR EASY SHAFT ROTATION
APPROXIMATE VERTICAL MOTION OF ASSEMBLY

FIGURE 12. *The construction details of the ball bearing device which inhibits the application of horizontal components, to the rocking beam due to imperfect motion of the beam lifter.*

6. The Observed Arrestment Error

The quantitative evaluation of the arrestment error was accomplished by running the test instrument through many arrestment cycles (as defined in section 3) so that errors associated with slow drift could be effectively eliminated. The error in read-out indication could be demonstrated to be negligible. For the experiments here described the instrument was not artificially damped, and the beam period initially used was 32 sec.

Apart from the comparison (in section 6.1 below) of the "rocking-beam" arrestment system (compare section 5.4) with the "constant-load" system (compare section 5.3) it was found necessary to investigate (in section 6.2) the influence of the beam-swing period (in section 6.3), the occasional large arrestment errors, and (in section 6.4) the influence of external vibrations.

6.1. Comparison of "Rocking-Beam" With the "Constant-Load" Arrestment System

The first test was performed by using the "rocking-beam" arrestment in the "partial-arrest" mode (as described in section 5.4). The same 1-kg brass weight was used to load the pan during each operating cycle. The data taken during this experiment is shown in figure 13A. The standard deviation of the balance indication for one single observation from the estimated mean (shown by the dotted line) is about 15 μg, that is 1.5×10^{-8} of the load. The data indicates that at unpredictable intervals an arrestment error of about 150 μg (1.5×10^{-7} of the load) can occur (see further discussion in section 6.3).

The rest of the test program was conducted on the mode of arrestment in which knives and flats were maintained in contact under constant load throughout the operating cycle (see description in section 5.3). Several evaluation runs were made—a typical set of data is shown in figure 13B. The standard deviation in this run is about 5 μg (5×10^{-9} of the load) which does not differ significantly from the standard deviation of 4.8 μg based on 80 points taken in several similar experiments. As predicted in section 4 the "constant-load" arrestment is significantly superior to the "rocking-beam" system.

6.2. The Influence of Beam-Swing Period on Arrestment Errors

When by sensitivity adjustment the beam-swing period was increased to 65 sec, the standard deviation associated with the arrestment error apparently increased (fig. 14, curve A).

A closer inspection of the experimental points, however, suggests that the error associated with one of the arrestment cycles is abnormally high. If one concludes that the disturbance to the balance during this cycle was unusually large and that it should therefore be rejected as unrepresentative, one can reinterpret the same data as in curve B in figure 14. The standard deviation is now about 3 μg, that is slightly better than for the shorter beam-swing period.

6.3. The Occasional Large Arrestment Error

For all the runs so far described it soon became obvious that occasional very large arrestment errors were typical. These could not just be explained by a statistical spread of random results; nor could they be predicted by any irregularities in balance handling. It may be mentioned in passing that a possibly similar effect is associated with the operation of the NPL balance [8], where occasional observations are rejected for presumed mishandling of an arrestment system in which skill is known to play a considerable part.

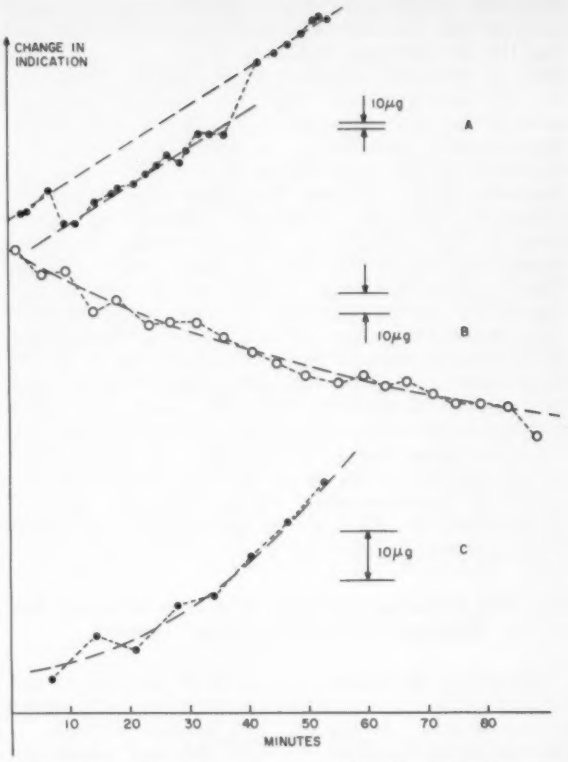

FIGURE 13A. *Variations in the indicated change in mass, plotted as a function of time when run through 24 operating cycles (defined in the text of the report) using the rocking beam method of arrestment.*

B. *Variations in the indicated change in mass, plotted as a function of time when run through 24 operating cycles using the constant load method of arrestment.*

In this experiment the frequency of the beam system as 1/32 c/s.

C. *Variations in data when the instrument is operated at 1/65 c/s in a low vibration ambient.*

6.4. The Influence of External Vibrations

The occasional unpredictable jump in balance indication became of great importance to this study of arrestment errors. Rejection of some observations is properly resisted by experimenters. Without such rejection the observed arrestment error and ultimate weighing precision is appreciably affected by these occasional unpredictable jumps in balance indication.

It was ultimately discovered that when all vibrational disturbances (nearby ventilation motors and air-conditioning compressors) were removed the occasional large shifts in indication did no longer occur. The observed arrestment error was reduced from 5 to about 3 μg (see fig. 13C).

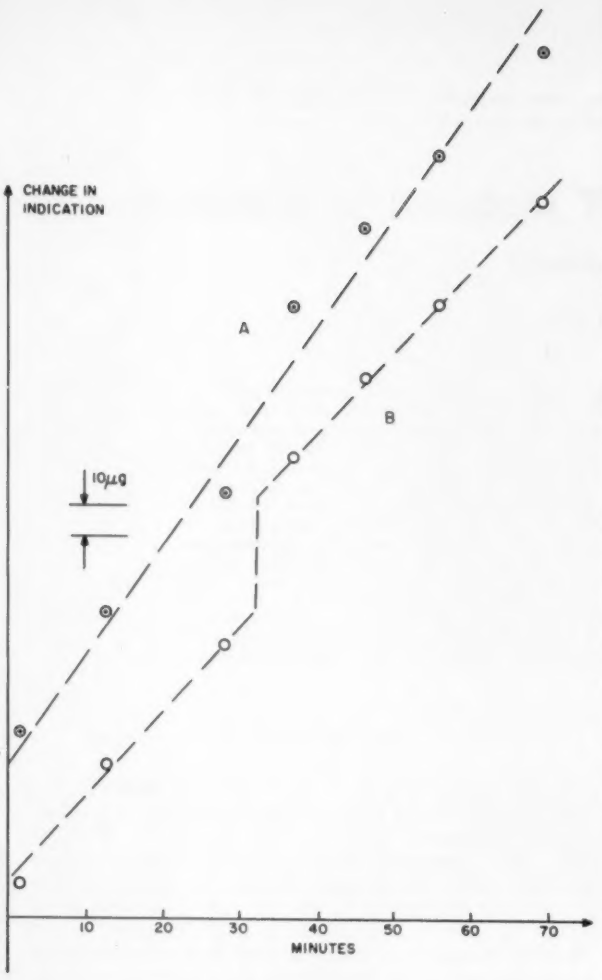

FIGURE 14A. *Variations in indicated change in mass during seven operating cycles.*

Balance frequency was 1/65 c/s.

B. *This is the same data as was presented in figure 14A but with most of the data spread forced into one major shift.*

The authors wish to express appreciation of the generous assistance and guidance received from many members of the NBS staff during the conduct of this study. L. B. Macurdy, J. M. Frankland, D. P. Johnson very graciously contributed both practical and theoretical assistance. We are especially indebted to H. S. Peiser for continual encouragement and support throughout this work, and for help in the preparation of the manuscript.

Richard Smith, instrument maker, contributed many practical ideas used in the construction of the apparatus. He was frequently called upon to devise an assembly to perform a particular function with no guidance in the mechanical design. Without his valued assistance it would have been difficult indeed to have conducted this study.

Bernard Wasko of the Voland Corporation kindly supplied the knife edges and flats.

7. References

[1] H. E. Almer, Response of microchemical balances to change in relative humidity, J. Research NBS **64C,** 281 (1960).

[2] H. A. Bowman and L. B. Macurdy, Gimbal device to minimize the effects of off-center loading on balance pans, J. Research NBS **64C,** 277 (1960).

[3] H. E. Almer, L. B. Macurdy, H. S. Peiser, and E. A. Weck, Weight calibration schemes for two-knife-edge direct reading balances, J. Research NBS **66C,** 33 (1961).

[4] H. S. Peiser, State mass standards, report of the 45th National Conference of Weights and Measures, June 8, 1960; p. 45.

[5] T. W. Lashof and L. B. Macurdy, Testing a quick-weighing balance, Anal. Chem. **26,** 707 (1954).

[6] A. H. Corwin, Weighing technique of organic chemistry Vol. I, Physical Methods of Organic Chemistry 3d Ed., pt. I, ch. III (Interscience Publishers, Inc., New York, 1959).

[7] M. Theissen, Trav. et Mem. Bureau International Pois et Meas., 5, pt. 2 (1886).

[8] F. A. Gould, A knife-edge balance for weighings of the highest accuracy, Proceedings of the Physical Society B **62,** 817 (1949).

[9] L. B. Macurdy (private communication).

(Paper 67C3–133)

JOURNAL OF RESEARCH of the National Bureau of Standards—C. Engineering and Instrumentation
Vol. 67C, No. 3, July–September 1963

Determination of Residual Thiosulfate in Processed Film

Chester I. Pope

(May 1, 1963)

The Crabtree-Ross procedure, employing the reaction of thiosulfate with mercuric chloride to form a turbid solution is the usual test for residual thiosulfate in processed film. Qualitative tests showed that in this procedure part of the precipitate remains in the gelatin layer of the film, causing the reported concentration of thiosulfate to be too low. When residual thiosulfate was measured in the presence of image silver, the image silver contributed an additional component to the turbidity. A new test procedure was developed which also employs mercuric chloride as the precipitant but which reveals 2 to 3 times as much residual thiosulfate as does the Crabtree-Ross procedure. Residual silver causes the formation of additional turbidity which is determined as residual thiosulfate. A trace of gelatin is dissolved from the film during the thiosulfate test, the amount depending on film type. The trace of gelatin had a pronounced effect on the amount of turbidity. The addition of a known amount of gelatin to the test solution masked the effect of dissolved gelatin, making it possible to prepare one calibration curve for all types of film. A new method of measuring the residual silver in processed film was developed. A photoelectric nephelometer was used to measure the turbidity.

1. Introduction

The reaction of thiosulfate with mercuric chloride to form a precipitate is the basis for a turbidity test which has been used for the past 30 years to determine the residual thiosulfate in processed film. The test is known in the literature as the Crabtree-Ross hypo test [1].[1] In the test a sample of film is immersed in a solution of mercuric chloride and potassium bromide and the turbidity is compared visually or by a photoelectric instrument with that produced in standard solutions containing known amounts of thiosulfate.

Analytical results have been reported [3, 4] to indicate that the Crabtree-Ross test measures all of the residual thiosulfate in processed film. However, the analysis of such small quantities of thiosulfate by chemical methods is subject to considerable error. It has been suspected that some of the precipitate formed in the reaction of thiosulfate with mercuric chloride remains in the gelatin layer, giving low values for the thiosulfate content. Also the comparison or standard solutions in the Crabtree-Ross test are not always reproducible and sometimes vary as much as 50 percent for the 5 μg standard, depending on how rapidly the thiosulfate was mixed in the preparation of the solutions.

It has been shown that potassium bromide can eliminate all of the thiosulfate from film after fixation [5]. A new thiosulfate test procedure has been developed in which the residual thiosulfate is extracted from the film by treating the sample in a solution of potassium bromide. The mercuric chloride is added after removal of the film sample. In the new procedure, any residual silver in the form of a silver thiosulfate complex is removed by the potassium bromide. The silver then reacts with the halide present in the test solution to form a precipitate which adds to the turbidity formed by the thiosulfate. The effect of gelatin on the turbidity in the thiosulfate test procedure was determined.

Qualitative tests were made to show that part of the precipitate remains in the gelatin layer when the Crabtree-Ross test procedure is used. The effect of the image silver on the turbidity in the Crabtree-Ross test procedure was also investigated. A new test method was developed for determining the residual silver in processed film by measuring the transmission density of a silver image developed from the silver in the residual silver thiosulfate complex.

2. Test Methods

The solutions and experimental procedures used in this investigation for determining the residual thiosulfate in processed film are given below. The films were 35 mm. The area of the film test sample was 1 in.[2] Round samples were punched from unperforated film with a special punch and rectangular samples were cut from perforated film using a metal stencil. Two or more specimens were tested for each determination of residual thiosulfate content. Two or more standard solutions were made in each run

[1] Figures in brackets indicate the literature references at the end of this paper.

to determine the turbidity for each thiosulfate concentration and prepare a calibration curve. The tests were made at room temperature (23 to 27 °C).

The processing solutions used in preparing the film samples were the same as those described in a previous publication [5]. Samples of 35 mm film 10 in. in length were developed 5 min, treated in a stop bath 30 sec, fixed in a fresh acid hardening bath or one containing 8 g of silver per liter, and washed in running tap water for selected times at different water temperatures to obtain a range of residual thiosulfate concentrations in the processed film. The thiosulfate-free film samples used in the tests were obtained by fixing in a fresh bath and removing the residual thiosulfate in the washing process—no thiosulfate eliminators were used. The thiosulfate concentrations are expressed in terms of anhydrous sodium thiosulfate ($Na_2S_2O_3$) in micrograms per square inch ($\mu g/in.^2$).

2.1. New Thiosulfate Test Procedure

Solution A_0

Potassium bromide	50.00 g.
Water to make	1 liter.

Solution A

Potassium bromide	50.00 g.
Water to make	980 ml.
Filter and add 0.10% gelatin solution	20 ml.

Solution B

Mercuric chloride	50.00 g.
Water to make	1 liter.

Solution A should be stored in a refrigerator and brought to room temperature before use.

The solutions were made up with distilled water and filtered through highly purified filter paper. The mercuric chloride was dissolved at room temperature. The potassium bromide, mercuric chloride, and the sodium thiosulfate ($Na_2S_2O_3 \cdot 5H_2O$) used in the thiosulfate standard solutions were of reagent quality, meeting ACS specifications. The gelatin was photographic grade.

The solutions were delivered from burets to 19 mm by 105 mm round cuvettes. The tip of the buret containing solution B was widened to permit delivery of 5 ml in about 5 or 6 sec. From the buret, 5 ml of solution A_0 or A was added to the cuvette. The test sample of film was folded twice with the emulsion side facing in and placed in solution A_0 or A for 15 min. The cuvette was agitated frequently during the immersion period. The sample was removed with a glass rod having a toe on the bottom end. The surface liquid was squeezed off as much as possible during removal. Then 5 ml of solution B was added from the buret and the cuvette was swirled immediately to insure rapid mixing of the solutions. The mixture was also stirred with the glass rod for a few seconds. The cuvette was wetted on the outside, wiped dry with soft tissue, and allowed to stand 30 min before the turbidity was measured.

Standard solutions were prepared by adding known amounts of sodium thiosulfate to 5 ml of solution A_0 or A, thoroughly mixing, adding 5 ml of solution B, and proceeding as described above in testing film. The standard solutions containing known amounts of thiosulfate were prepared as described in the American Standards Association method [2] for determining thiosulfate in processed film. No correction was made for the increase in volume of the test solution with the addition of the thiosulfate solution, since the error introduced is negligible.

2.2. Crabtree-Ross Thiosulfate Test Procedure

The following solution was made up with distilled water and filtered through highly purified filter paper:

Potassium bromide	25.00 g.
Mercuric chloride	25.00 g.
Water to make	1 liter.

The potassium bromide and mercuic chloride were of the same reagent quality as used above.

From a buret or pipet 10 ml of the above solution was added to a cuvette. The film sample was folded with the gelatin side in and immersed in the test solution for 15 min without agitation. Then the sample was removed, the solution was stirred with a glass rod, and the cuvette was allowed to stand 15 min before the turbidity was measured. The standard solutions containing known amounts of sodium thiosulfate were prepared and added as described in the American Standards Association method [2] referred to in section 2.1.

2.3. Turbidity Measurement

The turbidities of the test solutions were measured with a Coleman No. 9 nephelometer. In this instrument, a collimated beam of light from a tungsten lamp passes into the test solution, the light scattered at right angles to the exciting beam is detected by two photocells, and the output of the photocells is indicated on a meter. The nephelometer was calibrated by a Coleman turbidity standard of 74 units before each measurement. This standard did not change within a period of a year relative to other Coleman standards of 10, 18, 33, and 74 units. For readings above 130 units, the nephelometer was adjusted to make the standard of 74 units read 10 or 5 on the scale, making each unit on the scale equal to 7.4 or 14.8 units, respectively. The cuvettes were matched Coleman A grade. For the measurement, the cuvette was placed in a well containing sufficient distilled water to cover its three windows.

3. Results and Discussion

3.1. Effect of Time and Temperature on the Extraction of Thiosulfate From Processed Film

The treatment of processed microfilm and motion picture film for 15 min in solution A_0 at room temperature (23 to 27 °C) was found to be sufficient to

extract the residual thiosulfate and residual silver from the film sample. Clear (image-free) samples fixed in a fresh bath and in a bath containing 8 g of silver per liter were tested. Some of the samples were treated a second time in solution A_0 to determine if any measurable amount of thiosulfate remained. No thiosulfate was found in samples having a low residual thiosulfate concentration but 1 to 2 μg per in.^{2} was found in microfilm and 1 to 5 μg per in.^{2} was found in motion picture film having a residual thiosulfate concentration of 30 to 100 μg per in.^{2} Most of the thiosulfate was removed during a 5-min treatment in solution A_0. Extending the time to 30 min did not yield more thiosulfate than a 15-min treatment. As an example of the rapidity of the removal of the thiosulfate from the film, one sample of microfilm, containing 29 μg of thiosulfate per in.^{2} after fixation in a bath containing 8 g of silver per liter, tested 20 μg per in.^{2} after treatment for 1 min in solution A_0. Any turbidity resulting from the residual silver adds to that formed by the residual thiosulfate and is determined in the new test procedure as thiosulfate.

Tests were made to determine the amount of residual thiosulfate extracted from film by distilled water. Clear (image-free) samples were treated in 5 ml of distilled water, removed, and 0.25 g of potassium bromide added to give a 5-percent solution of potassium bromide before the addition of the 5 ml of solution B. About 30 percent of the residual thiosulfate was extracted from samples of microfilm containing 8, 14, 17, 34, 54, and 59 μg of thiosulfate per in.^{2} after fixation in a fresh bath. Only 1 to 3 μg of thiosulfate was extracted from samples of microfilm containing 14, 25, 31, 34, 44, and 46 μg of thiosulfate per in.^{2} after fixation in a bath containing 8 g of silver per liter. The bromide ion in solution A_0 decomposed the residual silver thiosulfate complex making the thiosulfate and silver soluble.

The effect of temperature on the extraction of the residual thiosulfate by solution A_0 was investigated. Tests were made at room temperature and a lower temperature on the same strip of film at the same time. After extraction, the specimens at the lower temperature were brought to room temperature before the addition of solution B. One sample of microfilm extracted at 7 to 9 °C tested 14 μg of thiosulfate per in.^{2} and at 26°, 17½ μg/in.^{2}; and a second sample at 13 °C tested 13 μg/in.^{2} of thiosulfate and at 26 °C, 15 μg/in.^{2} Both samples had been fixed in a bath containing 8 g of silver per liter. From the above data it may be inferred that a change of 3 °C in solution A_0 would cause an error of about ½ μg of thiosulfate per in.^{2}

3.2. Effect of Gelatin on the Turbidity in the Thiosulfate Test

Solution B was added to solutions of A_0 containing 5, 10, 20, and 40 μg, respectively, of sodium thiosulfate. Then the tests were repeated, except that 1-in.^{2} samples of clear (image-free) thiosulfate-free film were immersed in solution A_0 for 15 min and removed before the addition of the thiosulfate and solution B. The turbidities are shown in table 1 for different types of film and the above thiosulfate concentrations. For solutions containing more than 5 μg of thiosulfate, the turbidity of the solutions treated with film were much higher than the controls. The turbidities for microfilm specimens differed from those for motion picture film. The results suggested that the turbidity might be increased by an agent extracted from the film such as gelatin, causing a more highly dispersed precipitate. Turbid test solutions treated with film appeared bluer than those not treated. The turbidities in table 1 were reproducible to within 5 percent for each type of film. It appeared at first that a calibration curve would have to be prepared for each type of film, but this would have made the test procedure impractical.

Tests were then made to determine the effect of gelatin on the turbidity of the test solutions. Small concentrations of gelatin were added to solution A_0 containing known concentrations of sodium thiosulfate after which the required amount of solution B was added. It was found that traces of gelatin significantly increased the turbidity in the thiosulfate test solution. As little as 3 parts of gelatin in a billion caused a detectable change of the turbidity in the thiosulfate test solution!

TABLE 1. *Effect of different films on the turbidity in the thiosulfate test when solution A_0 was treated with 1 square inch of image-free thiosulfate-free film*

Thiosulfate added after removal of film	No film treatment. Data taken from calibration curve	Turbidimetric units				
		Microfilm			Motion picture film	
		A	B	C	A	B
Micrograms						
5	11	14	13	13	9	12
10	42	96	86	75	114	123
20	146	333	325	296	245	263
40	339	632	610	614	488	562

In order to evaluate the effect of gelatin concentration on turbidity, a 0.10-percent gelatin solution was made up as follows: About 10 g of photographic grade gelatin were heated in 600 ml of distilled water at 50 to 60 °C for 1 hr with frequent stirring. About 200 ml of the warm solution were filtered through 2 layers of highly purified filter paper. The solid content of the filtrate was determined by pipeting 10 ml into a tared 20 ml beaker, heating in an oven at 100±2 °C for 24 hr, and weighing the beakers and residue. From the weight of the solid residue in the 10 ml aliquot the volume of the filtrate containing 1 g of gelatin was calculated and this volume of filtrate was diluted to 1 liter with distilled water to obtain the 0.10-percent gelatin solution. A commercial food gelatin gave the same results as the above photographic gelatin, but it developed a fungus growth after storage for 8 weeks in a refriger-

ator, while the photographic grade has remained stable for 8 months in a refrigerator.

The effect of gelatin concentration on the turbidity in the thiosulfate test was determined for 10, 20, and 40 μg of sodium thiosulfate by adding different amounts of gelatin to solution A_0. Solution A_0 was made up to 1000 ml less the volume of gelatin solution to be added, filtered, and the gelatin solution added. The gelatin solution was added after filtration to avoid any effect of the filter paper on the concentration of the gelatin. In the tests, the thiosulfate was added to solution A_0 containing gelatin, followed by solution B. In figure 1 the gelatin concentrations are plotted against turbidimetric units for the 3 thiosulfate concentrations. These curves show that very low concentrations of gelatin in the test solution (1 to 10 μg per 10 ml of test solution) have a large effect on measured turbidity in the thiosulfate test. Between 50 and 200 μg per 10 ml of test solution, however, the change in measured turbidity is very slight. The data in figure 1 suggest that the effects of different amounts of gelatin dissolved from different types of film might be eliminated by increasing the gelatin concentration in the test solution.

A concentration of 100 μg of gelatin in 5 ml of the extracting solution A_0 was selected for the new thiosulfate test procedure and is hereafter designated solution A. Tests were then made to determine if treatment of different types of clear (image-free) thiosulfate-free film in solution A would give the same turbidity for a given thiosulfate concentration. Samples of 1 in.^{2} of film were immersed in solution A for 15 min and then removed before the addition of thiosulfate and solution B. Samples of three different microfilms and two motion picture films were tested at 5 thiosulfate concentrations (5, 10, 20, 40, and 80 μg per 10 ml of test solution). The measured turbidities for each concentration agreed within experimental error with the corresponding turbidities obtained for each of the above thiosulfate concentrations when solution A was not treated with a film. These results demonstrated conclusively that the effect on measured turbidity of gelatin dissolved from the film had been eliminated.

The nephelometer calibration curve shown in figure 2 was prepared by plotting measured turbidities as a function of thiosulfate concentration. The plotted values were an average of five or more determinations. In this new test procedure the rapid mixing of solutions, A and B, and the added gelatin formed a reproducible turbidity. The curve in figure 2 shows a sharp change between 6 and 8 μg of thiosulfate, but is linear from 9 to 100 μg. Figure 3 is an enlarged scale of a portion of figure 2 showing more clearly the sharp change in the calibration curve for the lower thiosulfate concentrations, those of chief concern in microfilm practice. In the Crabtree-Ross test procedure the turbidity readings for the standard solutions were not always reproducible and sometimes varied as much as 50 percent for the 5 μg standard. The rate of mixing of the thiosulfate in the test solution appears to affect the particle size of the precipitate.

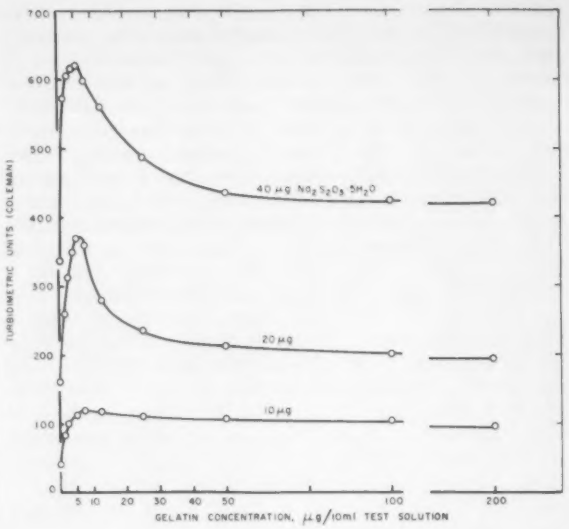

FIGURE 1. *Effect of gelatin concentration on the turbidity formed by the reaction of mercuric chloride with thiosulfate after the addition of 5 ml of solution* B *to 5 ml of solution* A_0 *for 3 thiosulfate concentrations.*

The concentration of sodium thiosulfate is shown on the curves.

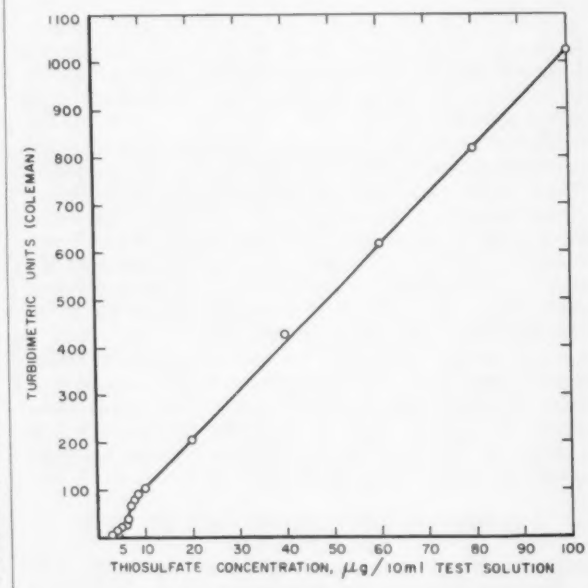

FIGURE 2. *Nephelometer calibration curve showing the turbidity formed by the reaction of mercuric chloride with thiosulfate after the addition of 5 ml of solution* B *to 5 ml of solution* A.

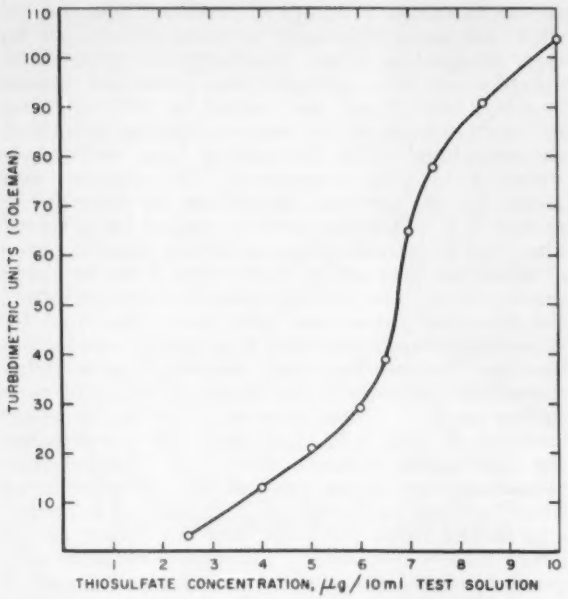

FIGURE 3. *An enlarged scale of the calibration curve in figure 2 for the low sodium thiosulfate concentrations.*

A trace of thiosulfate is held by the film in the thiosulfate test. It was found that the 1-in.^{2} microfilm samples removed 0.03 to 0.05 ml of solution A. This loss was determined by weighing, in a tared glass stoppered bottle, three 1-in.^{2} samples, before and after treatment in solution A. The loss of this amount of solution does not introduce any significant error, especially for the low residual thiosulfate concentrations. Tests were made by treating solutions of A containing 10 to 70 μg of thiosulfate with clear (image-free) thiosulfate-free microfilm to determine the error caused by removing the film sample from solution A. There was a loss of about 1μg of thiosulfate per in.^{2} regardless of the thiosulfate concentration. If the film sample was not removed before the addition of solution B, the sample sometimes interfered with the formation of the precipitate giving low turbidity values. Evidently the film absorbed the thiosulfate in the emulsion or on the film base. A correction of 1 μg might be applied. This correction is not significant for high thiosulfate concentrations, but it may be desirable to add it at concentrations below 20 μg per in.^{2} for accurate determination of residual thiosulfate.

3.3. Comparison of the New Test Procedure With the Crabtree-Ross Test Procedure

Unexposed strips of 35-mm film, cut 10 in. in length, were developed, treated in a stop bath, fixed, and washed at different water temperatures and for different times to obtain image-free samples with a range of residual thiosulfate concentrations. The film strips were stored about 2 to 3 weeks before testing. Analysis of the residual thiosulfate content was made by the two procedures at the same time on the same strip of film in each run. A calibration curve was prepared for the Crabtree-Ross test procedure and calibration curves for the new procedure are shown in figures 2 and 3. Samples of 1 in.^{2} of film were cut or punched from the strip, alternate samples 1 and 3 being used in one procedure and 2 and 4 in the other. The duplicate in both procedures generally gave the same residual thiosulfate content, occasionally differing by ½ to 1 μg in the low thiosulfate concentrations and 1 to 2 in the high. The average residual thiosulfate concentrations of the duplicate samples for the two procedures are given in table 2 for microfilm and motion picture film after fixation in a fresh bath and a bath containing 8 g of silver per liter. The thiosulfate concentrations for the new procedure were not corrected for the 1 μg of thiosulfate per in.^{2} which is normally absorbed by the film. As shown in table 2, the new test procedure measured 2 to 3 times as much residual thiosulfate in processed film as the Crabtree-Ross test procedure.

TABLE 2. *Comparison of residual thiosulfate concentrations obtained from the new thiosulfate test and the Crabtree-Ross thiosulfate test for the same sample of image-free film*

Thiosulfate, micrograms per square inch

Microfilm			Motion picture film		
Film brand	New procedure	Crabtree-Ross procedure	Film brand	New procedure	Crabtree-Ross procedure
	Fixed in a fresh bath				
A	2	0	A	28	11
A	7	4½	A	87	28
A	19	6½	A	110	32
A	22	12	B	16	7
A	55	27	B	50	18
B	5	2	B	78	28
B	7½	4			
B	19	10½			
B	43	19			
B	90	42			
	Fixed in a bath+8 g of silver per liter				
A	9½	3	A	64	18
A	25	7	A	88	23
A	38	12	B	6½	4½
A	62	18	B	52	19
B	8	2½	B	78	28
B	39	10			
B	70	18			

The lower residual thiosulfate concentrations measured by the Crabtree-Ross procedure may be attributed to the precipitation of some of the reaction product from the thiosulfate and mercuric chloride within the gelatin layer of the film. Thus, only a part of the thiosulfate is extracted to form a precipitate in the test solution. The presence of a precipitate in the gelatin layer after treatment in the Crabtree-Ross test solution was determined qualitatively by dissolving the gelatin and observing the turbidity of the solution. One-in.^{2} samples from clear (image-free) microfilm containing 0 and 50 to 70 μg of residual thiosulfate were treated in the Crabtree-Ross test solution for 15 min, washed 10

min, and treated in 10 ml of a ½-percent solution of pancreatic enzyme at about 55 °C for 30 min to dissolve most of the gelatin. On visual inspection, there was considerably more turbidity in the enzyme solution for films containing residual thiosulfate than the one containing none. The precipitate in the enzyme solutions for films containing thiosulfate appeared bluish, but the blank was brownish gray. In other tests on microfilm having a high residual thiosulfate concentration, the turbidity remaining after solution of the gelatin roughly corresponded to the difference of residual thiosulfate content measured by the new test procedure and the Crabtree-Ross test procedure. In another test, 1-in. samples of clear (image-free) microfilm containing 17, 39, and 51 μg of thiosulfate were treated in 10 ml of the Crabtree-Ross test solution for 15 min, washed 10 min, and heated in 10 ml of a 5-percent solution of citric acid at 70 to 80 °C for about 1 hr to dissolve the emulsion. There was considerably more turbidity in the solutions for films containing residual thiosulfate than for the one containing none. The degree of turbidity was in the same order as the residual thiosulfate concentrations of the films whether estimated visually or measured with the nephelometer. Again the precipitate in the solutions for the films containing residual thiosulfate was bluish, but the blank was brownish to gray. When the above solutions were made alkaline with concentrated ammonium hydroxide, most of the turbidity in the sample containing no thiosulfate was eliminated while the solutions for films containing thiosulfate became quite bluish and the turbidities were in the same order as the residual thiosulfate contents when estimated visually or measured with nephelometer.

The presence of a precipitate in the gelatin layer was also shown by measuring the transmission density of the film sample after treatment in the Crabtree-Ross test solution. Clear (image-free) microfilm samples containing 0, 60, 70, 103, and 150 μg, of residual thiosulfate per in.^{2} were treated for 15 min in the Crabtree-Ross test solution, washed 15 min, dried, and the transmission density of the samples measured. The untreated microfilm had a density of 0.07. The control sample having 0 μg of thiosulfate per in.^{2} had a density of 0.08; 60 μg, 0.09; 70 μg, 0.10; 103 μg, 0.11; and 150 μg 0.13. The above data showed that a precipitate was present in the gelatin layer and its density increased from 0.01 to 0.05 above that of the control.

The above results explain why the Crabtree-Ross test procedure gave low values for the residual thiosulfate content in processed film. The gelatin effect on the turbidity was not investigated for the Crabtree-Ross test procedure, but it is probably small since the test solution is acid.

3.4. Effect of the Image Silver on the Crabtree-Ross Test Procedure

Residual thiosulfate contents determined by the new test procedure and the Crabtree-Ross test procedure in the silver image of processed film did not show the same difference as those determined for clear (image-free) film. Flash-exposed strips of 35-mm film, cut 10 in. in length, were developed, treated in a stop bath, fixed, and washed for different times to obtain samples with a range of residual thiosulfate concentrations. The thiosulfate tests were made within 4 hr after processing. The samples were tested by the two test procedures as described in section 3.3. The comparative results for a microfilm fixed in a fresh bath and a bath containing 8 g of silver per liter are given in table 3 for an image density of 5. The residual thiosulfate contents from the two test procedures were about the same for thiosulfate concentrations of 20 μg per in.^{2} and higher, but the Crabtree-Ross test procedure gave higher thiosulfate contents in the range of 10 μg of thiosulfate per in.^{2} Other tests on microfilm for image densities of 0.02, 0.72, 1.62, and 2.48 showed that the thiosulfate contents from the Crabtree-Ross procedure were about one-half the value obtained from the new procedure at a density of 0.02, but approached those from the new procedure as the image density increased. Thiosulfate contents indicated by both procedures became about equal at image densities of 4 to 5. The above results show that the Crabtree-Ross test procedure gives higher residual thiosulfate contents in the presence of image silver than in clear (image-free) film and this difference may result from the addition of silver to the test solution forming a turbidity of silver halide. In the Crabtree-Ross test procedure the silver in the image is bleached by the mercuric chloride, forming silver halide in the film. Any residual thiosulfate present could form a soluble silver thiosulfate complex which migrates into the test solution where it decomposes to form an additional turbidity of silver halide and is measured along with that formed by the reaction of thiosulfate with mercuric chloride.

TABLE 3. *Comparison of residual thiosulfate concentrations obtained from the new thiosulfate test and the Crabtree-Ross thiosulfate test for microfim having a density of 5.*

Fixed in a fresh bath		Fixed in a bath +8 g of silver per liter	
New procedure	Crabtree-Ross procedure	New procedure	Crabtree-Ross procedure
Thiosulfate, μg/in.^{2}			
9	14	11	16
12	16	20	21
18	21	31	29
24	23	57	43

Different amounts of silver as silver nitrate were added to the Crabtree-Ross test solution and the turbidities measured. The standard silver solutions were made up and added by the same method used for the standard thiosulfate solutions. Figure 4 shows the calibration curve obtained by plotting the turbidimetric units against the silver concentration in the Crabtree-Ross test solution. The calibration curve showed that the turbidity of the silver halide varied linearly with the silver concentration and also

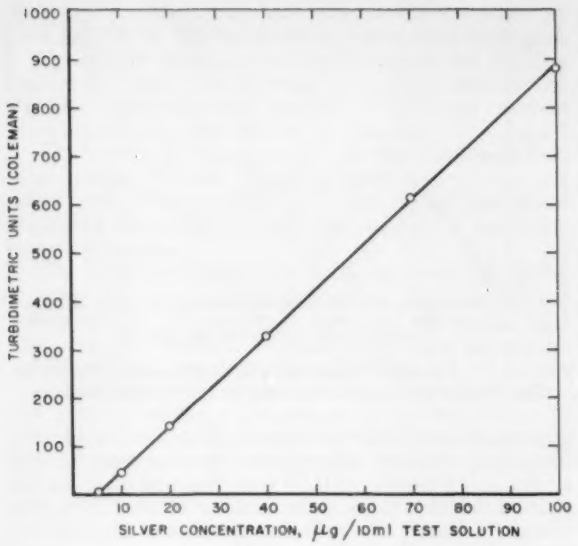

FIGURE 4. *Calibration curve showing the turbidity formed by silver added as silver nitrate to 10 ml of the Crabtree-Ross thiosulfate test solution.*

that a small amount of silver in the test solution would add appreciably to the turbidity in the thiosulfate test. For example, 20 μg of silver gave a turbidity reading of 142 as compared to 204 for 20 μg of thiosulfate shown in figure 2.

The effect of image silver on the turbidity in the Crabtree-Ross test procedure was further investigated by adding a known amount of thiosulfate to processed microfilm. A 0.05 ml solution containing 20 μg of sodium thiosulfate was pipeted onto 1-in.^{2} samples of thiosulfate-free film punched from clear (image-free) strips and strips having an image density of 5, evaporated to dryness in an oven at 50 °C, and the residual thiosulfate determined at the same time by the two test procedures. Duplicate samples were used for each test in the clear and image areas. The amount of residual thiosulfate found by the new test procedure in exposed film (image density 5) was about the same as that found in clear film. In one run 19 μg of sodium thiosulfate were measured in the clear film and 17 μg in the exposed film; in a second run, there was 17 μg in the clear film and 16 μg in the exposed film. The above results showed that the residual thiosulfate was accurately determined in the presence of image silver if allowance is made for some loss of thiosulfate due to its tendency to react with silver to form silver sulfide. A trace of thiosulfate may also be oxidized by exposure to air during oven drying.

The amount of residual thiosulfate found by the Crabtree-Ross procedure in exposed film (image density 5) was more than that found in an unexposed film. In one run, 11 μg of sodium thiosulfate were measured in the clear film and 17 μg in the exposed film. In a second run, there were 12 μg in the clear film and 19 μg in the exposed film. The results show that the exposed film tested higher in residual thiosulfate than the clear film, indicating that some of the silver in the bleached image had migrated into the test solution. The amount of thiosulfate found by the Crabtree-Ross test procedure in the clear film was less than was found by the new test procedure, due to the retention of some of the precipitate in the gelatin layer, as shown in section 3.3.

3.5. Test for Residual Silver in Processed Film

Residual silver in processed film is present as a silver thiosulfate complex. Appreciable amounts of residual silver may cause fading or yellowing of the image due to the formation of silver sulfide. A large concentration of residual silver in the film would indicate that the fixing bath contained too much silver for adequate removal of the silver thiosulfate complex during a normal washing procedure. A fresh fixing bath leaves no measurable residual silver in the film, but as silver accumulates in the fixing bath the tendency for the silver thiosulfate complex to remain in the film increases. The silver thiosulfate complex is more difficult to remove in the washing process than the thiosulfate. As the fixing bath approaches exhaustion the residual silver in the film becomes high and some of it remains after prolonged washing.

The test for residual silver in processed film [6] now in use is only qualitative. In this test the film is treated with a 0.2-percent solution of fused sodium sulfide and a yellow stain is produced if sufficient residual silver is present. Tests showed that at high residual silver concentrations a stain density of only 0.02 was produced in microfilm and 0.04 in motion picture film. A more sensitive and quantitative test was needed to indicate the amount of residual silver present in processed film. It has been shown [5] that a 0.1-percent solution of potassium iodide will react with the residual silver thiosulfate complex in processed film to precipitate silver iodide in the film. An investigation was made to determine if the silver in the silver thiosulfate complex could be converted to silver in the film and the amount of residual silver indicated by measuring the transmission density of the silver.

Samples of unexposed microfilm and motion picture film were fixed in a bath containing 8 g of silver per liter and washed for different times to obtain a range of residual thiosulfate concentrations accompanied by high residual silver concentration. It was found that the residual silver in the silver thiosulfate complex could be converted to a silver image by treating it in a developer containing 2 g of potassium iodide per liter, while exposing it to light. The optimum concentration of potassium iodide was 1½ to 3 g per liter of developer solution. If there was less than 1½ g of potassium iodide per liter, not all of the residual silver was converted to image silver and if above 3 g, some of the silver iodide passed into solution before development. For the test procedure, 2 g of potassium iodide per liter of developer solution was used. The following developers were used in the experimental work and gave the same results:

Developer A

Amidol, 2,4-diaminophenol dihydrochloride	5.0 g.
Sodium sulfite, anhydrous	30.0 g.
Potassium iodide	2.0 g.
Water to make	1 liter.

Developer B

Monomethyl *p*-aminophenol sulfate	3.1 g.
Sodium sulfite, anhydrous	45.0 g.
Hydroquinone	12.0 g.
Sodium carbonate, anhydrous	67.5 g.
Potassium iodide	2.0 g.
Water to make	1 liter.

The developer should be fresh and developer A should be made up just before use. The film sample was treated in the developer solution for 20 min with occasional stirring while exposed to a 100-w tungsten lamp located 6 in. from the surface of the solution, treated 1 min in a stop bath containing 12 ml of glacial acetic acid per liter, and washed 15 min. The densities of the silver images obtained for the different thiosulfate concentrations were very reproducible and correlated well with the thiosulfate concentrations. Silver in the image was identified qualitatively by dissolving the image in nitric acid and obtaining a precipitate of silver chloride after the addition of sodium chloride. Film samples of the silver image were immersed in water for 5 min and, after removal of the surface water, they were bleached over concentrated hydrochloric acid, dried, and redeveloped with light in developer A. The same density could be redeveloped, indicating that the image was silver.

One set each of unexposed 35 mm samples, cut 10 in. in length, from a microfilm and a motion picture film, respectively, were fixed in a bath containing 8 g of silver per liter and washed at 25° C for different times to obtain a range of residual thiosulfate concentrations. Then samples from strips having different residual thiosulfate concentrations were developed together in Developer A, one set being run for microfilm and one for motion picture film. The transmission densities of the developed samples were measured and the density of the film base subtracted from the density readings. The density of the silver image for each sample was plotted against its respective residual thiosulfate concentration and curves for the microfilm and the motion picture film are shown in figure 5. The data in the curves show that the silver density developed from the residual silver is proportional to the residual thiosulfate concentration for the lower thiosulfate concentrations and becomes nearly constant at the higher concentrations. The test method may be used to study the exhaustion of a fixing bath under controlled conditions, since the appearance of appreciable concentrations of residual thiosulfate will signal difficulty in removing the silver thiosulfate complex in the washing process.

In a microfilm with a residual thiosulfate concentration of 130 μg per in.^{2}, a density of 0.16 was obtained, while in the sodium sulfide test [6] a stain

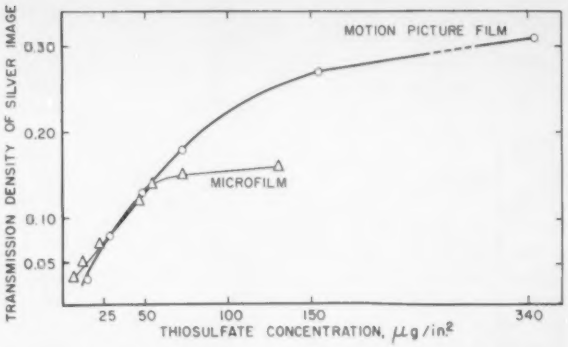

FIGURE 5. *Density of silver image formed from the silver in the silver thiosulfate complex versus the thiosulfate concentration.*

density of only 0.02 was found. In a motion picture film for a residual thiosulfate concentration of 154 μg per in.^{2}, a density of 0.27 was obtained while in the sodium sulfide test a stain density of only 0.04 was found. Clearly, the new test method is much more sensitive than the sodium sulfide test.

Tests were made for residual silver on microfilm and motion picture film fixed in a fresh bath by the new test method and no residual silver could be detected in microfilm samples containing up to 240 μg of residual thiosulfate per square inch and motion picture samples containing up to 500 μg per in.^{2}

4. Summary

A new test procedure was developed for the determination of residual thiosulfate in processed film. This procedure indicates that the residual thiosulfate present in clear (image-free) processed film is 2 to 3 times that indicated by the Crabtree-Ross test procedure. In the course of development of the new test procedure, it was found that a trace of gelatin dissolved from the film sample produced a considerable change in the measured turbidity. The amount of gelatin dissolved depended on the type of film being tested. A separate nephelometer calibration curve might have been prepared for each type of film, but such a procedure would be impractical. Instead the effect of gelatin concentration in the test solution was investigated. The data showed that the addition of 100 μg of gelatin to the test solution would eliminate the effect of gelatin dissolved from the film, thus making it possible to prepare a single calibration curve for all types of film. For accurate results at low thiosulfate concentrations a correction of 1 μg per in.^{2} should be added to the value obtained turbidimetrically.

In the new procedure the thiosulfate was extracted from 1 in.^{2} of film by treatment in 5 ml of a 5-percent solution of potassium bromide solution containing 100 μg of gelatin, and 5 ml of a 5-percent solution of mercuric chloride was added after removal of the film sample. A nephelometer was used to measure the turbidities. A calibration curve was prepared at 25 °C$\pm$2 °C. The temperature of the solutions

during the thiosulfate test should be the same as that at which the calibration curve was prepared.

Qualitative tests showed that some of the precipitate in the Crabtree-Ross test procedure remained in the film during the test, causing low values of residual thiosulfate concentration to be reported.

When a silver image containing residual thiosulfate was tested by the Crabtree-Ross test procedure, there was evidence that some of the image silver migrated into the test solution, adding a turbidity of silver halide.

The new test procedure may be used for determining the residual thiosulfate in film containing image silver. However, it has been shown [5] that the test for residual thiosulfate in film should be made with an image-free area of film.

A new test method was developed for determining the residual silver in processed film. The silver in the silver thiosulfate complex was developed to a silver image and its transmission density measured.

(Paper 67C3–134)

5. References

[1] J. I. Crabtree and J. F. Ross, A method of testing for the presence of sodium thiosulfate in motion picture films, J. Soc. Motion Picture Engrs. **14,** 419–426 (1930).

[2] American Standard Method for Determining the Thiosulfate Content of Processed Black-and-White Photographic Films and Plates, PH4.8–1958 (American Standards Association, Inc., 10 East 40th St., New York 16, N.Y.).

[3] J. I. Crabtree, G. T. Eaton, and L. E. Muehler, The removal of hypo and silver salts from photographic materials as affected by the composition of the processing solutions, J. Soc. Motion Picture and Television Engrs. **41,** 14 (1943).

[4] E. P. Przybylowicz, C. W. Zuehlke, and A. E. Ballard, An evaluation of the Crabtree-Ross procedure for residual hypo in processed film, Photo. Science and Engr. **2,** No. 3, 148–153 (1958).

[5] C. I. Pope, Stability of residual thiosulfate in processed microfilm, Journal of Research National Bureau of Standards, Vol. **67C** (Eng. and Instr.), No. 1, 15–24 (1963).

[6] American Standard Method for Indicating the Stability of the Images of Processed Black-and-White Films, Plates, and Papers, PH4.12–1954 (American Standards Association, Inc., 10 East 40th St., New York 16, N.Y.).

JOURNAL OF RESEARCH of the National Bureau of Standards—C. Engineering and Instrumentation
Vol. 67C, No. 3, July–September 1963

Drag Compensation and Measurement With Manned Satellites: Feasibility Study[1]

R. M. Langer [2] and J. P. Vinti

(April 19, 1963)

Even at low altitudes approximating those of manned earth-satellites it is feasible to use external jets to maintain a satellite in a purely gravitational orbit. With the jets off, it is possible to measure the drag, air density, and time of passage through perigee, by means of observations aboard the satellite. Intermittent operation of the jets should permit achievement of both objectives.

Many artificial satellites have had masses of about 10^6 gm and effective areas of some 5 m^2. At a height of 200 km the resulting drag amounts to some 6×10^4 dynes or about 6×10^{-5} of the weight. At 300 km the drag is one-tenth of this. Accurate knowledge of this drag is essential in determining the atmospheric density at high altitudes and in reducing the observed orbit to determine the figure of the earth. For the second purpose it would be better to be able to eliminate the drag than to correct for it.

So far drag measurement has been done only by difficult reductions of the orbits of unmanned satellites. Drag cancellation has not been done but a means has been discussed, involving automatic instrumentation. In this note we propose several methods for drag measurement or compensation that can be achieved either by automatic means in an unmanned satellite or by the astronaut in a manned satellite. The numerical values here presented may help to decide in different missions whether manning or automation is more appropriate. For greater vividness and conciseness, however, we now speak mostly in terms of a manned satellite.

First consider drag cancellation. To do so, we note that Pugh [1],[3] Lange [2], and others have suggested the use of external jets to neutralize the drag on an unmanned double satellite. This would require using a sensing device to detect approach of the inner satellite toward the outer one and a servomechanism to transmit the resulting signals to the external vernier jets. These jets in turn would produce enough acceleration of the outer satellite to keep the inner satellite centered. With neglect of very small gravitational interactions of the inner satellite with the outer and of small electromagnetic interactions of the inner satellite with the instrumentation, the outer satellite, and with the outside surroundings, the only force on the inner satellite would be external gravitation. Since the outer satellite is moving in the same orbit as the inner, the observed orbit is purely gravitational.

In place of this unmanned double satellite, if we use a manned space capsule, with the astronaut as sensing device and control system, we can eliminate certain difficulties. This procedure would be analogous to the use of a test pilot in a manned plane, while the automatic unmanned double satellite would correspond to an inertially guided unmanned plane, which came much later. The advantages of an automatic system will become important when one seeks prolonged, large scale, highly precise observations. Meanwhile we need not delay making some basic observations by means of astronauts' reports and data, which may be of great help in preparing elaborate space laboratories in the future.

To maintain a manned capsule in a gravitational orbit, the astronaut would continually or intermittently adjust some external jets, to keep a small test object within some tolerable distance from the capsule's center of mass. For protection against air currents and stray fields, the test object should be enclosed in an evacuated and electromagnetically shielded housing.

To examine the feasibility of such a procedure, consider a jet of compressed air escaping through a simple converging nozzle of 1 mm diameter from a chamber at 6 atmospheres. Producing 6×10^4 dynes thrust throughout a circular orbit at 200 km height would require 6.8 kg of air. For an elliptic orbit of eccentricity $\epsilon=0.03$ and the same perigee, it would take only 1.6 kg. For perigee at 300 km these figures would drop by more than a factor 10. Moreover, use of a divergent portion with the nozzle would also improve matters considerably.

[1] Research supported by the National Aeronautics and Space Administration, U.S.A.
[2] Consultant to the National Bureau of Standards, J. R. M. Bege Co., Arlington, Mass.
[3] Figures in brackets indicate the literature references at the end of this paper.

A chemical propellant giving the big rocket specific impulse of 300 kg force sec/kg mass (300 "sec"), if efficient micro-vernier jets become available, would be 6 times more economical of mass. Thus the satellite need not go very high to make man-controlled drag compensation feasible. At these relatively low altitudes all the appreciable harmonics of the earth's gravitational field will still be well represented, so that the resulting gravitational orbits should be very suitable for deducing the coefficients of the various harmonics. Furthermore, as will appear later, the relatively high drag can actually be used to improve the accuracy of determination of time of passage through perigee, by means of a separate experiment performed by the astronaut.

The astronaut may measure the drag at intervals between jet thrusts, having previously oriented the capsule so that it presents a constant projected area. To do this he may be furnished two identical torsion systems, with twist axes in the same plane but mounted at right angles to each other, each carrying a seismic mass of about 100 g about 1 cm off axis. He first rotates the torsion plane manually to produce maximum and equal twists for both torsion systems, whereupon it becomes normal to the drag force. He then orients the capsule for minimum drag by adjusting jets that rotate it until its long axis becomes perpendicular to the plane of the torsion axes and thus parallel to the drag.

In our example the satellite of mass 10^6 g, moving at a height of 200 km, experiences a drag force of 6×10^4 dynes and a drag deceleration of 6×10^{-2} cm/sec^2. This leads to a torque of 6 dyne cm on each torsion system. If the sensitivity is 100 dyne cm per radian, the twist will be 3 deg, enough for easy measurement, although the systems will be rather sluggish, with response times from 6 to 10 sec. However, since 10 sec corresponds to only about 0.5 deg change in eccentric anomaly, such a torsion system should allow easy following of the changes in drag occurring in elliptic motion with small eccentricity. Such measurements of the drag should provide valuable information concerning both the orbit and the atmosphere. The astronaut can monitor height, eccentricity, and position in orbit with little dependence on terrestrial observers. Of greatest importance, he can determine accurately the time of passage through perigee, since the drag has a sharp maximum there even when the eccentricity is as small as 0.005.

Another method of measuring the drag would be simply to have the astronaut measure the distance $s=\frac{1}{2}a_Dt^2$ traversed in a short time t by a small test object as it drifts through the capsule under the influence of the effective gravitational field $\boldsymbol{a}_D$. Here $\boldsymbol{a}_D=\boldsymbol{F}_D/m_s$, the negative of the drag acceleration of the satellite. Thus in our above example, with $a_D=6\times10^{-2}$ cm/sec^2, we have $s=3$cm if $t=10$ sec.

Two difficulties arise. In order that $-\boldsymbol{F}_D/m_s$ should be the only field acting on the test object it is necessary to eliminate centrifugal and Coriolis forces arising from the changing orientation of the capsule. To do so one could orient the capsule inertially, relative to the fixed stars, by some method of attitude control. But then the projected area would keep changing, so that one could not readily deduce the atmospheric density from the drag.

If one orients the capsule tangentially, as proposed in the above paragraphs on the accelerometer, there arise the apparent forces. It is easy, however, to correct for them by purely kinematical calculations, since one knows the rotational motion of a capsule which is tangentially oriented. Moreover, their effect is small. In our above example, the centrifugal acceleration is negligible and the Coriolis acceleration does not exceed 1/50 of the drag acceleration.

A question arises about body motions of the astronaut or accelerations produced by automatic equipment on board. Four measures could be taken to reduce such effects: (a) balance the accelerations; (b) arrange them to be transverse to the satellite motion; (c) shock-mount and filter out these motions; (d) suspend the motions during observations of the drag. Even breathing could be suspended during the five or ten second duration of such a measurement, but it is not at all certain that this would be necessary. Thus the ballistocardiograms of Smith and Bryan [3] show no long-periodic accelerations attributable to breathing even though their system had as good a response at 0.1 c/s, where breathing would show up, as in the frequency range of 2 to 10 c/s important in recording accelerations produced by the heart beat.

Ballistocardiographic measurements by Smith [4], on the other hand, furnish reassuring statistics concerning the irremovable effects of the heart beat on drag measurements. Each of 50 normal persons was firmly attached to a platform free to swing in reaction to the heart beat. The double amplitudes of displacement ranged from 0.035 mm to 0.09 mm, with a most frequent double amplitude of about 0.06 mm. The normal peak displacement from mean position was thus about 0.03 mm.

Since the mass in these measurements was about 100 kg, the corresponding displacement in the case of an astronaut firmly attached to a 1000 kg capsule would be only 0.003 mm. Comparison of this figure with the 3-mm excursion of the test body inside a satellite at 300 km (Mercury at apogee) shows a possible error of only 1 part in 1000. Thus neither heart beat nor breathing need interfere with a drag measurement, even if we do not adopt the special measures a, b, and c listed above.

To recenter the test object, the astronaut has only to turn on and adjust the jets for drag compensation before the object collides with its housing. The orbit will then remain essentially gravitational. By combining all three of the methods here described, using intermittent drag compensation, one could obtain a gravitational orbit and take many measurements of the drag and thus of the air density, all in one flight. A manned satellite so instrumented should then provide valuable geophysical and bioastronautic data, along with experience in design and operation of a primordial zero-g laboratory.

To conclude, note that nothing we have said above is intended to discourage the use of automatic unmanned satellites. Our aim has rather been to find further important functions for astronauts in those manned flights that are now being planned or will be planned in the future. They in turn may lead both to better automatic and better manned space laboratories.

(Paper 67C3–135)

References

[1] Pugh, G. E., WSEG Research Memorandum No. 11 (Weapons System Evaluation Group, Washington 25, D.C., 1959).

[2] Lange, Benjamin, Feasibility study for a purely gravitational orbit satellite, unpublished memorandum based on research done at Stanford University, Stanford, California, and supported by the Lockheed Missiles and Space Company general research program.

[3] Smith, J. E., and Bryan, S., Am. Heart J. **45,** 715 (1953).

[4] Smith, J. E., Am. Heart J. **46,** 692 (1953).

686-132—63——5

JOURNAL OF RESEARCH of the National Bureau of Standards—C. Engineering and Instrumentation
Vol. 67C, No. 3, July–September 1963

Surface Flame Propagation on Cellulosic Materials Exposed to Thermal Radiation

D. Gross and J. J. Loftus

(April 11, 1963)

The results of a series of flame-spread tests are summarized and analyzed to delineate the importance of the physical and thermal properties in surface flame propagation on simple and composite slabs. The data are in accordance with relationships for the transient surface temperature rise for irradiated opaque and chemically inert slabs and support a simple concept for the spread of flame on the surfaces of cellulosic materials exposed to thermal radiation; viz, that flame propagation consists of progressive ignition of the solid when a characteristic temperature is reached.

1. Introduction

The result of a standardized flame-spread test [1][1] performed on a single material or on a composite assembly is reported in terms of an arbitrary flame-spread index. This index is defined as zero for noncombustible asbestos-cement board and may range in the hundreds or even thousands for materials of very rapid flammability. It has been shown [2] that the flame-spread index is composed of two multiplicative factors: (a) a flame-spread factor representing the ignition sensitivity of the material, and (b) a heat evolution factor representing the maximum rate of heat generation. Although flame-spread index values for a wide variety of typical building finish materials have been published [3, 4, 5, 6], a systematic evaluation of the important physical and thermal properties which govern the surface propagation of flames is incomplete. This paper summarizes the results of tests performed to define the significance of ignition sensitivity for cellulosic materials and to analyze and delineate some important parameters in flame propagation. The primary objective of the analysis was to extend a simple surface ignition concept to a flame propagation situation by considering the propagation of flames as a series of progressive surface ignitions of thermally irradiated material. In actual fires, the predominant mode of heat transfer is by radiation, generally from adjacent flaming surfaces. Although all tests were performed using the radiant panel test method, the analysis and interpretation are considered likely to be applicable to surface propagation of flame on most irradiated combustible materials.

2. Apparatus and Test Procedure

The apparatus used for the tests has been described in detail [1, 3]. As shown in schematic form in figure 1, it consists of a radiant panel heat source, a frame for support of the test specimen, and associated measuring equipment.

[1] Figures in brackets indicate the literature references at the end of this paper.

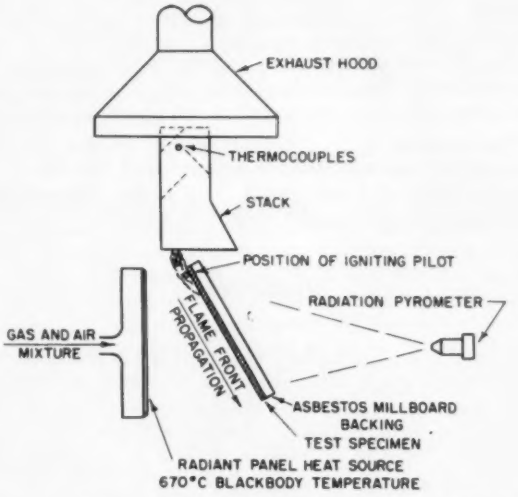

FIGURE 1. *Schematic diagram of radiant panel apparatus for flame-spread measurement.*

The radiant panel consists of a cast iron frame enclosing a 12-in. wide by 18-in. high porous refractory material. The panel is mounted in a vertical plane, and a premixed gas-air mixture supplied from the rear is burned in intimate contact with the refractory surface to provide a radiant heat source. The energy output of the panel, which is maintained by regulating the gas flow according to the indication of a radiation pyrometer, is that which would be obtained from a blackbody of the same dimensions operating at a temperature of 670 °C (1,238 °F). A stack placed under an exhaust hood and above the test specimen receives the hot products of combustion and smoke.

For test, the 6- by 18-in. specimen backed by a sheet of asbestos millboard was placed in a metal holder and mounted on a supporting frame, facing the radiant panel and inclined 30 deg to it. A pilot igniter fed by an air-acetylene mixture served both

to initiate flaming at the upper edge of the test specimen and to ignite combustible gases rising from the specimen. Observations were then made of the progress of the flame front, the occurrence of flashes, etc., as well as the temperature rise of the stack thermocouples. For some tests, an electrical timer calibrated in minutes and decimal fractions to hundredths was used for recording the time of occurrence of events during the tests. However, for tests involving very rapid flaming, a hand-operated switch was used to actuate an event marker on a high-speed recorder. The test duration was 15 min, or until sustained flaming had traversed downward the entire 18-in. length of specimen, whichever time was less.

The flame-spread index, I_s, was computed as the product of the flame-spread factor, F_s, and the heat evolution, Q, thus:

$$I_s=F_sQ \tag{1}$$

where

$$F_s=1+\frac{1}{t_3}+\frac{1}{t_6-t_3}+\frac{1}{t_9-t_6}+\frac{1}{t_{12}-t_9}+\frac{1}{t_{15}-t_{12}}. \tag{2}$$

The symbols t_3 . . . t_{15} correspond to the times in minutes from specimen exposure until arrival of the flame front at a position 3 . . . 15 in., respectively, along the length of the specimen and

$$Q=0.1\Delta\theta/\beta \tag{3}$$

where 0.1 is an arbitrary constant, $\Delta\theta$ is the observed maximum stack thermocouple temperature rise for the specimen minus the maximum temperature rise observed with a thick asbestos-cement board substituted for the specimen, and β is a calibration constant representing the maximum stack thermocouple temperature rise per unit heat input rate using a calibrating diffusion-type gas burner placed near the top of an asbestos-cement board specimen during normal operation of the radiant panel [1, 3]. To maintain the established numerical consistency of eq (1), and for convenience, English units (Btu, °F, min) were employed in eqs (1), (2), and (3).

Prior to test, all specimens and composite assemblies were conditioned by placing them in an oven at 140 °F for a 24-hr period and then allowing them to reach moisture equilibrium (constant weight) at 73 °F and at one of three relative humidities (17%, 50%, and 86%). The low and high humidity conditions were achieved by placing a tray containing an appropriate saturated salt solution at the bottom of each of two closed containers into which the specimens were suspended. Each container lid was fitted with a fan to provide adequate air circulation and a hygrometer element for measuring relative humidity. A room maintained at 73 °F and 50 percent rh by a conventional central air conditioning system was used for achieving moisture equilibrium at this intermediate relative humidity in all other specimens.

3. Analysis

A rigorous analysis of the radiation-induced ignition process would require consideration of chemical decomposition reactions, surface charring and contraction, variation in thermal properties with temperature, diffusion and mixing of combustible volatiles, and other complex conditions. Fortunately, the ignition behavior of cellulosic materials appears to closely follow the most simple theoretical postulate for temperature variation; i.e., the opaque, constant property, and chemically inert solid [7]. Thus, no consideration is given to the possible effects of absorptance and diathermancy, chemical decomposition, supply of volatiles, etc., the primary objective being to extend the simple postulate to a better understanding of the propagation of flames along surfaces.

The equation for the temperature rise, θ, of an opaque inert slab of thickness l, density ρ, thermal conductivity k and heat capacity c, subjected to constant irradiance I on one face and losing heat by Newtonian cooling through a coefficient H from both faces is complex [8].

However, the solution is of the form

$$\theta=\frac{I}{H}f\left(\frac{x}{l},\frac{kt}{\rho cl^2},\frac{Hl}{k},\right), \tag{4}$$

where x is the distance in the slab measured from the irradiated surface and t is time. Simms [7] has given approximations for the two cases of interest, namely thin and thick materials.

3.1. Thin Materials

For thin materials (in which a linear temperature gradient exists) and for very small values of the Nusselt number Hl/k, an approximation to the rise in temperature of the irradiated surface, θ_s, is given in reference [7] as

$$\theta_s=\frac{I}{2H}\left[1-e^{-\frac{Ht}{\rho cl}}\right]. \tag{5}$$

The term $Ht/\rho cl$ is the ratio of the energy lost by cooling to the heat content of the material, and is termed a cooling modulus.

3.2. Thick Materials

For thick materials, the surface temperature rise is the same as that for a semi-infinite solid and the relation [7, 9] is

$$\theta_s=\frac{I}{H}\left[1-e^{b^2}\text{erfc } b\right] \tag{6}$$

where

$$b=H\sqrt{\frac{t}{k\rho c}} \tag{7a}$$

and the complementary error function is

$$\text{erfc}\ (b)=1-\text{erf}\ (b)=\frac{2}{\sqrt{\pi}}\int_b^\infty e^{-\xi^2}d\xi \qquad (7b)$$

In the radiant panel flame-spread test, the irradiance varies along the surface of the specimen with the distance from the top [3]. If ignition of a given material may be represented by a characteristic surface temperature [7], then, for thin materials, this temperature is reached at the same position along the length of the specimen (same I and H) at exactly the same time, if the ρcl product is the same. For thick materials a similar situation exists if the $k\rho c$ product is the same. In other words, the ignition time (at each position) should be directly related to either ρcl or $k\rho c$. The product $k\rho c$ is commonly referred to as the thermal inertia for surface heating. Since the flame-spread factor F_s consists of a series of reciprocal time periods, inverse relationships of hyperbolic form are to be expected between F_s and ρcl for thin materials and between F_s and $k\rho c$ for thick materials.

3.3. Composite Materials

A solution for the surface temperature rise of a composite slab, in which the surface of the upper finite skin is irradiated in a spatial nonuniform manner (with or without surface heat loss), is unknown to the authors. However, examination may be made of the governing parameters in the following equation derived in reference [10] for the temperature rise, θ_s, on the surface of a composite material consisting of a finite skin of thickness l_1 (thermal properties k_1, ρ_1, c_1, where the thermal diffusivity $\alpha_1=k_1/c_1\rho_1$) over a substrate extending to infinity (thermal properties k_2, ρ_2, c_2, α_2) as the surface is heated without losses by constant irradiance I:

$$\theta_s=\frac{2I\sqrt{\alpha_1 t}}{k_1}\left[\frac{1}{\sqrt{\pi}}+2\sum_{n=1}^{\infty}\left(-\frac{1}{\gamma}\right)^n \text{ierfc}\ \frac{nl_1}{\sqrt{\alpha_1 t}}\right], \qquad (8)$$

where

$$\gamma=\frac{\sqrt{k_2\rho_2c_2}+\sqrt{k_1\rho_1c_1}}{\sqrt{k_2\rho_2c_2}-\sqrt{k_1\rho_1c_1}}=f\left(\frac{k_2\rho_2c_2}{k_1\rho_1c_1}\right)=f(\sigma). \qquad (9)^2$$

From this equation, the time, t, for a given surface temperature rise to be accomplished is a complicated function of $k_1\rho_1c_1$, l_1^2/α_1 and $\frac{k_2\rho_2c_2}{k_1\rho_1c_1}$. Griffith and Horton [10] illustrate that for a given skin material and for each time of heating, a critical thickness exists such that for greater thickness the composite assembly behaves essentially as a wall of infinite thickness of the skin material. For such cases, the substrate may be ignored so that the equation for the surface temperature reduces to that for a homogeneous thick wall, namely,

$$\theta_s=\frac{2I}{\sqrt{\pi}}\sqrt{\frac{t}{k_1\rho_1c_1}}, \qquad (10)$$

and the critical thickness is given very closely by

$$l_1'=\sqrt{\pi\alpha_1 t}. \qquad (11)$$

It is important to note from eqs (8), (10), and (11) that the surface temperature rise depends upon the thermal inertia $k\rho c$ while the critical thickness depends upon the thermal diffusivity, $\alpha=k/\rho c$.

4. Results and Discussion

While the analytical expressions for simple slabs listed in section 3 are strictly applicable only to uniformly irradiated slabs, the form in which the thermal and physical parameters appear is useful in interpreting the present data. These data were obtained using an experimental setup in which there is a nonuniform spatial irradiation, and interest has been confined to the travel of flames from the region of higher to the region of lower irradiance. While the expressions do not take into account heat flow in the direction of flame travel, this will occur in the actual test, particularly for highly conductive veneers and substrates, and for sandwich constructions. In addition, variations in the surface heat transfer coefficient are to be expected for the experimental arrangement used.

4.1. Thin Materials

To examine the effect of board thickness on flame propagation, veneers of balsa wood and hardboard were obtained or prepared in various thicknesses. These ranged from 0.071 to 1.26 cm for the balsa veneers and from 0.081 to 0.635 cm for the hardboard veneers. These materials were chosen because of their readily measurable rates of flame propagation, uniformity in structure (especially the hardboard) and availability. The hardboard veneers were cut from a single large sheet and planed to constant thickness. The density was uniform to ± 10 percent for all veneer thicknesses. However, the balsa wood sheets, obtained from a commercial source, varied in density by a factor of more than 2. In contrast to the standard flame spread test procedure, for this test series the veneers were supported at the edges only, leaving an enclosed air space of 1.27 cm between the back of the veneer and a backing sheet of 1.27-cm-thick asbestos millboard.

The ranges of measured thickness and densities, and average values of F_s and I_s are given in table 1 for specimens conditioned to equilibrium in relative humidities of 17, 50, and 86 percent. The average coefficient of variation for the F_s values listed was 4 percent for the hardboard specimens and 16 percent for the balsa specimens. Generally, four replicate tests were performed.

The effect that the relative humidity of the conditioning atmosphere has on surface flammability of materials has been given [2] for thick specimens of spruce, fiberboard, and hardboard. Since moisture vapor is readily dissipated from thin unsupported veneers, the relative change in F_s (and I_s) was not as large for the thin as for the thick hardboard specimens.

[2] As corrected.

TABLE 1. *Surface flammability test results for balsa and hardboard veneers*

Material	Thickness range	Density range	Flame spread factor, F_s^*			Flame spread index, I_s^*		
			17% rh	50% rh	86% rh	17% rh	50% rh	86% rh
	cm	*g/cm³*						
Balsa	0.071–0.081	0.206–0.279	67.7	55.9	54.4	410	317	325
	.147– .155	.120– .150	63.3	70.8	.....	417	404	.....
	.300– .305	.157– .221	41.1	35.7	.....	442	392	.....
	1.25 –1.26	.083– .147	62.6	45.3	.....	457	284	.....
Hardboard	0.081–0.086	0.975–1.04	17.5	18.5	15.4	314	302	255
	.150– .155	1.00 –1.04	10.9	10.2	.....	254	232	.....
	.297– .318	0.986–1.08	6.64	5.97	.....	207	175	.....
	.584– .635	.865–1.00	5.47	4.80	3.64	160	154	84

*All F_s and I_s values represent averages for 4 individual test specimens.

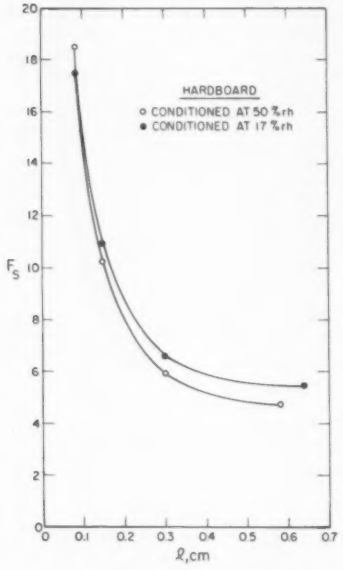

FIGURE 2. *Effect of veneer thickness on flame-spread factor for hardboard.*

An inverse relationship between the flame-spread factor and the thickness of veneer was found to hold for the hardboard specimens, as shown in figure 2. A thickness of approximately 0.4 cm may be taken as the approximate dividing region between thin and thick hardboard specimens, inasmuch as further increases in thickness appear to produce very little change in F_s.

Account was taken of the large density variations of the thin (0.08 to 0.30 cm) balsa specimens in the plot of F_s versus ρcl of figure 3. Individual values (rather than averages of four) were plotted for two conditioning humidities. Also included are the average values for thin (0.08 to 0.32 cm) hardboard specimens. Using a generalized CGS system of units [3] the data may be approximated by a relation of hyperbolic form:

$$F_s=5+\frac{1.5}{\rho cl}. \qquad (12)$$

[3] l: cm, ρ: g/cm³, c: w sec/g °C, k: w/cm °C.

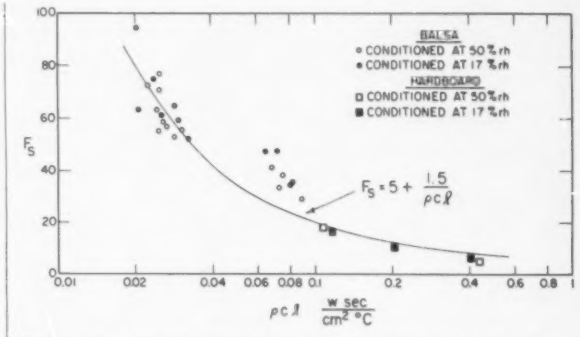
BALSA
○ CONDITIONED AT 50 %rh
● CONDITIONED AT 17 %rh
HARDBOARD
□ CONDITIONED AT 50 %rh
■ CONDITIONED AT 17 %rh
$F_s = 5 + \frac{1.5}{\rho c l}$
F_s
$\rho c l$ $\frac{w \text{ sec}}{cm^2 °C}$

FIGURE 3. *Flame-spread factor* versus *ρcl for thin balsa and hardboard veneers.*

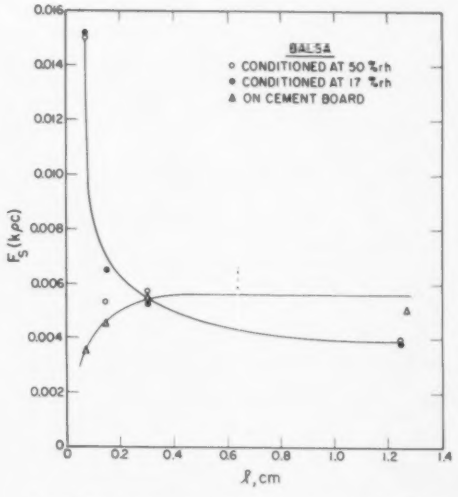

GU 4 *Effect of veneer thickness on modified flame-spread factor for balsa.*

Because of the inverse relationship between F_s and thermal inertia for thick materials, a second method for examining the combined effects of thickness and density is illustrated in figure 4. Here, the modified flame-spread factor, F_s $(k\rho c)$, for balsa (with no substrate) is seen to decrease with increasing thick-

ness and to approach a limiting value at a thickness of about 0.6 cm. The thermal conductivity values were taken at the measured density from room temperature values of cross-grain thermal conductivity of dry balsa [11, 12]. The effect of using an asbestos-cement board substrate with varying thickness of balsa veneer is also illustrated in figure 4 and will be discussed later.

4.2. Thick Materials

A survey of previous flame-spread data for thick cellulosic materials revealed a good correlation between flame-spread factor and thermal inertia (fig. 5). The data shown include the 1.2-cm-thick balsa woods conditioned at 17 and 50 percent rh, the 0.6-cm-thick hardboard, and a wide variety of other cellulose-base materials all conditioned at 50 percent rh. The specific heat and thermal conductivity values were taken from handbook sources and refer to dry material at room temperature. For materials which ranged from balsa (ρ=0.08 g/cm^3) to hardboard (ρ=1.08 g/cm^3), and including paper, cotton, fiberboard, plywood and nine varieties of natural wood, the data were closely represented by the relation

$$F_s=5+\frac{0.003}{k\rho c}. \qquad (13)$$

The fact that cellulosic materials do vary in their surface temperatures for ignition may explain part of the departure of the empirical relationships obtained experimentally (figs. 3 and 5) from that of a true hyperbola. On the basis of measured times for pilot ignition of woods exposed to uniform low-level irradiance [13], it was found that the calculated surface temperatures for ignition of cellulosic materials varied from 300 °C for hardboard to 390 °C for balsa, approximately, and the calculated surface temperatures were definitely related to thermal properties. Furthermore, the actual gaseous ignition process, not considered in this analysis, must likewise be a function of material properties.

4.3. Composite Materials

Another series of tests was performed to examine the effect of the type of substrate on the flame-spread factor of composite assemblies. The test specimens consisted of thin veneers (0.08 cm thick) of both balsa and hardboard cemented to a variety of relatively thick noncombustible substrates ranging from felted calcium silicate, a very good insulator, to conductive aluminum alloy. A thin coating of fire-retardant adhesive was used and sufficient pressure was applied during the drying process to ensure good thermal contact. Except for the thickest composite assemblies, all assemblies were backed up with the standard 1.27-cm-thick asbestos millboard backing. As shown in table 2 and in figure 6, the thermal inertia of the substrate has a very strong effect on the flame-spread factor of composite assemblies with thin surface veneers.

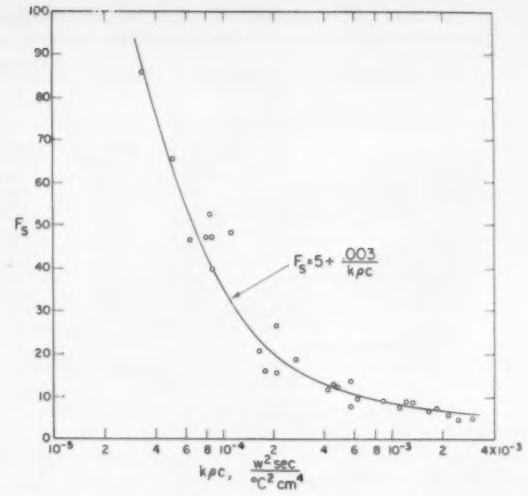

FIGURE 5. *Effect of thermal inertia on flame-spread factor for thick cellulosic materials.*

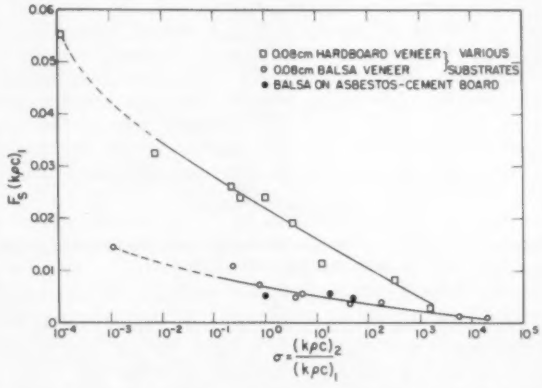

FIGURE 6. *Effect of thermal inertia ratio on modified flame-spread factor for a composite assembly with thin surface veneer.*

Although this was noted in previous studies [4, 6], neither the range of substrate properties nor the importance of the thermal inertia parameter had been fully explored. Furthermore, analysis of previous data on the basis of thermal inertia is complicated by the combustible nature of most of the substrates used in the earlier studies and their contribution (of heat) to flame propagation.

For example, it may be noted that a replot of previous flame-spread index data (fig. 3 of reference 4) on the basis of the F_s ratio rather than the I_s ratio results in an equally good (or better) correlation (see fig. 7). In addition, the F_s ratio approaches unity very closely for a finish thickness of 0.4 cm. That the ratio is higher than unity for composite materials with thin veneers even when the heat contribution of the substrate is not a factor, is obvious

TABLE 2. *Effect of substrate on surface flammability of composite assemblies with balsa and hardboard veneers*

Substrate	Thickness l	Density ρ	Thermal conductivity k	Specific heat c	Thermal inertia $k\rho c$	Balsa*		Hardboard*	
						F_s	I_s	F_s	I_s
	cm	*g/cm³*	*w/cm °C*	*w sec/g °C*	*w² sec/°C² cm⁴*				
None (air)	1.27	0.0012	0.000260	1.01	3.16×10^{-7}	55.9	317	18.5	302
Calcium silicate	0.635	.40	.000649	0.837	2.17×10^{-4}	28.2	142	10.9	172
Gypsum board	.698	.82	.00107	.837	7.35×10^{-4}	33.2	34	8.79	154
Asbestos millboard	1.27	.86	.00121	1.05	1.09×10^{-3}	25.1	47	8.08	75
Asbestos cement	0.474	1.88	.00745	0.837	1.17×10^{-2}	15.3	17	6.39	57
Granite	2.54	1.68	.0218	.795	2.91×10^{-2}	17.4	25	3.88	20
Stainless steel	0.670	8.00	.260	.502	1.04	7.18	13	2.74	10
Stainless steel	.061	7.94	.260	.502	1.03	20.1	85	10.1	166
Alluminum alloy	2.54	2.70	2.03	.921	5.05	4.22	3	1.00	0.2
Alluminum alloy	0.635	2.69	2.03	.921	5.03	12.0	19	4.98	40
Aluminum alloy	.051	2.69	2.03	.921	5.03	23.4	85	12.3	190

*Veneer 0.08 cm thick.

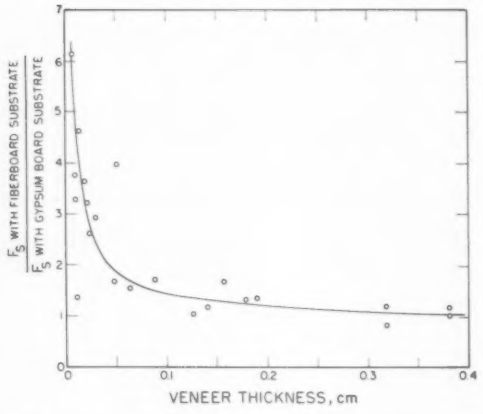

FIGURE 7. *Effect of veneer thickness on flame-spread factor ratio for two substrates.*

in terms of the findings of figure 6, namely, that for a composite material with a thin veneer, the value of F_s is higher with a substrate of lower $k\rho c$. Since $k\rho c$ (gypsum board substrate) $>k\rho c$ (fiberboard substrate) for composite materials with thin veneers,

$$\frac{F_s \text{ with fiberboard substrate}}{F_s \text{ with gypsum board substrate}}>1.$$

Several additional tests were performed to illustrate the effect of (a) the thickness of veneer and (b) the thickness of substrate on the flame-spread factor of composite assemblies. The first effect is clearly shown in figure 4 for various thicknesses of balsa veneers applied to an asbestos-cement board substrate. The substrate is most effective in reducing the (F_s) $(k\rho c)$ product for the thin veneers, but its influence becomes insignificant when the veneer thickness exceeds the critical thickness (0.6 cm).

Account may also be taken of the veneer thickness in the plot of figure 6 if the substrate is considered to consist of the portion of the balsa veneer exceeding 0.08 cm (but less than 0.6 cm) in combination with a thick asbestos-cement substrate. An "effective" thermal inertia, $(\overline{k\rho c})_2$, was calculated from the equation

$$(\overline{k\rho c})_2=\left(\frac{l-0.08}{0.6-0.08}\right)k_1\rho_1c_1+\left(\frac{0.6-l}{0.6-0.08}\right)k_2\rho_2c_2 \qquad (14)$$

where $0.08\leq l\leq 0.6$ cm.

The effective thermal inertia reduces to that of the substrate, $k_2\rho_2c_2$, when the veneer thickness is 0.08 cm. It becomes equal to that of the veneer, $k_1\rho_1c_1$, for a veneer thickness of 0.6 cm. Using the effective thermal inertia of the substrate, these data, shown as closed circles, were plotted along with the bulk of the data for 0.08-cm-thick balsa and hardboard veneers in figure 6.

Using eq (8), typical curves were calculated and are shown in figure 8 for "specific temperature rise" θ_s/I on the surface of a composite material in terms of the thickness l_1 of the veneer and the thermal inertia ratio $\sigma=k_2\rho_2c_2/k_1\rho_1c_1$ of substrate to veneer. It may be seen that, for veneers less than the critical thickness $(\sim\sqrt{\pi\alpha_1 t})$, the specific temperature rise will

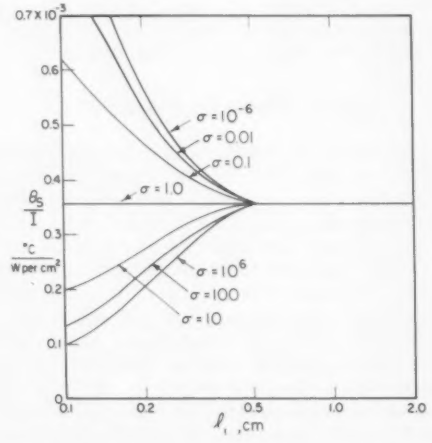

FIGURE 8. *Specific surface temperature rise for a composite material in terms of the veneer thickness (l_1) and the thermal inertia ratio (σ).*

Time: 100 sec, $k_1=.001$, $\alpha_1=.001$.

be greater than or less than the semi-infinite value (i.e., $\sigma=1$) according as the thermal inertia ratio is less than or greater than 1. It is clear that no finite amount of insulating or conductive substrate will permit attainment of the same surface temperature rise at the same time as the semi-infinite material. However, it is possible by employing the relationship of eq (11) to estimate the equivalent thickness of substrate which, when combined with a thin (i.e., less than critical) veneer, will yield the equivalent critical veneer thickness. If the critical thickness of balsa is taken to be 0.6 cm, then, for the same time and a balsa veneer thickness of 0.08 cm, the equivalent thickness of substrate may be estimated by

$$l_2'=\sqrt{\frac{\alpha_2}{\alpha_1}}\,(l_1'-l_1)=\sqrt{\frac{\alpha_2}{\alpha_1}}\,(0.6-0.08). \qquad (15)$$

Equivalent substrate thicknesses based upon a critical thickness of 0.6 cm for balsa and 0.4 cm for hardboard are listed in table 3. It may be noted that the thickness of the asbestos-cement substrate and the thickest stainless steel and aluminum alloy substrates used were each less than the equivalent thickness. Consequently, the limiting values of F_s for such assemblies were not fully reached. As expected, a wide range in the flame-spread factor was observed for composite assemblies of 0.08 cm balsa and hardboard veneers on varying thicknesses of aluminum alloy and stainless steel substrates (see table 2). In fact, for the hardboard veneer on 2.54-cm-thick aluminum alloy, the flame-spread factor was reduced to 1.0, corresponding to the complete absence of surface flaming. It should be mentioned that the application of a thin combustible veneer on a relatively thin, highly conductive substrate with an insulating backing board forms a unique sandwich construction. In the orientation of the flame-spread test, this type of construction is ideally suited to longitudinal rather than normal heat flow in the substrate, and this may have increased the rate of flame travel (and therefore F_s) for the thin metallic substrates.

TABLE 3. *Equivalent substrate thickness for thin (0.08 cm) veneers of balsa and hardboard*

Substrate	Actual thickness l_2	Thermal diffusivity α_2	Equivalent substrate thickness	
			Balsa veneer $\alpha_1=0.00223$	Hardboard veneer $\alpha_1=0.000892$
	cm	*cm²/sec*	$l_2'=0.52\sqrt{\alpha_2/\alpha_1}$ *cm*	$l_2'=0.32\sqrt{\alpha_2/\alpha_1}$ *cm*
Calcium silicate	0.635	0.00194	0.489	0.476
Gypsum board	.698	.00155	.437	.428
Asbestos millboard	1.27	.00135	.408	.398
Asbestos cement	0.474	.00473	.760	.745
Granite	2.54	.0122	1.23	1.20
Stainless steel	0.061–0.670	.0646	2.82	2.76
Aluminum alloy	.051–2.54	.816	10.0	9.78

It is interesting to note that asbestos millboard ($\alpha=0.00135$) which is used as the backing material in the standard flame-spread test has a critical thickness of 1.95 cm at a time of 900 sec corresponding to the maximum duration of test exposure. Although the backing used is only 1.27 cm thick, it does provide a common heat sink for all materials and may be considered semi-infinite for the important early portion of every test.

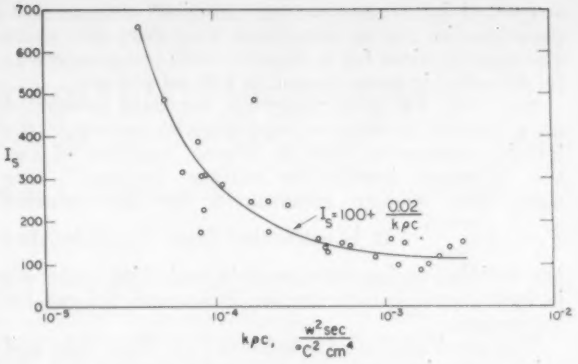

FIGURE 9. *Effect of thermal inertia on flame-spread index for thick cellulosic materials.*

While surface propagation of flame in the flame-spread test is related predominantly to the ignition sensitivity of the material (here expressed as the flame-spread factor F_s), fire spread in actual situations also depends upon the rate of heat release by the burning surfaces. The magnitude of the rate of heat release depends mainly upon the thickness involved in the flaming and the material density. Study of the Q values for the hardboard veneers shows a steady increase for thicknesses from 0.08 cm to 0.32 cm with little further increase for the 0.64-cm thickness. The combination of a decreasing flame-spread factor and an increasing heat evolution factor with thickness tends to yield a flame-spread index for which the variation with thickness is moderate. The effect of thickness upon I_s is shown in table 1. Examination of the influence of substrate properties for composite assemblies was made with the same thickness of balsa and hardboard veneers, and therefore the I_s values in table 2 follow very closely the trend of F_s. Because of the effect of density upon Q and since the thickness involved in flaming varies for different materials, a plot of I_s versus $k\rho c$ for all the thick cellulosic materials tested (see fig. 9) shows considerably more scatter than that shown for F_s in figure 5. The data may be represented approximately by the relation

$$I_s=100+\frac{0.02}{k\rho c}. \qquad (16)$$

5. Summary

Surface flame propagation measurements using the radiant panel test method have shown that the ignition sensitivity (flame-spread factor F_s) for thin balsa and hardboard veneers was an inverse function of both thickness and density. The data were analyzed in terms of the approximate relationship

suggested by Simms for the transient surface temperature rise for an irradiated thin slab, for which the time required for a characteristic temperature to be achieved is proportional to the ρcl product.

Similarly, for thick materials, the data assembled on a variety of cellulosic materials showed that the ignition sensitivity was an inverse function of $k\rho c$, the "thermal inertia for surface heating." The data were closely represented by the relation $F_s=5+\frac{0.003}{k\rho c}$. It is estimated from the data that the dividing region between thin and thick materials is approximately 0.6 cm for balsa and 0.4 cm for hardboard.

The good correlations achieved for both thin and thick materials support a simple concept for the spread of flame on the surfaces of cellulosic materials exposed to thermal radiation, namely that flame propagation consists of progressive ignition of the solid when a characteristic temperature is reached.

For a composite assembly consisting of a thin veneer over a semi-infinite substrate, the flame-spread factor was shown to be a function of the ratio of the thermal inertia of substrate to veneer. This is in accordance with the functional relationship for the transient surface temperature rise for composite assemblies. For veneers less than a critical thickness ($\sim\sqrt{\pi\alpha_1 t}$), the specific temperature rise at any given time will be greater or less than the semi-infinite value according as the thermal inertia ratio is less than or greater than 1. The substrate has the most effect upon the surface temperature with the thinnest veneer and with the greatest change in $k\rho c$ value from that of the veneer. For thin veneers over highly conductive substrates such as metals, estimates have been made which indicate that the equivalent critical substrate thickness may be several times that tested. This provides an explanation for the observed wide variation in flame-spread factor with metal substrate thickness.

Since fire spread depends on the rate of heat release as well as the ignition sensitivity, the combined effect was also evaluated, and for thick cellulosic materials the data were represented by the relation,

$$I_s=100+\frac{0.02}{k\rho c}.$$

6. References

[1] Interim Federal Standard No. 00136a (Comm.-NBS) (June 30, 1961). Available from General Services Administration Regional Offices.

[2] A. F. Robertson, Surface flammability measurements by the radiant panel method, ASTM, Special Technical Publication (1963) (in press).

[3] A. F. Robertson, D. Gross, and J. J. Loftus, A method for measuring surface flammability of materials using a radiant energy source, ASTM Proc. **56,** 1437–53 (1956).

[4] D. Gross and J. J. Loftus, Flame spread properties of building finish materials, ASTM Bulletin, 56–60 (May 1958).

[5] D. Gross, Flame-spread measurements by the radiant panel flame-spread method, Forest Products J. **10,** 33–36 (Jan. 1960).

[6] D. Gross and J. J. Loftus, Surface flammability of fire-retardant and conventional paint assemblies, Fire Res. Abstr. and Rev. **3,** 151–8 (1961).

[7] D. L. Simms, Ignition of cellulosic materials by radiation, Combustion and Flame **4,** 293–300 (Dec. 1960).

[8] H. S. Carslaw and J. C. Jaeger, Conduction of heat in solids, 2d Ed., Sec. 3.11 (Clarendon Press, Oxford, 1959).

[9] D. I. Lawson, L. L. Fox, and C. T. Webster, The heating of panels by flue pipes, Fire Research Special Report No. 1, Dept. of Scientific and Industrial Research and Fire Offices, Committee, London (1952).

[10] M. V. Griffith and G. K. Horton, The transient flow of heat through a two-layer wall. Proc. Phys. Soc. **58,** 481–7 (1946).

[11] International Critical Tables (McGraw-Hill Book Co., New York, N.Y.).

[12] T. W. Watson, Heat Transfer Section, NBS (private communication).

[13] A. J. Buschman, Jr., Fire Research Section, NBS (private communication).

(Paper 67C3–136)

JOURNAL OF RESEARCH of the National Bureau of Standards—C. Engineering and Instrumentation
Vol. 67C, No. 3, July–September 1963

Parallel Reversible Permeability Measurement Techniques From 50 kc/s to 3 Gc/s*

Cletus A. Hoer and R. D. Harrington

(April 30, 1963)

New measurement techniques are described for determining the complex reversible permeability of ferrimagnetic materials from 50 kc/s to 3 Gc/s with d-c fields applied parallel to the rf fields in toroidal specimens. In the 50 kc/s to 50 Mc/s range, emphasis is directed towards recent improvements in the rf permeameter. For measurements in the 50 Mc/s to 100 Mc/s range, the feasibility of using variable length re-entrant cavities with quarter wavelength chokes is demonstrated. Two half-wave variable length cavities are described for obtaining reversible permeability data in the 100 Mc/s to 3000 Mc/s range. A technique for avoiding the use of quarter wavelines for isolating the d-c and rf circuits in these half-wave cavities is emphasized and represents a definite improvement over corresponding slotted line methods. A brief description of the d-c circuitry developed for these measurements as well as some typical spectrum data is also given.

1. Introduction

Considerable effort has been directed in recent years towards the study of the magnetic spectra of ferrite and garnet materials in the radio and microwave frequency ranges. This work is in general concerned with an evaluation of the frequency spectrum of the initial complex permeability ($\mu_i^* = \mu_i' - j\mu_i''$) in which only an rf field is applied to the sample or the measurement of the reversible complex permeability ($\mu^* = \mu' - j\mu''$) in which a d-c magnetic field is superimposed on the rf field. Several investigations of the dependence of the initial permeability spectrum on the composition of ferrites, the temperature environment, etc., have also been reported. However, the reversible permeability spectra studies with the applied d-c fields appears to be one of the more promising techniques for gaining further information concerning the resonance and relaxation phenomena observed in the magnetic spectra. Nevertheless, there has been relatively little work in this area compared to the effort that has been directed towards initial permeability spectra measurements.

Previous studies of the parallel reversible permeability spectra of ferrites as a function of frequency with applied d-c fields have been confined to measurements covering relatively limited frequency ranges such as the radiofrequency range or the microwave range [1–5].[1] These investigations have utilized primarily inductance coil measurements for obtaining data at lower frequencies or slotted line techniques for obtaining information at higher frequencies. It is the purpose of this paper to describe the use of the radiofrequency permeameter, and variable length re-entrant and half-wave length cavities for obtaining the reversible permeability of ferrimagnetic toroidal materials over the frequency range from 50 kc/s to 3 Gc/s with d-c fields applied parallel to the rf fields. Recent improvements in the permeameter as well as some of the advantages of variable length half-wave coaxial cavities over slotted lines for measurements of this type will be emphasized.

2. Radiofrequency Permeameter, 50 kc/s to 50 Mc/s

The advantages of the radiofrequency permeameter over inductance coil methods or coaxial transmission line techniques for initial permeability measurements at frequencies below 50 Mc/s have been discussed in the literature [6]. The satisfactory results obtained using the permeameter made it seem reasonable to extend its application to the measurement of reversible permeability. Therefore, the permeameter was modified to make parallel reversible permeability measurements by enclosing it in a d-c coaxial line as shown in figure 1. The d-c coaxial line may enclose the whole permeameter [7] as in figure 1a or only that part which encloses the sample, figure 1b. Both methods were used, and although the latter design is more difficult to make, it proved to be the better instrument. If the d-c coaxial line encloses the whole permeameter, the d-c field is applied to the primary core as well as to the sample being measured. The varying d-c field changes the characteristics of the primary which results in errors that are difficult to correct. The coupling between rf and d-c circuits is greater when the whole permeameter is enclosed, creating a need for filters in the d-c circuit from below 1 Mc/s to 50 Mc/s. When the primary was not enclosed by the d-c coaxial line, as in figure 1b, the primary was not affected by the d-c current, and filters were

*This work was partially supported by the Department of the Navy under a Bureau of Ships contract.

[1] Figures in brackets indicate the literature references at the end of this paper.

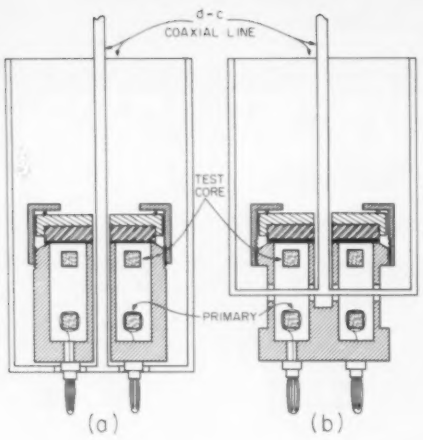

FIGURE 1. *Radiofrequency permeameter with d-c coaxial line to provide a d-c field parallel to the rf field.*

The d-c coaxial line in (b) cuts through the center of the permeameter to avoid applying the d-c field to the primary core.

needed only above 4 Mc/s. These filters are parallel L–C circuits tuned to have a maximum impedance at the frequency at which measurements are being made. The maximum impedance Z_{max} of such an L–C circuit at a frequency ω is approximately

$$Z_{max}=\frac{Q}{\omega C}$$

In addition to the requirements of high Q and low resonating capacitance, C, the characteristics of the filter must not change appreciably with greatly varying d-c currents. Good results were obtained with large powdered iron SF cores wound with bare No. 8 soft copper wire. The capacitors were small, variable mica capacitors. Up to 400 amps were applied for short periods of time with no significant change in Z_{max}. It was necessary to use a filter in both d-c leads to completely eliminate all external rf paths. Each filter was connected separately and tuned to give a maximum Q for the permeameter with the secondary closed and empty. These filters, the d-c leads, and connections for water cooling the center conductor of the d-c coaxial line are shown in figure 2. An exploded view of the permeameter and d-c coaxial line is shown in figure 3.

The measurement of reversible permeability is made in the same way as is the initial permeability, except for the application of the d-c field. A recent study of the permeameter equations for evaluating μ' and μ'' has resulted in a set of exact equations which are independent of the transformer characteristics [8]. The permeameter is represented by a T-network which is evaluated at a given frequency using a stable, low loss standard sample of known μ' and μ''. Using a standard sample in calibrating the permeameter, the procedure in measuring the reversible permeability of a sample is to measure the

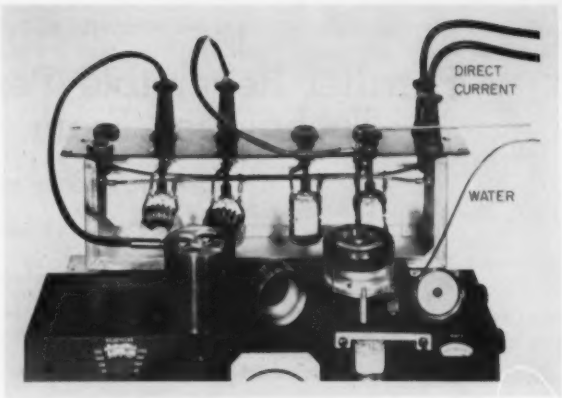

FIGURE 2. *Permeameter with d-c outer conductor (left) and shorting plate (right) removed.*

The filters are shown behind the Q-meter.

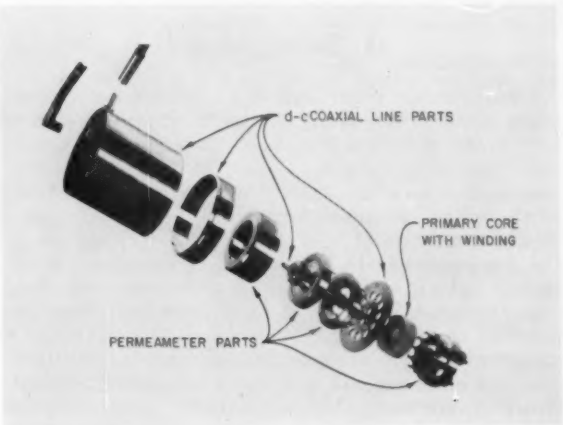

FIGURE 3. *Exploded view of permeameter of the type shown in figure 1b showing how d-c coaxial line is constructed through center of the permeameter.*

input impedance, Z_{in}, of the permeameter for the following conditions:

1. Secondary open; $Z_{in}\equiv Z_1$.
2. Secondary closed; no sample enclosed; $Z_{in}\equiv Z_0$.
3. Secondary closed; standard sample of known impedance Z_s enclosed; $Z_{in}\equiv Z_{f'}$.
4. Secondary closed; test sample enclosed; $Z_{in}\equiv Z_f$.

The d-c current is then turned on and Z_f measured at each desired value of current. The permeability, μ', and loss, μ'', of the test sample are then calculated at each current setting from

$$\mu''+j(\mu'-1)=\frac{Z_s}{\omega L_a}\left(\frac{Z_{f'}-Z_1}{Z_{f'}-Z_0}\right)\left(\frac{Z_f-Z_0}{Z_f-Z_1}\right) \qquad (1)$$

where L_a is the equivalent air inductance of the test sample and ω is the angular frequency. All input impedances (Z_1, Z_0, $Z_{f'}$, Z_f) are measured with the d-c leads connected to the coaxial line surrounding the permeameter.

3. Variable Length Re-entrant Cavity, 50 to 100 Mc/s

The upper frequency limit of the permeameter is about 50 Mc/s. Above 50 Mc/s slotted lines or cavities are in general used for initial permeability measurements. Slotted lines have been used in the 50 to 100 M/cs range but are cumbersome due to their large length. Somewhat smaller re-entrant cavities have also been used in the same frequency range by noting variations in either capacity or frequency for determining their resonant properties [9–12]. Measurements with a re-entrant cavity may also be made in terms of variations in length of the cavity [9]. The latter method has several advantages over the variable capacitance or the variable frequency method in that no capacity calibration need be made or no expensive frequency measuring equipment is needed. It is also possible to more easily minimize errors due to supports and discontinuities in the line which may become significant at higher frequencies.

On the basis of the above information, an investigation was carried out to determine if a variable length re-entrant cavity can be adapted for obtaining reversible permeability measurements. As in the case of the permeameter, it is necessary to isolate the d-c and rf circuit from each other. However, above 50 Mc/s it is difficult to use lumped circuit chokes for this purpose. On the other hand, the successful use of quarter wavelength transmission lines for this purpose by other investigators using slotted lines for their reversible permeability measurements suggests that the quarter wave choke method may also be applicable for re-entrant cavities.

The arrangement which we have found to give the best results is shown in figure 4. In this case the d-c current passes through the center conductor of the cavity in order to provide the circumferential field in the vicinity of the sample. The d-c current was confined to the center conductor by placing a thin sheet of insulation between the mounting flange of the quarter wavelength short and the cavity. No rf current could be detected in the d-c circuit outside of the cavity when the choke was tuned to approximately a quarter wavelength. It was observed that the setting of the quarter wavelength line is not critical for completely isolating the d-c and rf circuits.

The complex permeability may be evaluated from a determination of the change in the resonance length and Q of the cavity due to insertion of the sample. The equations and procedure for obtaining data are the same as those given in the next section describing variable length half-wave coaxial cavities. Essentially the same equations have also been given by van der Burgt, Gevers, and Wijn [9] who describe a variable length re-entrant cavity for initial complex permeability measurements. However, in their instrument, copper rings having the same dimensions as the sample were measured in order to obtain simplified equations.

The restrictions on the use of such instruments noted by the above authors such as high Q, small

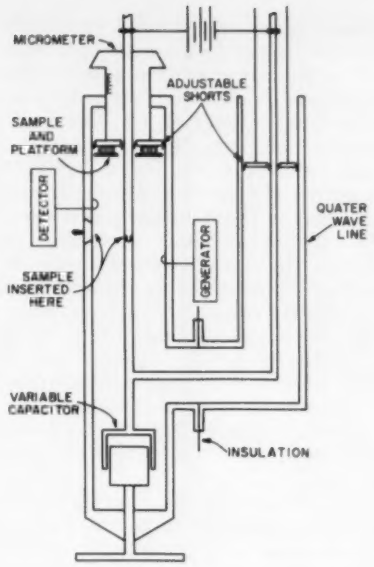

FIGURE 4. *Variable length re-entrant cavity with quarter wavelength line used from 50 to 100 Mc/s.*

The length of the quarter wavelength line relative to the reentrant cavity will in general be somewhat greater than indicated in the above simplified schematic.

length changes, etc., are also applicable to our instrument. A Q of several hundred, obtained with our instrument, appears to be satisfactory for determining the loss of most materials from 50 to 100 Mc/s. In addition, we have found it necessary to give consideration to possible errors due to temperature changes of the center conductor resulting from the large d-c currents required to obtain the bias fields. Such errors can be either eliminated by water cooling the center conductor or corrected for by making two identical runs, one with the sample in the cavity and one with the cavity empty. In our case, the latter method proved to be more feasible since some mechanical difficulty was experienced in obtaining water cooling in a cavity of this type.

4. Variable Length Half-Wave Cavities, 100 to 3000 Mc/s

The combination lumped and transmission line circuitry used in the previously described re-entrant cavity may result in somewhat more difficulty in the mechanical design of the instrument and in the rigorous analysis of the working equations than is the case for completely distributed parameter systems. As such, most magnetic spectra studies of the initial complex permeability in the range above about 100 Mc/s have utilized slotted line techniques. Somewhat less information has been reported on the use of variable length coaxial half-wave cavities for obtaining data of this type [13].

The measurement of parallel reversible permeability at these higher frequencies has been confined exclusively to the use of slotted lines in which the d-c circuit is isolated from the rf circuit by means of a quarter wavelength line [1, 3, 4]. On the other hand, an examination of variable length cavities suggests that an insulated d-c conductor could be placed through a hollow rf center conductor of such a cavity and thereby isolate the d-c from the rf signal without the use of a quarter waveline. Because of this advantage and our previous successful use of variable length cavities for initial permeability measurements, we developed two variable length cavities with hollow center conductors containing insulated d-c conductors. No coupling between the rf and d-c circuits was observed in either instrument. Since complete isolation is obtained without the use of a quarter waveline, this is a distinct advantage over slotted line techniques for reversible permeability measurements.

The design of both of these cavities was based on the Chipman method for impedance measurements [14]. Both cavities were mounted in a vertical position in order to avoid any supports on the center conductor. One of the instruments was designed for measurements below 300 Mc/s, while a smaller, more precise instrument was used for obtaining data above 300 Mc/s.

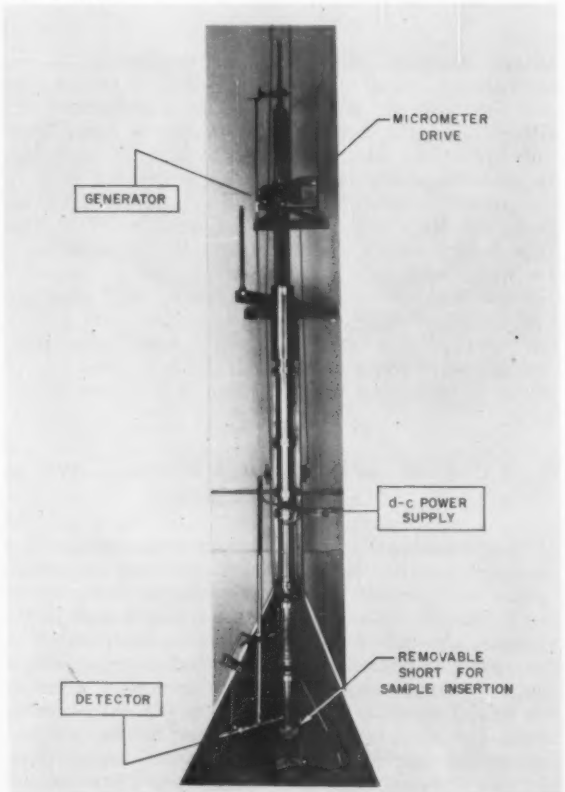

FIGURE 5. *Half-wave variable length cavity used at 100 Mc/s, 200 Mc/s, 300 Mc/s, etc.*

The larger instrument shown in figure 5 is presently designed for obtaining data at frequencies in the vicinity of 100, 200, and 300 Mc/s using 1, 2, or 3 half wavelengths respectively. The Q at these frequencies varies from 400 to 700. Continuous frequency coverage at these low frequencies would require a rather long micrometer drive. In lieu of this approach, the line has been constructed in removable sections to provide for coarse adjustments in length if information at other frequencies should be desired in the future. The general features of the instrument are similar to those shown in figure 6 which is actually a schematic for the higher frequency cavity described below.

Although the above described cavity can be used above 300 Mc/s, it was more convenient to design and construct a smaller, more precise instrument capable of continuous frequency coverage for measurements from 300 to approximately 3000 Mc/s. As in the case of the larger cavity, multiple half wavelengths can be used to obtain resonance at the higher frequencies. In addition, this cavity has the added advantage of a continuously variable coarse adjustment of length for changing the frequency range of the instrument. This adjustment was obtained by

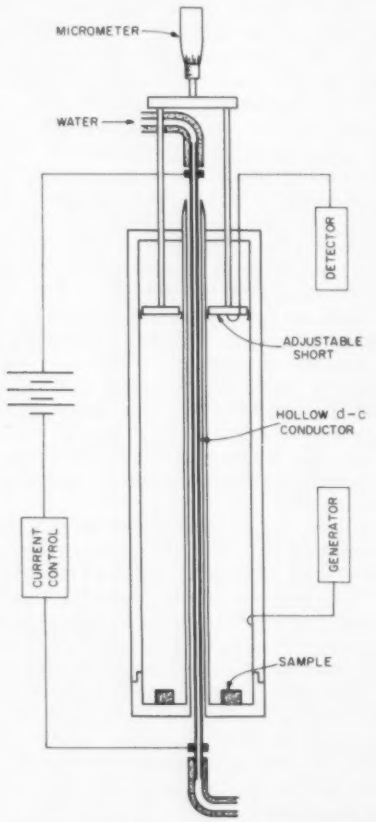

FIGURE 6. *Drawing of the 300–3000 Mc/s variable length cavity.*

A d-c field is applied to the sample by sending direct current through a d-c conductor which is placed inside of and insulated from the hollow rf center conductor.

threading the outside conductor of the cavity for a considerable distance as can be seen in figure 7. The cavity also has a higher Q, ranging from 500 to 3000, depending on frequency. To avoid any discontinuities near the sample at high frequencies, the center conductor and shorting plate of the 300 to 3000 Mc/s cavity were constructed as one piece as can be seen in figure 6. This arrangement gives a uniform distribution of rf current around the center conductor where it joins the shorting plate, and hence a uniform rf field for the sample which rests on the shorting plate. The cavity is opened for inserting the sample by removing the whole center conductor-short assembly. The cavity was prevented from heating up when the direct current was applied by making the d-c conductor out of ⅛ in. tubing through which water was circulated for cooling.

The complex permeability may be readily evaluated from a determination of the changes in resonant length and Q of the cavity when the sample is inserted. The toroidal sample which is placed against the shorted end of the line has a thickness small compared to a quarter wavelength in the material in order that dielectric effects do not influence the magnetic permeability measurements. Our experience has indicated that it is not difficult to obtain sufficiently thin ferrites so that the dielectric effect is negligible at least to 1 Gc/s and in some cases to 3 or 4 Gc/s.

For sufficiently small changes in the parameters of high quality lines, the complex permeability ($\mu^* = \mu' - j\mu''$) may be calculated from the equations

$$\mu' - 1 = \frac{\Delta L}{d}$$

$$\mu'' = \frac{\Delta l_f - \Delta l_e}{2d}$$

where it is assumed that the sample of thickness d has the same radial dimensions as the coaxial line. The remaining quantities in the equations are obtained from the following length measurements.

ΔL=The difference between the resonance length of the empty cavity and the resonance length of the cavity when the sample is placed against the short.

Δl_e=The difference between the two lengths of the empty cavity for which the power level is ½ the maximum value at resonance.

Δl_f=The difference between the two lengths of the cavity with the sample for which the power level is ½ the maximum value at resonance.

An excellent analysis of variable length cavities for initial permeability measurements in which these equations are developed in essentially the above form has been given by Eichacker [13, 15]. His work also demonstrated that variable length lines and slotted lines both work with the same evaluation formula. In this respect, it should be noted that the above equations have also been obtained in similar form by other authors using slotted line techniques [16].

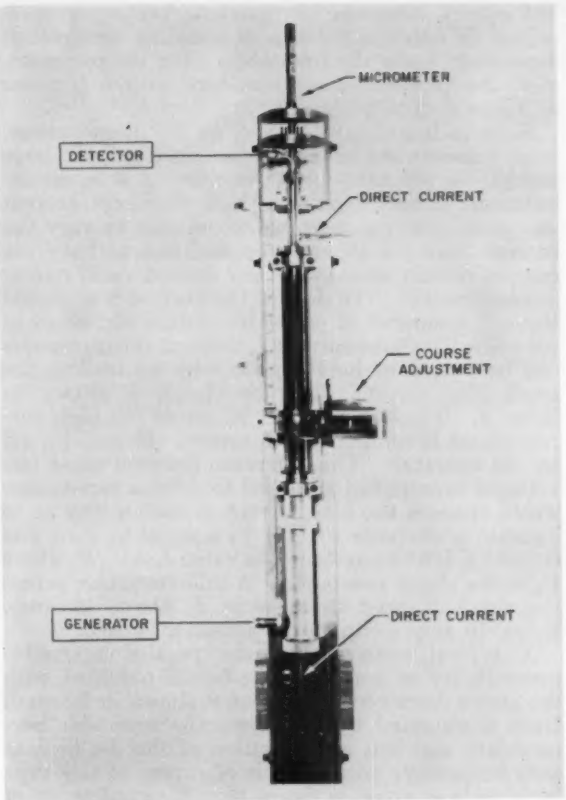

FIGURE 7. *Half-wave variable length cavity used at 300–3000 Mc/s.*

In many cases, it may not be convenient to obtain samples which have the same radial dimensions as the coaxial line. However, following the approach used by Bady and Franklin [10], the above equations may be written in the following form for loose fitting samples.

$$\mu' - 1 = \frac{\log \frac{B}{A}}{\log \frac{b}{a}} \frac{\Delta L}{d}$$

$$\mu'' = \frac{\log \frac{B}{A}}{\log \frac{b}{a}} \frac{(\Delta l_f - \Delta l_e)}{2d}$$

where the toroidal sample of inner radius a and outer radius b is located in the coaxial line of radii A and B.

5. Associated Equipment and Results

The rf equipment used with the half-wave cavities and re-entrant cavity consisted of commercially available signal sources with pads and matching stubs for the input circuit as well as facilities for monitoring the frequency of the system. The out-

put circuit consisted of matching stubs and calibrated IF detector systems or standing wavemeters depending upon the frequency. For the permeameter, the impedances are measured with a Q meter or Maxwell-type bridge.

Since in the cavities as well as the permeameter, large currents are needed to obtain d-c fields large enough to saturate many samples, a 6 v nickle-cadmium battery capable of high discharge current was used. It was desirable to be able to vary the current from 0.5 to 500 amp and also to have the current remain constant at any desired value during a measurement. To do this the current was passed through a number of power transistors connected in parallel. The large current I_c through the transistors can be varied or held constant by controlling the small bias current I_B. The circuit is shown in figure 8. The voltage drop V_s across the high current shunt is compared to a control voltage, V_c, set by the operator. The difference between these two voltages is amplified and used to drive a servomotor which changes the bias current in such a way as to increase or decrease I_c until V_s is equal to V_c. The current I_c is held constant at a value $I_c = V_c/R_s$ where R_s is the shunt resistance. A millivoltmeter across the shunt is used to measure I_c above 10 amp. Below 10 amp a clip on d-c ammeter is used.

A typical spectrum of the parallel reversible permeability of a magnesium ferrite obtained with the above described equipment is shown in figure 9. Data is obtained by measuring the reversible permeability and loss as a function of the d-c field at each frequency. An example of curves of this type for μ' only is given in figure 10. A complete set of these curves at all desired frequencies enables the spectrum to be obtained for any desired current. This data indicates that the above described equipment provides a highly satisfactory method for obtaining reversible permeability spectra information.

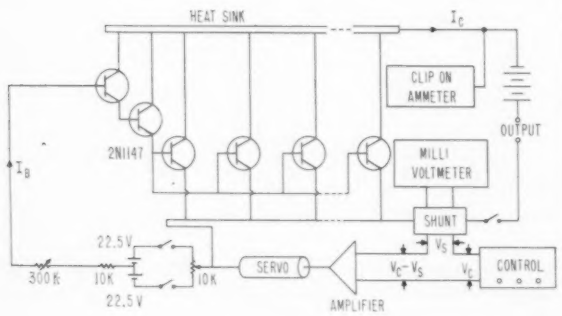

FIGURE 8. *Direct current control for varying or holding constant large d-c currents.*

The output current I_c passed by the power transistors is controlled by the bias current I_B. A control voltage V_c is compared to V_s and the difference amplified to drive a servo which adjusts I_B in such a way so as to increase or decrease I_c until $V_s = V_c$. I_c is changed by changing V_c.

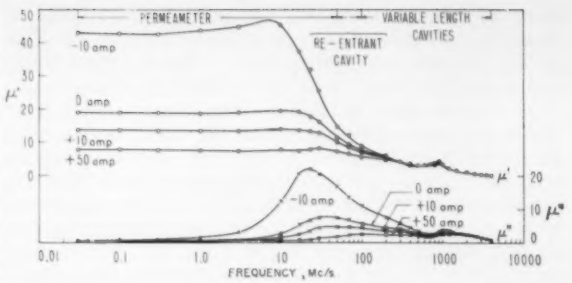

FIGURE 9. *Typical spectrum of the parallel reversible permeability of a magnesium ferrite.*

Data obtained from curves such as shown in figure 10. Sample dimensions outside diameter = 0.961 in., inside diameter = 0.678 in., thickness = 0.040 in.

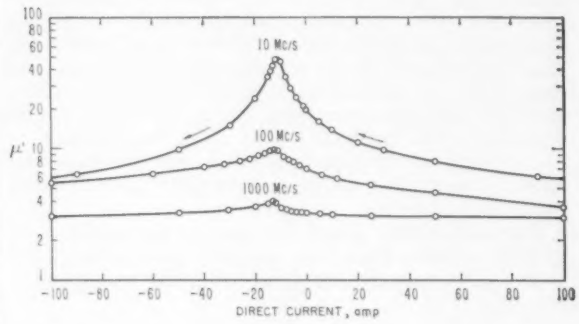

FIGURE 10. *Typical results of parallel reversible permeability versus applied d-c current.*

The sample was cycled at ±100 amps several times before measurements were made in the direction indicated by the arrows.

The authors thank W. A. Pittman for making the many measurements and calculations, and M. B. Lindell and G. A. Boschen for construction of the instruments.

6. References

[1] Brastins, A., and Williams, E. M., Separation of magnetic losses in UHF ferrites, IRE Trans. Instr. **I–10,** No. 2-63–67 (Sept. 1961).

[2] Fomenko, L. A., An investigation of magnetic spectra of of solid solutions of some NiZn-ferrites in the radio frequency range, Soviet Physics JETP **3,** No. 1, 19–28 (Aug. 1956).

[3] Harvey, R. L., Gordon, I., and Braden, R. A., The effect of a d-c magnetic field on the UHF permeability and losses of some hexagonal magnetic compounds, RCA Review **22,** 648–657 (Dec. 1961).

[4] Miles, P. A., Westphal, W. B., and von Hippel, A., Dielectric spectroscopy of ferromagnetic semiconductors, Reviews of Modern Physics **29,** No. 3, 279–307 (July 1957).

[5] Lombardini, P. P., Schwartz, R. F., Ferrites for high-power R-F tuning, Elec. Mfg. **62,** 60–71 (Aug. 1958).

[6] Haas, P. H., A radio-frequency permeameter, J. Research NBS **51,** No. 5, 221–228 (Nov. 1953) RP2454.

[7] Rasmussen, A. L., Hess, A. E., R-F permeameter techniques for testing ferrite cores, Elec. Mfg. **61,** No. 5, 86 (May 1958).

[8] Hoer, C. A., Rasmussen, A. L., Equations for the radio-frequency magnetic permeameter, J. Research NBS **67C,** (Eng. and Instr.) No. 1, 69–76 (Jan.–Mar. 1963).

[9] van der Burgt, C. M., Gevers, M., Wijn, H. P. J., Measuring methods for some properties of ferroxcube materials, Philips Technical Review **14,** No. 9, 245–256 (Mar. 1953).

[10] Bady, I., Franklin, R. J., Measurement of permeability and Q of magnetic materials over the frequency range of 50 to 500 Megacycles, Engineering Report 1159, Signal Corps Engineering Laboratories, Fort Monmouth, N.J. (Sept. 30, 1955) Published in 1957 IRE National Convention Record **5,** Pt 5, 137–145 (1957).

[11] Lindenhovius, H. J., van der Breggen, J. C., The measurement of permeability and magnetic losses of non-conducting ferromagnetic materials at high frequencies, Philips Research Reports **3,** 37–45 (Feb. 1948).

[12] Harrington, R. D., Powell, R. C., Haas, P. H., A re-entrant cavity for measurement of complex permeability in the very-high-frequency region, J. Research NBS **56,** No. 3, 129–134, (Mar. 1956) RP2657.

[13] Eichacker, R., A material-characteristics test assembly for determining the electromagnetic material constants of solid and liquid media at frequencies between 30 and 7000 Mc and temperatures between −60 and +240 °C, Rohde and Schwarz-Mitteilungen, No. 11, 185–205 (Dec. 1958), English Edition (Aug. 1959).

[14] Ginzton, E. L., Microwave measurements, p. 287 (McGraw-Hill New York, N.Y., 1957).

[15] Eichacker, R., Stoffmessung mit Messleitungen, Rohde and Schwarz-Mitteilungen, No. 15, 15–27 (Apr. 1961).

[16] Conrad, E. E., Porter, C. S., Doctor, N.J., and Franklin, P. J., Extension of the "thin-sample method" for the measurement of initial complex permeability and permittivity, J. Appl. Phys. **27,** No. 4, 346–350 (Apr. 1956).

(Paper 67C3–137)

JOURNAL OF RESEARCH of the National Bureau of Standards—C. Engineering and Instrumentation
Vol. 67C, No. 3, July–September 1963

Publications of the National Bureau of Standards*

Selected Abstracts

An absolute calibration of the National Bureau of Standards Thermal Neutron Flux, E. J. Axton, *J. Research NBS* **67A** (*Phys. and Chem.*), *No. 3, 215–230* (*May–June 1963*).
The NBS Thermal Neutron Flux has been calibrated in terms of the gold thermal neutron capture cross section. The effective thermal neutron (below cadmium cutoff energy) flux density is estimated to be 4307 ± 2 percent n/cm^2 sec in September 1961. This figure is in agreement with a recent value quoted by the NBS.

Purity analysis of highly purified materials by time-temperature cryometry, G. S. Ross and H. D. Dixon, *J. Research NBS* **67A** (*Phys. and Chem.*), *No. 3, 259–263* (*May–June 1963*).
Visual observation of the freezing and melting of compounds in cells used for the determination of purity has uncovered some heretofore unexpected behavior. This behavior has been correlated with certain difficulties experienced in the measurement of purity, particularly when the sample is very pure. Means for partially reducing these difficulties are proposed and procedures for increasing the accuracy of purity measurements are described.

Analysis of families of curves, J. Mandel and F. L. McCrackin, *J. Research NBS* **67A** (*Phys. and Chem.*), *No. 3, 271–279* (*May–June 1963*).
A systematic approach is presented for fitting empirical expressions to data depending on two variables. The problem can also be described as the simultaneous fitting of a family of curves depending on a parameter.
The proposed method reduces a surface fitting problem to that of fitting a few functions of one variable each. First, the surface is expressed in terms of these one-variable functions, and using an extension of two-way analysis of variance, the accuracy of this fit is assessed without having to determine, at this point, the nature of one-variable functions. Then, the one-variable functions are fitted by customary curve-fitting procedures.
For illustration, the method is applied to two sets of experimental data.

A controlled atmosphere chamber, C. L. Gordon and R. B. Johannsen, *J. Research NBS* **67A** (*Phys. and Chem.*), *No. 3, 281–283* (*May–June 1963*).
An inert atmosphere chamber for the transfer of reactive materials is described. It has the advantages of being inexpensive and easily cleaned, and can be evacuated.

The meaning of Betti's reciprocal theorem, C. Truesdell, *J. Research NBS* **67B** (*Math. and Math. Phys.*), *No. 2, 85–86* (*Apr.–June 1963*).
It is demonstrated that Betti's reciprocal theorem represents a criterion for the existence of a stored-energy function.

Effect of molecular weight on viscoelastic properties of polymers as predicted by a molecular theory, H. Oser and R. S. Marvin, *J. Research NBS* **67B** (*Math. and Math. Phys.*), *2, 87–90* (*Apr.–June 1963*).
Calculations have been made covering the predictions of a model representing the viscoelastic behavior of rubberlike polymers for molecular weights greater then M_c, M_c being the lower limit of the range in which the viscosity is proportional to $M^{3.4}$. A pronounced difference in the character of G'' is predicted for polymers with molecular weights between 5 and 10 times M_c as compared with those whose molecular weights are outside this range.

Asymptotic behavior of the current on an infinite cylindrical antenna, K. S. Kunz, *J. Research NBS* **67D** (*Radio Prop.*), *No. 4, 417–431* (*July–Aug. 1963*).
An asymptotic expression is obtained for the currnet distribution on the outside surface of an infinitely long, perfectly conducting, hollow cylindrical antenna that is fed by an infinitesimally narrow circumferential gap. This asymptotic expression involves two series. The first series is expressed in reciprocal powers of $\log (2|z|/j\Gamma^2 ka^2)$, where $|z|$ is the distance from the gap, $\log \Gamma$ is Euler's constant, k is the propagation constant, and a is the radius of the antenna. The second series is a similar series multiplied by 1 $(k|z|)$. The first series is dominant and its first five terms yield values for the magnitude and phase of the current that for even moderately thick antennas (circumferences as large as $\lambda/3$) are accurate to within about one percent in as close as $\lambda/3$ of the gap. This is shown by a comparison of the values of the current obtained from these terms with the numerically computed values of Duncan (1962). Asymptotic expressions for the current found in the literature resemble the first term of this dominant series and are accurate only at relatively large distances from the gap—except for very thin antennas.

On the statistical theory of electromagnetic waves in a fluctuating medium (I), K. Furutsu, *J. Research NBS* **67D** (*Radio Prop.*), *No. 3, 303–323* (*May–June 1963*).
The subject of electromagnetic wave scattering by a randomly varying medium is reviewed giving special emphasis to the technical method of approach. The symbolic representation of Maxwell's equations is introduced to make it easier to survey the whole subject and to formulate the equations. The Feynman diagram method is applied to the computation of the correlation of the fields at different points in space to any order of approximation. The differential equation to be satisfied by the latter correlation function is also derived from another point of view. Then, the theory is developed on the "renormalization" of the constants, i.e., the effective propagation constant in a fluctuating medium and the effective coupling constant between the field and the medium, etc.; the explicit expression of the former is obtained to the first order of approximation. The dispersion relation is derived as a connected problem. In Part II of this series of papers, a fundamental theory of statistics of the electromagnetic field in a fluctuating medium will be developed. In Part III, a few applications to tropospheric scattering will be given.

Analysis and synthesis of nonuniform transmission lines or stratified layers, G. Latmiral, G. Franceschetti, and R. Vincinguerra, *J. Research NBS* **67D** (*Radio Prop.*), *No. 3, 331–345* (*May-June 1963*).
Nonuniform lossless or lossy transmission lines or layers used as broadband matching or absorbing devices are studied. When the refraction index, $n(x)$, and the characteristic impedance $Z_0(x)$, are given, the reflection spectrum, $\rho_0(\eta) = \rho_0 (4\pi/\lambda)$, for $x=0$ can always be computed by solving numerically a Riccati differential equation (RDE). (Analysis)
Conversely, not only for $n=$const [Bolinder, 1950, 1956] but also for $n(x)$ real and $\mu=\mu_0$, a tapered transformer can be synthesized starting from a given $\rho_0(\eta)$ spectrum by using Fourier transform techniques. (Synthesis)
For broadband absorbers, the synthesization procedure can be approximately applied, under certain conditions, to only the part of the spectrum which represents the reflection of the matched (lossy) line.

NBS viscometer calibrating liquids and capillary tube viscometers, R. C. Hardy, *NBS Mono. 55* (*Dec. 26, 1962*), *20 cents.*
Most measurements of viscosity are made with relative viscometers. These instruments must be calibrated with

liquids whose viscosities are known. NBS provides a series of 10 oils for this purpose. Their viscosities range from 0.02 to 450 poises and their temperature coefficients of viscosity range from 2.1 to 9.4 percent per degree C. When properly stored the oils may remain usable for from two months to one year but prompt use is recommended. The less viscous oils are more stable. Representative types of glass capillary tube viscometers and their use are discussed briefly. Contrary to common belief, it is not necessary to calibrate these instruments at the temperature of use since the temperature coefficients of the instruments are small and correction if necessary can be calculated. Instruments in which the effective volume of charge is not adjusted at the test temperature may require adjustment of their calibration constants to compensate for thermal expansion of the test liquid. Correction formulas for this and other errors or conditions are presented.

Equipment characteristics and their relation to system performance for tropospheric communication circuits, A. F. Barghausen, F. O. Guiraud, R. E. McGavin, S. Murahata, and R. W. Wilber, *NBS Tech. Note 103* (*Jan. 15, 1963*), *$1.00.*

The performance of a tropospheric communications system, either within the line of sight or beyond the line of sight, is directly dependent on the operating characteristics of the equipment.

Performance predictions of a communications system are made on the basis that equipment will operate in a prescribed manner. The degree of success of the communications system will depend largely upon how well these predicted values correspond to the actual operating values.

Consideration is given to those portions of the equipment that have definite effect upon the operating performance. Specific items of equipment and methods for determining their performance are considered. Representative results in light of the present state of the art permits an evaluation of an actual system in terms of realizing an "optimum" system.

In systems that do not have the "optimum" characteristics desired, consideration is given to laboratory devices which may alleviate these deficiencies. Future systems should consider incorporating these devices as development permits.

The construction of calorimeters for the measurement of absorbed dose, B. Petree and G. Ward, *NBS Tech. Note 163* (*Nov. 1962*), *25 cents.*

Direct measurements of energy locally absorbed in irradiated materials can be made with adiabatic calorimeters of suitable design. Design criteria imposed by requirements of accuracy include limitations on size and complexity. Small calorimeters of simple design with precision better than one percent at dose rates above one rad per second have been developed. Details of fabrication, auxiliary equipment and performance are described.

Detection of high altitude nuclear detonations using the VLF phase shift technique, A. G. Jean and D. D. Crombie, *IEE Trans. Nuc. Sci.* **NS–10,** *242–253* (*Jan. 1963*).

It is well known that nuclear detonations at heights of about 30 km or more can create large increases in the electron density of the upper atmosphere not only in the general area of the blast but also in areas remote from it. In this paper, the effects of such nuclear explosions on the lower ionosphere are considered. The influence of these ionospheric changes on the propagation of VLF signals is then discussed from the point of view of the detection of such nuclear explosions.

The measurement of voltage by the use of the Stark effect, Y. Beers and G. L. Strine (*Intern. Conf. Precision Electromagnetic Measurements, Boulder, Colo., 1962*), *IRE Trans. Instr.* **I–II,** *171* (*Dec. 1962*).

The theory of the Stark effect is reviewed with regard to its possible application of measuring voltages. It is pointed out that the effect can be used only to measure relative voltage and that the accuracy is likely to be limited by the accuracy with which the electrode separation can be determined. Therefore, the most sophisticated types of molecular frequency standards may not be required. The Stark method appears to hold a particular advantage for the measurement of high voltage since no voltage divider is required. Also, two possible methods of comparing ac voltages to dc voltages are discussed. Finally, an expermental Stark voltmeter employing a millimeter wave Fabry-Perot absorption cell is discussed. Calculations concerning $J=2\rightarrow3$ transition of methyl cyanide at 55 Gc indicate that in principle the precision obtainable with a field strength of 10^4 volts/cm should be in the neighborhood of one part in a million, if field inhomogeneities can be neglected.

A National Bureau of Standards gas thermometer, L. A. Guildner, *Book, Temperature, Its Measurement and Control in Science and Industry* **3,** *Pt. 1, 151–155* (*Reinhold Publ. Corp., New York, N.Y., 1962*).

At the National Bureau of Standards a constant-volume gas thermometer will be used to determine differences between the International Practical Temperature Scale of 1948 and the Kelvin thermodynamic scale. The gas thermometer bulb is a 500 cc sphere of platinum-20% rhodium alloy. It is connected to a pressure-sensitive diaphragm for separating the gas thermometer from a mercury manometer. With large menisci, the positions of the mercury crowns can be accurately detected by capacitance. The height of mercury is measured by Hoke end standards. A "tilt meter" measures variations of the manometer base from level.

Intensive effort is being made to reduce random and systematic errors. The bulb is thermostated uniformly by a copper furnace. The physical characteristics of the gas thermometer will be determined experimentally. Measurements will be made with a second thermometer bulb and with more than one gas. Determinations will be made for different masses of each gas in order to extrapolate to zero pressure.

It is planned to measure near the fixed points and at intermediate temperatures from 100 °C to 960 °C. A final set of measurements will determine the ratio of the thermodynamic temperatures of the steam and triple points of water.

Quartz crystals at low temperatures, P. R. Simpson and A. H. Morgan, *Proc. 13th Annual Symp. Frequency Control, pp. 207–231* (*Aug. 1959*).

The results of measurements performed at NBS Boulder Laboratories on certain characteristics of high precision quartz crystal oscillator units at temperatures below the normal ambient range are described with particular emphasis on frequency stability. Included are some details on the cryogenic ovens used, their temperature control devices and performance. The oscillators developed for driving the crystal units and the frequency measuring systems employed will also be discussed. Various disturbing influences such as recharging the cryostats with refrigerant, shock and vibration, filament voltage variations on the oscillator tubes, and others, will be mentioned.

Resistance thermometry in the liquid helium temperature region, M. H. Edlow and H. H. Plumb, *Book, Temperature, Its Measurement and Control In Science and Industry* **3,** *Pt. 1, 407–411* (*Reinhold Publ. Corp., New York, N.Y., 1962*).

Carbon and impurity doped germanium resistors have been investigated for use as precision secondary thermometers in the liquid helium temperature region. Three germanium resistors supplied by Bell Telephone Laboratory (86Ω, 59Ω, and 21Ω) have been thermally cycled from 300 °K to 4.2 °K and their resistances have been found to be reproducible to within 1 millidegree when temperatures were derived from a controlled surface vapor pressure, and within ½ millidegree (except for one that had been repaired) when temperatures were derived from a vapor pressure thermometer whose tubing is jacketed through most of the liquid helium. Five impurity-doped germanium resistors supplied by Texas Instruments Inc. have been thermally cycled from 300 °K to 4.2 °K and yield reproducibilities ranging from 2 to 10 millidegrees. Preliminary calibrations of the Bell Laboratory 59Ω and 21Ω and the Texas Instruments Inc. 125Ω resistors have been made from 4.21 °K to 2.16 °K at every 0.1 °K. The data were fitted to a curve of the form $\log R+k/\log R=A+B/T$ by means of the 704 computer. The standard deviations of the data from this equation for the 125Ω and 59Ω resistors are $\leqq1$ millidegree; for the 21Ω resistor, the standard deviation is $\leqq3.3$ millidegrees.

An improved resistance thermometer bridge, J. P. Evans, *Book, Temperature, Its Measurement and Control in Science and Industry* **3,** *Pt. 1, 285–289 (Reinhold Publ. Corp., New York, N.Y., 1962).*
Details of an improved Mueller bridge are given. The bridge has a range 0 to 422 ohms in 1 microhm steps. The important new features are (1) the addition of a decade with 1 microhm steps, (2) the use of mercury wetted contact switches for the 1, 0.1, and 0.01 ohm decades as well as for the 10 ohm decade and the 100 ohm coils, (3) the use of totally enclosed wafer type switches for the four lower decades, (4) the inclusion of a circuit which permits the instrument to be used as a four terminal decade resistor, (5) provision for digital read-out of the bridge dial settings, and (6) electrical guarding and shielding of the measuring circuit so that sensitive electronic null detectors may be used.

Lasers, T. R. Lawrence, *J. Wash. Acad. Sci.* **53,** *25–34 (Feb. 1963).*
A general survey on the present state of lasers is presented.

Thermophysical properties of zirconium hydrides, R. L. Beck and T. B. Douglas, *Trans. Am. Soc. Metals* **55,** *1075–1076 (1962).*
Attention is called to the emphasis by metallurgists and physical chemists of different sets of properties of metal hydrides, but it is pointed out that almost all properties indicate and are influenced by the phase-field boundaries. The author (of the paper discussed) shows commendable caution in interpreting data in terms of these boundaries. More two-way approach to immobile equilibria is recommended, and the writer cites some of his own experience. One heat capacity reported, while not precise, agrees with a recent correlation by the writer of the Zr-H system. The writer criticizes the implication that two coexistent phases have the same heat capacity. He points out that an ideal heat-capacity curve has a discontinuity on entering a two-phase field and that for a given simple composition the heat capacity in the latter field is always greater than in an adjacent one-phase field.

Measurement of electron density and temperature in dense plasmas by application of line broadening theory, J. B. Schumaker, Jr., and W. L. Wiese, *Book, Temperature, Its Measurement and Control in Science and Industry* **3,** *Pt. 1, 575–579 (Reinhold Publ. Corp., New York, N.Y., 1962).*
The electron density and temperature in arc plasmas have been determined by the deliberate introduction of a trace of hydrogen as a thermometer. The electron density is obtained by spectrophotometric measurement of the line profile of one of the Balmer lines and comparison with the theoretical profiles recently calculated by Griem, Kolb, and Shen. The temperature is then calculated from the electron density using the usual equilibrium equations of statistical mechanics for reacting gases.

A study of stability of high temperature, platinum resistance thermometers, J. P. Evans and G. W. Burns, *Book, Temperature, Its Measurement and Control in Science and Industry* **3,** *Pt. 1, 313–318 (Reinhold Publ. Corp., New York, N.Y., 1962).*
The National Bureau of Standards is studying the performance of platinum resistance thermometers in the range 630.5° to 1063° C. A number of thermometers with temperature sensing resistors of several designs, various protecting tube materials, and two types of platinum wire have been constructed. Thermometer stability was tested by heating the thermometers for long times at high temperatures and periodically determining the thermometer resistance at 100° and 0° C. The constancy of the ratio of these resistances, R_{100}/R_0, is taken as an indicator of thermometer stability. It is shown that stable thermometers can be made. The stability of the thermometers is found to be affected by the rate of cooling from high temperatures. This cooling rate effect is explained by the quenching-in of point defects in platinum.

Theory and methods of optical pyrometry, H. J. Kostkowski and R. D. Lee, *Book, Temperature, Its Measurement and Control in Science and Industry* **3,** *Pt. 1, 449–481 (Reinhold Publ. Corp., New York, N.Y., 1962).*
A detailed review of the theoretical methods of optical pyrometry and the application of these methods at the National Bureau of Standards in realizing and dispersing the International Practical Temperature Scale above 1063° C is presented. In the theoretical presentation, the concepts of effective and mean effective wavelengths are introduced, and various equations relating these parameters to each other and other physical quantities are derived. The important features of precision visual optical pyrometers are discussed and a number of blackbody sources and tungsten strip lamps described. Detailed experimental procedures and results of primary and secondary calibrations of optical pyrometers at NBS are given. Finally, recommendations for achieving high precision and accuracy and the fundamental limitations in visual optical pyrometry are presented.

The role of temperature in our measuring system, A. G. McNish, *Book, Temperature, Its Measurement and Control in Science and Industry* **3,** *Pt. 1, 129–132 (Reinhold Publ. Corp., New York, N.Y., 1962).*
Temperature is taken, together with length, mass, and time, as one of the completely independent quantities which form the basis of our measuring system. This is noteworthy in that temperature is an intensive quantity while the other three are extensive quantities. The unit of temperature, like the units of length, mass, and time is independent of all units of the system, being like them, embodied in its proper standard.
It is possible to construct a system in which temperature is not regarded as an independent quantity but one expressible in terms of length, mass, and time. However, in such a system the unit of temperature could not be realized with anything like the accuracy required for good measurements This is because the relationship between temperature and length, mass, and time has not yet been measured with an accuracy approaching that with which each of these quantities itself can be measured. Specifically, the gas constant has never been very accurately determined.
The present practice of regarding temperature as an independent quantity affords a procedure for the most accurate measurement of temperature.

The determination of absolute temperatures from sound velocity measurements, G. Cataland, M. H. Edlow, and H. H. Plumb, *Book, Temperature, Its Measurement and Control in Science and Industry* **3,** *Pt. 1, 129–132 (Reinhold Publ. Corp., New York, N.Y., 1962).*
Absolute temperatures were derived from determinations of the velocity of sound in a gas and the acoustical interferometer was used for the velocity measurements. For an ideal gas, the velocity of sound is directly proportional to the square root of the absolute temperature; in the case of a real gas, corrections must be made which involve virial coefficients of the gas in a pressure expansion. Since these corrections are a function of pressure, it is desirable that velocity measurements for absolute temperature determinations be conducted at the lowest practical pressures (the real gas approaches the state of an ideal gas).
An acoustical interferometer has been constructed at the National Bureau of Standards and has been used, with helium gas as a thermometric material, to determine absolute temperatures at 4.2° K. When temperatures thus derived are compared with absolute temperatures associated with liquid helium vapor pressures, the difference between the two temperatures is 10 millidegrees. While this result is of a preliminary nature, it does justify continued investigations for determining absolute temperatures by sonic methods.

Ranking laboratories by roundrobin tests, W. J. Youden, *Mater. Res. Std.* **3,** *No. 1, 9–13 (Jan. 1963).*
This paper presents a scoring method for laboratories participating in roundrobins. For each material the laboratory with the highest numerical result is given the rank of one, the laboratory with the next highest result is given the rank of two, and so on until the lowest of L results is given the rank L. A laboratory is scored by summing its ranks for all the materials. The paper includes a new statistical table that gives lower and upper limits for scores that correspond to five percent probability. Because systematic

errors operate to produce extreme scores, the table should be useful in singling out laboratories with pronounced systematic errors.

The error rate in a multiple-frequency-shift system and the output signal/noise ratio in a frequency modulation and a pulse-code-modulation/frequency-shift system, H. Akima, *Intern. Conf. Satellite Communication, pp. 305–310 (Nov. 22–28, 1962).*
Based on the assumption of a fading-free signal and an additive white Gaussian noise, the element and symbol error rate in an MFS (multiple-frequency-shift) system are evaluated, and the output SNR (signal-to-noise ratio) in an FM (frequency-modulation) and a PCM-FS (pulse-code-modulation-frequency-shift) system are determined theoretically. The signal to noise characteristics of an SSB (single-sideband), an FM, and a PCM-FS system are compared with each other.

A differential thermocouple voltmeter, J. E. Griffin and F. L. Hermach, *AIEE Trans., Pt. I. Communications and Electronics No. 63, Article No. 62-819, 338–344 (Nov. 1962).*
An a-c voltmeter has been developed to indicate directly in percent the difference between an unknown voltage and the settings of the dials of the instrument. It is accurate to 0.05% from 5 cps to 10 kc at 1 to 700 volts. Two 10-ma thermoelements are used; one in series with an a-c decade resistor, and the other energized from a constant-voltage d-c source (zener diode). A built-in galvanometer, calibrated in percent of the input voltage, indicates the difference between the two thermocouple output emfs and has a resolution better than 0.01%. The instrument was designed for rapidly calibrating other voltmeters. It can also be used for ac-dc difference measurements (frequency response tests) to 0.02%.

Cavitation problems in cryogenics, R. B. Jacobs and K. B. Martin, *J. Basic Eng.* **82,** *756–757 (Sept. 1960).*
Cavitation problems in cryogenics are not unique to cryogenics. A basis for the prediction of cavitation characteristics is developed and discussed. Cavitation problems with cryogenic pumps, flow meters and flow of saturated liquids are discussed. It is concluded that research into basic problems involving metastability, nucleation, vapor-phase dynamics, etc., is needed.

Color tests for antioxidants, E. J. Parks, L. T. Milliken, and F. J. Linnig, *Rubber Age* **92,** *No. 257–261 (Nov. 1962).*
A method involving the use of color and precipitation tests is presented for the qualitative identification of five antioxidants commonly used to protect crude SBR. They are: PBNA (phenyl-beta-naphthyl-amine), BLE (reaction product of acetone and diphenylamine), Stalite (mixture of heptylated and octylated diphenyl amines), Wingstay S. (mixture of styrenated phenols), Polygard (mixture of aklylated aryl phosphites). The use of several series of selected tests avoids the need to distinguish between shades of color and helps to eliminate uncertainties resulting from contamination or the possible presence of other stabilizers. The method stresses simplicity and rapidity of operation. Laboratory instrumentation is not involved. Only 10 to 15 minutes are required to complete the series of tests necessary for the identification of antioxidants present in normal quantities. Traces (10 to 100 ppm) of staining antioxidants (PBNA and BLE) are also detected in rubber protected primarily by usual amounts (about 1.25%) of nonstaining antioxidants (Stalite, Wingstay S., and Polygard). The individual tests necessary to detect these trace quantities require no more than 30 minutes in some cases, and as little as 10 minutes in others.

Widely separated clocks with microsecond synchronization and independent distribution system, T. L. Davis and R. H. Doherty, *IRE WESCON, Conv., Pt. 5, pp. 3–17 (1960).*
In a majority of timing applications, a problem exists in setting two or more clocks to agree with one another. Present techniques using WWV or other high frequency broadcasts allow clocks to be synchronized within 1 millisecond. This paper describes a method which offers an improvement in synchronization of three orders of magnitude.
Microsecond synchronization is obtained by use of the Loran-C navigation system as the link between a master clock at Boulder, Colo., and any slaved clock anywhere in the Loran-C service area.
The timing system also includes a unique method for distribution of several time code formats on a single UHF channel.

A low impedance Maxwell bridge for measuring torodially-shaped magnetic materials from 1 Kc to 100 Kc, A. L. Rasmussen and R. C. Powell, *Proc. IRE* **50,** *2505–2506 (Dec. 1962).*
A specially designed Maxwell bridge extends the range of coaxial magnetic measurements several orders of magnitude lower in frequency and complex permeability than possible with previous equipment. This bridge measures from 1 Kc to 100 Kc the quantities of 10^{-11} to 10^{-6} henrys, $10^{-7} \times$ (frequency in Kc) to 10^{-1} ohm and loss tangent (the reciprocal of the Q) 10^{-3} to 10 using toroidally-shaped magnetic materials without the difficulties normally encountered from multiple windings and contact resistance.

Germanium vacuum ultraviolet Ritz standards, V. Kaufman and K. L. Andrew, *J. Opt. Soc. Am.* **52,** *No. 11, 1223–1227 (Nov. 1926).*
The number of Ge I Ritz standards below 2000Å has now been increased to approximately 100 lines with estimated uncertainties not exceeding 0.0009Å, 68 of which have estimated uncertainties of 0.0003Å. This extension is the end product of a systematic Fabry-Perot interferometric investigation which has extended the former interferometric region of 2019–4685Å to 12069Å. Ninety-five interferometrically determined levels of Ge I are given, 72 of which have been improved by this effort.
Twenty-three lines of Ge II were also measured interferometrically leading to 20 improved energy levels of this spectrum and to estimated splittings of the $ng^2G(n{=}5, 6, 7)$ terms. From the improved levels, twelve Ge II Ritz standards from 999 to 1966Å have been calculated with estimated uncertainties not exceeding 0.0009Å. An improved series limit of Ge II calculated from the nf^2F and ng^2G term series is 128 521.3 cm^{-1}. This value made use of improved levels of this work and as yet unpublished data furnished by Shenstone.

Microwave Doppler measurements of the ionization front in cylindrical shock waves from exploding wires, D. L. Jones and R. M. Gallet, *Exploding Wires* **2,** *127–144 (1962).*
Strong cylindrical shock waves from exploding wires have been measured by microwave Doppler techniques. The results obtained simultaneously on two or three independent frequencies are in very good agreement and show that the ionization front is well defined. The Taylor-Lin similarity blast wave theory for the shock wave propagation is well verified over distances up to 6 or 7 cm under the present conditions. Systematic results for the determination of shock wave energy and the efficiency for shock production in air over a range of pressures, wire diameters, and stored electrical energy are presented. Relative to optical methods used in the same problem the present technique is more sensitive and perhaps more precise.
It is remarkable that very good reflections are still consistently obtained when the shock Mach number falls below 3 in air. From the calculated temperature and ionization in the shock front, the expected electron density should then be negligible. This effect is probably a result of the pre-excitation of the gas ahead of the shock front, caused by ultraviolet radiation from the wire explosion or from the advancing shock front itself. There is also a relatively weak precursor ionization, for which recent microwave absorption measurements have indicated electron densities of the order of 10^{11} cm^{-3} several centimeters ahead of the front.
The good reflection at low Mach numbers permits one to show that the similarity theory is still valid until Mach number 4 or below, and permits one also to record the departure from this relation at larger radii.

Tests for contingency tables and Markov chains, S. Kullback, M. Kupperman, and H. H. Ku, *Technometrics* **4,** *No. 4, 573–608 (Nov. 1962).*

A number of useful tests for contingency tables and finite stationary Markov chains are presented in this paper based on the use of the notions of information theory. A consistent and simple approach is used in developing the various test procedures and the results are given in the form of analysis-of-information tables. Beginning with tests of hypotheses for a one-way table, tests of hypotheses of specified probabilities, independence, conditional independence, homogeneity of classifications, and symmetry are developed for contingency tables of two, three, four, and higher order classifications. For the Markov chains, the tests include the hypotheses of a specified matrix of transition probabilities, Markovity, and homogeneity of several realizations of Markov chains. Worked examples are given throughout the paper.

Comments on the limits to the refractive index at ground level as a radiometeorological parameter, B. R. Bean and G. D. Thayer, *Proc. IRE* **48,** *No. 8, 1498–1501 (Aug. 1960).*
This letter is in rebuttal to M. Misme's criticism of the authors' earlier article in the Proc. IRE. M. Misme points out that, granting his hypothesis, an exponential decrease of N with height is impossible in regions of the world where the specific humidity is greater than 10 gms/kg. He then reaches the conclusion that certain common applications of meteorological data to radio engineering problems are also not valid in these same areas of high atmospheric humidity. The authors' rebuttal consists of a demonstration that the experimental evidence is in marked disagreement with M. Misme's conclusions. By testing both M. Misme's hypothesis and their own original conclusions with new and independent experimental data from the arctic and the tropics, the authors conclude that their original model refractive index atmospheres have even broader application than originally supposed.

Interpretation of *p*H measurements in alcohol-water solvents, R. G. Bates and R. A. Robinson, *Proc. 7th Intern. Conf. Coordination Chemistry, Stockholm, Sweden, pp. 342–344 (1962).*
The liquid-junction potential between an aqueous salt bridge-reference electrode and solutions in ethanol-water solvents is shown to be dependent, as a first approximation, only on the solvent composition and not on the nature of the solute. The *p*H* appears to be the most practical unit for measuring the acidity of partially aqueous media.

The significance of transients and steady-state behavior in nonlinear systems, W. J. Hartman, *Proc. IRE Correspondence Section* **49,** *No. 3, 637 (Mar. 1961).*
The purpose of this note is to correct some mathematical errors made in a letter to the editor of the IRE by Wolf.

Measurements of effective temperatures of microwave noise sources, J. S. Wells, W. C. Daywitt, and C. K. S. Miller, *IRE Intern. Conv. Record, Pt. 3, 1200–1208 (Nov. 1962).*
The need for the calibration of gas discharge noise sources has existed for some time. In an effort to accommodate this need, work has been completed on a comparison system in X-band that uses a heated resistive wedge as a standard source of noise power.
The reference standard is based on Nyquist's Theorem and consists of a high temperature waveguide terminated by a suitably matched resistive element. The waveguide itself is one continuous piece with a heat sink on the flanged end. Two standards are in use; one of platinum—13 percent rhodium waveguide and the other of gold waveguide.
The comparison system is a modified radiometer of the type used by Dicke, the principal modification being the use of one arm for comparison purposes and the other arm for a reference. The powers from an unknown noise source and a standard noise source are compared through a single arm, and an indication of the ratio of the power levels is read as an attenuation difference on a precisely calibrated variable attenuator. The noise temperature of the unknown source is then determined from the attenuation difference, the temperature of the attenuator, and the effective noise temperature of the standard.
An error analysis includes sources of errors in the comparison system and in the standard source. The errors due to the comparison system consist of: mismatch and calibration errors associated with the precision variable attenuator; chart resolution uncertainty; switch uncertainty; and the ambient temperature uncertainty of the attenuator. For the standard source the errors include the mismatch factor of the standard (and also the corresponding one for the unknown source), errors due to the uncertainty in the temperature of the hot load, and the uncertainties in the calculation of the effective noise temperature.
All of these uncertainties will give a total error of 0.07 db in the excess noise ratio of a suitable unknown noise source to be calibrated.
The evidence of good repeatability in a set of measurements is presented along with the determination of the excess noise ratio of a commonly used, terminated, tube-in-mount noise source.

The calibration of temperature standards on the international practical temperature scale of 1948, J. P. Evans. *Proc. 17th Ann. Instrument.-Automation Conf. Exhibit, Instr. Soc. Am. Preprint No. 21-1-62 (New York, N.Y., Oct. 1962).*
The International Practical Temperature Scale of 1948 is maintained in this country by the National Bureau of Standards. This paper describes techniques used at NBS to calibrate temperature measuring devices on the scale and methods of transferring the scale to industrial temperature standards.

Mechanical properites of materials, R. H. Kropschot, *Book, Applied Cryogenic Engineering, Ed. R. W. Vance and W. M. Duke, 44–59 (John Wiley & Sons, Inc., New York, N.Y., 1962).*
The principal mechanical properties of materials from room temperature 300 °K (80 °F) to 4 °K (−452 °F) are summarized. The discussion includes the tensile strength, yield strength, toughness properties and why some materials having a certain crystal structure (face centered cubic) are more suitable for low temperature applications. The behavior of the materials that are commonly used in missile and space vehicles are portrayed by graphs and tables.

A sing-around velocimeter for measuring the speed of sound in the sea, M. Greenspan and C. E. Tschiegg, *Book, Underwater Acoustics, Lecture* **5,** *p. 87–101 (Plenum Press, Inc., New York, N.Y., 1962).*
The NBS–ONR underwater velocimeter is an instrument which automatically measures the speed of sound in the sea (it also finds use in the laboratory). The stability and precision of the instrument are adequate for all current uses. Models now being manufactured are transistorized and battery-powered, so that they can be used in the abyss. The principle of operation, together with construction details and performance characteristics, are given. The history of such instruments is briefly outlined, and the distribution of current models is indicated.

Refraction and dispersion of synthetic sapphire, I. H. Maltison, *J. Opt. Soc. Am.* **52,** *No. 12, 1377–1379 (Dec. 1962).*
The refractive indices of synthetic sapphire (Al_2O_3) were measured at selected wavelengths and the values of index range from 1.834 at 0.265 μ in the ultraviolet to 1.586 k at 5.58 μ in the infrared. A three-term Sellmeier dispersion equation of the form

$$n^2-1=\sum_i \frac{A_i\lambda^2}{\lambda^2-\lambda_i^2}$$

was fitted to the experimental data. Dispersive quantities were computed which estimate the optical performance to be expected from sapphire.

Polysulfide sealants: Part I. Formulation and application properties, D. A. George, L. Dunlap, and P. Stone, *Adhesives Age* **6,** *No. 2, 32–36 (Feb. 1963).*
The chemistry, formulation modifications, working properties, and factors affecting the working proportions of polysulfide sealants are discussed. The investigations shows that the working properties necessary for various applications can be obtained in polysulfide sealants.

Low temperature insulation, R. H. Kropschot, *Book, Applied Cryogenic Engineering, Ed. R. W. Vance and W. M.*

Duke, P. 152–169 (John Wiley & Sons, Inc., New York, N.Y., 1962).
The subject of cryogenic insulation has been divided into five categories: (1) high vacuum, (2) multiple layer, (3) powder, (4) rigid foam, and (5) supports. Recent data on the thermal conductivity and other properties of these insulations is presented in tabular and graphical form. Application of these insulations to cryogenic devices is discussed. In particular, the use of multiple layer insulation for insulating liquid helium and hydrogen containers is described. Some criteria for the comparison of different types of insulation are presented.

Precision of methods for measuring tensile strength, stretch, and tensile energy absorption of paper, T. W. Lashof, *Tappi* **46,** *No. 1, 52–59 (Jan. 1963).*
An interlaboratory study was conducted to evaluate the methods for tensile strength and stretch, and to evaluate a proposed method for measuring tensile energy absorption of paper. The study was made in accordance with Mandel's statistical linear model described in the tentative TAPPI Testing Practice T 1200. It is concluded that between-laboratory variability as compared with the within-laboratory variability is appreciable for the stretch method, but of only slight or negligible importance for the other methods. At higher values of stretch and tensile energy absorption the results are affected by the type of gripping jaw (flat or line) used, being greater for flat jaws. Values of precision are reported for within-laboratory replication, for within-laboratory comparison of materials, and for comparison of results between laboratories. Twelve replicate measurements are recommended; i.e., test results should be based on averages for 12 specimens.

Dimensional changes in dentures, G. C. Paffenbarger, J. B. Woelfel, and W. T. Sweeney, *Dental Practitioner* **13,** *No. 2, 64–69 (Oct. 1962).*
Four technic dentures and usually eight clinical dentures were made with eight different types of acrylic resins, a polystyrene, a vinylacrlyic copolymer, an epoxy resin and hard rubber. The dentures were processed with the equipment recommended by the manufacturer.
Thick dentures had less shrinkage on processing and less dimensional change during use, when wetted, dried in air and heated in water. Therefore, the denture should be made as thick as comfort and function will permit.
None of the dimensional changes of dentures that occurred during processing or in use could be detected clinically. The conventional acrylic resins processed with the usual dental technic of compression molding produced dentures that were just as stable in dimension as those produced by special resins and appliances.

Tunneling between a normal metal and a superconductor, J. Harden and R. S. Coller, *Cryogenics* **2,** *No. 6, 369–370 (Dec. 1962).*
The expression for the tunneling current through an insulating film between a normal metal and a superconductor was used to obtain a functional relationship between the energy gap and the inflection point of the current-voltage characteristic. For temperatures near the critical temperature, a more sensitive functional relationship was obtained between the energy gap and the slope at the origin of the current-voltage characteristic. The results are given in both graphical and tabular form.

Dislocations and chemical etch pits in copper, A. W. Ruff, Jr., *J. Appl. Phys.* **33,** *No. 12, 3392–3400 (Dec. 1962).*
The relation between chemical etch pits and dislocations has been studied in thin single crystal foils of copper. Both deformed and as-grown crystals in [111] orientations were employed. A procedure was developed for etching thin foils so that both the etch pits and dislocations were simultaneously revealed by transmission electron microscopy methods. Results are also presented from companion studies of unetched foils and replica studies of etched surfaces. Although a general relation was found between etch pits and dislocation emergence points, a one-to-one correspondence did not exist. A discussion is presented of other defects which may nucleate etch pits, including some experimental results on deformation-produced prismatic dislocation loops. The relation of the present results to dislocation studies by etching methods alone is mentioned.

Properties of a silica-reinforced polymer for dental restorations, R. L. Bowen, *J. Am. Dental Assoc.* **66,** *No. 1, 57–64 (Jan. 1963).*
The incorporation of vinylsilane-treated silica powder into an organic polymer reinforced the material. This reinforcement gave a number of properties more nearly matching those of hard tooth tissues than those obtained with unreinforced dental resin. When vinylsilane-coated silica (70%) was combined with a comonomer solution (30%), and the material allowed to harden, the hardening shrinkage and the coefficient of thermal expansion were decreased and the compressive strength, the modulus of elasticity, and the resistance to indentation were increased relative to direct filling resins. Compared with silicate cements, the reinforced resin had lower solubility and disintegration in water, was less affected by desiccation, and had higher tensile strength, but lower compressive strength.
The same resin filled with silican not having the vinylsilane surface treatment had inferior properties after equivalent immersion in water.

Mechanical basis of diffusion, C. Truesdell, *J. Chem. Phys.* **37,** *No. 10, 2336–2344 (Nov. 1962).*
Four types of theory of diffusion are distinguished, presented, and compared: kinematical, hydrodynamical, kinetic, thermodynamic. A simple mechanical theory, based upon recognizing the diffusive drags as forces that produce motions, is shown to include and unify all earlier attempts. In this theory a hypothesis of binary drags is formalized and shown to lead to the symmetry relations proposed originally by Stefan. The Onsager relations for pure diffusion are proved to be equivalent to Stefan's relations. Known results show that these relations hold as a first approximation in the kinetic theory of monatomic gas mixtures. Whether or not they hold in higher approximation is unknown.

Realistic estimates of error, W. J. Youden, *J. Instr. Soc. Am.* **8,** *No. 10, 57–58 (Oct. 1962).*
This paper emphasizes that the concept of the error in a measurement has meaning only in terms of the use to which the measurement is put. A method for the experimental estimate of realistic errors is given together with some efficient methods of tracking down the most important sources or error in a measurement.

Gas evolution from metal surfaces during fatigue stressing, W. L. Holshouser and J. A. Bennett, *Am. Soc. Testing Mater. Preprint* **62** *(June 1962).*
Numerous bubbles were observed to form under transparent pressure-sensitive tape applied to the surface of flat specimens stressed in reversed torsion. The bubbles were produced by hydrogen evolved at the surface of aluminum alloy or carbon steel specimens and appeared to be evidence of surface reactions associated with fatigue damage and crack propagation. Gas evolution started before any fatigue cracks could be detected. The effect was also observed on specimens stressed in reversed bending, but could not be produced by fluctuating stress smaller than that necessary to produce cracks nor by a single application of load of any magnitude. No gas evolution associated with fatigue damage could be observed on specimens of copper, brass, cadmium, nickel, stainless steel, tin, titanium, or zinc. The presence of the tape retarded the development of fatigue cracks in aluminum alloy and carbon steel specimens.

Conductive floors, F. L. Hermach, *Intern. Assoc. Elec. Inspectors News Bull., pp. 40–44 (July 1962).*
Electrically conductive floors are used to minimize hazards from electrostatic sparks in munitions plants and hospital operating rooms. This paper briefly describes such floors and their function, and discusses the safe limits of resistance.

Note on the Kubelka method of measuring water absorption of leather, R. L. Hebert and A. E. McDonell, *J. Am. Leather Chemists' Assoc.* **LVII,** *No. 9, 461–496 (Sept. 1962).*
The work done by the Joint ALCA–ASTM Committee on

the absorption of water by leather with the Kubelka method is described. The data for water absorption by leather obtained by two laboratories and an analysis for the precision of the Kubelka method are presented. A comparative statistical analysis of variance is also shown for the Kubelka and the ALCA E–30 methods. The committee decided that the results did not justify the adoption of the Kubelka method.

Intercomparisons of laboratory test results, J. Mandel. *Proc. Instr. Soc. Am. Paper* **44-3,** *5 pages (1962).*
The presence of experimental error in measurements makes it necessary to represent the process in terms of a statistical model. Such a model is presented and its use for the characterization of precision, both within- and between-laboratories, is illustrated.

Coatings formed on steel by cathodic protection and their evaluation by polarization measurements, W. J. Schwerdtfeger and R. J. Manuele, *Corrosion* **19,** *No. 2, 59t–68t (Feb. 1963).*
Three steel specimens were continuously exposed in the laboratory for almost 5 years in city water to which was added 3 percent by weight of sodium chloride. Two of these specimens were under continuous cathodic protection, one by current from a zinc anode and the other by current from a rectifier through a carbon anode. The third specimen was left to corrode freely.
As a result of the cathodic protection, carbonates and silicates formed protective coatings which eventually reduced the current density required for protection from about 5 to 0.02 ma/ft.^{2}. A coated specimen, after being without protective current for 32 days (including 12 days out of the salt water), required only 0.3 ma/ft.^{2} for initial protection.
The instantaneous corrosion rates on the coated specimens (scratched and unscratched) while without protective currents were measured by changes-in-slope (breaks) in polarization curves. The currents at which breaks occurred in the cathodic curves were found to be related to $\Delta V/\Delta I$ values from the curves which values in turn bore a relation to the corrosion rates as measured by weight loss.

Variance of radio frequency caused by atmospheric turbulence in line-of-sight transmissions, K. A. Norton, E. C. Barrows, M.C. Thompson, Jr., and H. B. Janes (*Intern. Conf. Precision Electromagnetic Measurements, Boulder, Colo., 1962*), *IRE Trans. Instr.* **I–II,** *153 (Dec. 1962).*
The frequency stability of a radio signal propagated over a line-of-sight path is reduced by time variations in phase velocity along the path. This instability caused by the atmosphere will produce errors in frequency measurements made by averaging a standard frequency transmission over a period of time T and also in time interval measurements made by counting the number of cycles of the standard frequency received during a period of time T. Recent measurements of the variations in phase of a received signal at microwave frequencies permit estimation of both types of error as a function of T. These atmosphere-induced errors are compared to the errors inherent in the best currently available oscillators and it appears that the latter source of error is dominant for line-of-sight paths through the atmosphere. The level and slope of the frequency spectra have been observed to vary over wide ranges with time and geographical location. The spectral form $W(f) \sim 2/3$ expected on the basis of the Obukhov-Kolmogorov theory of atmospheric turbulence has a slope which lies well within the range of observed slopes for the range of fluctuation frequencies from one cycle per day to one cycle per second.

Instrument for the continuous measurement of the density of flowing cryogenic fluids, C. E. Miller, R. B. Jacobs, and J. Macinko, *Rev. Sci. Instr.* **34,** *24–27 (Jan. 1963).*
This paper describes the development of a new electromechanical method of measuring the densities of flowing cryogenic fluids. The instrument uses a movable section of flow passage, vibrated transversely at a constant amplitude and frequency, as the sensing element. A Dynamometer, inserted between the flow passage and driver, continuously measures the acceleration reaction (a product of mass and acceleration) of the fluid in the passage. A measure of this reaction is also a measure of the fluid density in the passage. Performance results indicate that the densitometer should be well suited for service in liquid oxygen and nitrogen single and two phase flow systems, and with only minor changes for use with liquid hydrogen.

Third International Conference on Precision Electromagnetic Measurements, W. D. George, *Nature* **139,** *No. 4858, 921–929 (Dec. 8, 1962).*
A summary of the 1962 International Conference on Precision Electromagnetic Measurements.

Measurement of RF peak pulse power by a sampling-comparison method, P. A. Hudson, W. L. Hudson, W. L. Ecklund, and A. R. Ondrejka (*Intern. Conf. Precision Electromagnetic Measurements, Boulder, Colo., 1962*), *IRE Trans. Instr.* **I–II,** *280 (Dec. 1962).*
A method is described whereby rf peak pulse power may be measured by comparison with cw power at the same frequency. Comparison is made by first sampling the power in a small portion of the rf pulse width and subsequently sampling the same portion of the cw signal whose power level is accurately known. Sampling is accomplished with a fast SPDT coaxial solid-state switch synchronized with the rf pulse. A time delay network allows the sample to be taken anywhere along the rf pulse width. Estimated maximum error for peak power levels to 10 KW is 3%. High cw levels are not necessary since the switch is used in conjunction with directional couplers to cover the power ranges of interest.

Radiation of sound by ocean waves, R. K. Cook, *Proc. 4th Intern. Congress Acoustics, Preprint 043 (Organization Committee, Copenhagen, Denmark, 1962).*
Wave trains of finite or semi-infinite length and traveling at subsonic speeds on the surface of water can radiate sound power into the atmosphere. Radiation integrals for the trains are used to compute the amount of atmospheric infrasound produced by ocean waves. The computed amounts are compared with measured infrasound having periods near five seconds.

Calorimetric determination of half-cell entropy changes, J. M. Sherfey, *J. Electrochem. Soc.* **110,** *No. 3, 213–221 (Mar. 1963).*
The reversible heat effects ($T\Delta S$) of half-cell processes have been measured in a twin calorimeter consisting of a Dewar flask divided into two halves by means of a vertical partition. Both compartments contain the same electrolyte and each has an electrode. A hole in the partition, covered by filter paper, permits the passage of electrolytic current between the compartments. The total heat effect and the heat due to irreversible phenomena are measured separately for each compartment. The difference between these two gives the desired reversible heat.
The half-cells studied include copper in acid copper sulfate, silver in acid silver perchlorate, and silver-silver chloride in various chloride solutions. The effect of "transport entropies" on these measurements is outlined. Presently accepted theories of the "irreversible" or "steady-state" thermodynamics of electrolytic cells predict the equivalence of half-cell entropy data obtained by the present calorimetric method and data obtained from thermocell studies. This predicted agreement was not obtained in the case of the half-cell silver-silver perchlorate.

Measurement and standardization of dielectric samples, H. E. Bussey and J. E. Gray (*Intern. Conf. Precision Electromagnetic Measurements, Boulder, Colo., 1962*), *IRE Trans. Instr.* **II–I,** *162 (Dec. 1962).*
The selection of a material suitable for use as a standard of dielectric properties at microwave frequencies is discussed, and tests are described which indicate that a glass and a glass-ceramic are satisfactory for such standards. The probable accuracy of measurement of the real part of the dielectric constant is estimated at $\pm 0.3\%$. Loss measurements are discussed. A correction is developed for the error resulting from the small airgap often present around the sample in transmission line measurements. The effects of humidity and temperature variations are examined, and preliminary results of measurements to 800 °C are given.

Polysulfide sealants, Pt. II. Service Properties, D. A. George, F. Roth, and P. Stone, *Adhesives Age* **6**, *35ff (Mar. 1963).*
The service properties of 28 2-part polysulfide sealants normally used as aircraft and spacecraft cabin sealants were investigated. The tensile strength, peel strength, resistance to elevated temperatures, resistance to corrosion, and their effects on the surface of an acrylic plastic were found to vary widely with some formulations being excellent in one or more properties. Excellent adhesion was found between some of these formulations and such substrates as acrylic plastics, glass, aluminum alloys, magnesium alloys, stainless steel and titanium.

Spectrum analysis of extremely low frequency variations of quartz oscillators, W. R. Stkinson, L. Fey, and J. Newman, *Proc. IRE* **51**, *379 (Feb. 1963).*
The spectral density of the frequency fluctuations of quartz oscillators has been determined over a decade range centered at 1×10^{-6} c/s and over a two-decade range centered at 0.2 c/s. Throughout all of the lower range and the lowest decade of the upper range the spectral density was observed to increase with decreasing frequency. It is pointed out that theoretical treatments of oscillator noise often consider thermal noise as the source of frequency fluctuations, but that the results of such analyses do not yield spectra similar to those observed. A computational difficulty encountered in utilizing the measurements is mentioned and possible ways of avoiding this difficulty are suggested.

Improved sample holder for X-ray diffractometer furnace, E. M. Levin and F. A. Mauer, *J. Am. Ceram. Soc.* **46**, *No. 1, 59–60 (Jan. 1963).*
An improved sample holder for the NBS X-ray furnace is described. Advantages and disadvantages are discussed.

Pitfalls in determinations of the compressive strength of concrete, J. R. Dise, *Mod. Concrete* **26**, *No. 3, 48–51 (July 1962).*
Information about the causes of variation in results of compressive strength tests of concrete is widely scattered through the literature on concrete testing. Certain portions of this information have been assembled and correlated with field observations in a general discussion which should be of interest, and perhaps benefit, to concrete technicians who have not had an opportunity to do this for themselves.

Determination of lead in leaded steels by X-ray spectroscopy, B. A. Kilday and R. E. Michaelis, *Appl. Spectry.* **16**, *No. 4, 136–138 (1962).*
The determination of lead in leaded steel by X-ray spectroscopy is highly dependent on proper surface preparation because of the tendency toward smearing or removal of the lead. A metallographic preparation technique using diamond dust as the abrasive is shown to provide reproducible and accurate results even with large changes in the particle size of the lead. This work is part of a cooperative program with the United States Steel Corporation in the preparation of a leaded-steel spectrochemical standard. Although certain inhomogeneities, both linear and radial, were observed by X-ray spectroscopy in the rods tested, suitable material has been selected for use as the NBS spectroscopic standard.

Infrasonics, R. K. Cook, *McGraw-Hill Yearbook of Science & Technology, pp. 275–276 (1962).*
This is a summary article on natural sounds in the atmosphere at infrasonic frequencies. The article is based on
(1) STR 2528 in the Dec. 1960 issue of the Technical News Bulletin.
(2) NBS Report 7172 on sound waves caused by magnetic storms, approved for publication in the Jour. of Geophysical Research.
(3) S. K. Mitra, "The Upper Atmosphere," published in India in 1952.

Image-gloss test; Apparatus and procedure, W. N. Harrison, *Proc. Porcelain Enamel Inst. Forum* **23**, *154–163 (1962).*
Several improvements in an image-gloss test apparatus and procedure are described, some of which provide greater convenience and adaptability. Others yield a large increase in reproducibility. The attribute measured is psychophysical in nature, involving the observer's visual response to one aspect of gloss; much of the diminution in scatter of test results is attributable to the incorporation of testing principles that have proven effective in psychophysical research.
Modifications in the apparatus and procedure make it possible to obtain a given precision of a determination with one-fifth the man-hours required for observations before the improvements were made.
Results of a roundrobin test are given. Observations by a contingent who did not follow instructions had substantially greater scatter than readings on the same specimens made by the recommended procedure.

Shear strength of beams without web reinforcement containing deformed bars of different yield strengths, R. G. Mathey and D. Watstein, J. *Am. Concrete Inst.* **60**, *No. 2, 183–207 (Feb. 1963).*
The behavior of reinforced concrete beams failing in shear was investigated in a series of tests in which the shear span to depth ratio and the ratio of reinforcement were varied. Six types of deformed bars with nominal yield strengths ranging from 40,000 to 100,000 psi and different stress-strain characteristics were used as tensile reinforcement.
The diagonal tension crack formed in all the beam specimens at stresses in the reinforcement which were within the range that was essentially elastic. The shear strengths at diagonal tension cracking decreased roughly linearly as the corresponding maximum stresses in the reinforcement increased for beams with the same shear span to depth ratio.
An empirical formula is presented for estimating the shear strength corresponding to the diagonal tension cracking load of beams rectangular in cross section without web reinforcement. The shear strengths developed in the beam specimens are compared with values given in the ACI Building Code (1956) and with values computed from the formula recently proposed by the ACI–ASCE Joint Committee on Shear and Diagonal Tension (1962).

Thermometric cells for calibration of liquid-in-glass thermometers, D. P. Enagonio, *Book Temperature, Its Measurements and Control in Science and Industry* **3**, *Pt. 2, 219–230 (Reinhold Pub. Corp., New York, N.Y., 1962).*
The freezing temperatures of purified compounds contained in sealed glass cells were studied as standards for the calibration of mercury-in-glass thermometers. Methods of using cells containing phenol, naphthalene, and phthalic anhydride for this purpose are given, together with the reproducibility of the maximum freezing temperature as measured with mercury-in-glass and with platinum resistance, thermometers.

Cryogenic testing of structural solids, R. M. McClintock, *Eng. Quart.* **2**, *No. 1, 28–35 (Feb. 1962).*
The features of a new tensile cryostat are presented to exemplify techniques used in the design of equipment and the measurement of temperature and strain at low temperatures. This cryostat allows tensile testing of metals or plastics at any temperature between 4 and 300 °K.
Typical data illustrative of the behavior of solids at low temperatures are also presented.

Uncertainties in calibrations, W. J. Youden, *IRE Trans. Instr.* **I-II**, *Nos. 3 & 4, 133–138 (Dec. 1962).*
This paper discusses the errors in calibrating standards under the headings:
Introduction
Determination of the Uncertainty Associated with a Specified Comparison Procedure
How Should the Uncertainty be Stated?
Discussion
Summary

Experimental determination of the frequency ratio of optical harmonics, H. S. Boyne and W. C. Martin, *J. Opt. Soc. Am.* **52**, *No. 8, 880–884 (Aug. 1962).*
The frequency ratio of the fundamental 6940 A radiation from a pulsed ruby optical laser and the second harmonic generated piezoelectric crystals has been investigated by comparing the wavelengths of the first and second harmonics with known thorium spectral lines on photographs taken with a 15,000-lines per-inch grating spectrometer.
Two piezoelectric crystals, potassium dihydrogen phosphate

and quartz, and one ferroelectric crystal, triglycine sulfate, were used to generate the second harmonic. In each case the generated second harmonic is twice the frequency of the primary radiation to within the limits imposed by the line width of the primary radiation and the resolution of the instrument. These restrictions limit the accuracy of the experiment to ± 3 parts per million (ppm) for KDP, ± 6 ppm for quartz, and ± 4 ppm for TGS. Some spectral characteristics of high energy pulses from the ruby optical laser as they might affect this experiment are given.

Energy use and power demands in all-electric houses equipped with air-to-air heat pumps, J. C. Davis and P. R. Achenbach, *ASHREA J.* **4,** *No. 9, 87–95 (Sept. 1962).*
An analysis was made of metered electrical-energy usage and power demand for all purposes in 16 sample houses from a total of 1,535 houses constructed at Little Rock Air Force Base. The energy used for cooling and heating by the air-to-air heat pumps installed in these houses and the effect of the electrical energy used by other appliances on the heating and cooling loads of the houses were of primary interest. The data from the sample houses showed an average annual energy usage of 25,300 kwh per house, of which about half was used by the heat pump and its auxiliary resistance heaters, about one-fourth for water heating, and the remainder for the electric range and miscellaneous devices. The electrical energy used for heating and cooling each averaged about 2 kwh/degree-day per thousand square feet of inside floor area, using a 65 °F base for determining the degree-days in each case. It was found that the energy used by appliances, other than the heat pump, which contributed toward heating the house was about half the amount used by the heat pump during the winter months. The analysis revealed that the monthly maximum power demand for the entire housing area was probably caused by a moderately high sustained demand in many houses rather than a coincidence of the maximum demands in a smaller number of houses.

Ferroelectric switching and the Sievert integral, P. H. Fang and I. R. Stegun, *J. Appl. Phys.* **34,** *No. 2, 284–286 (1963).*
A connection between some ferroelectric switching functions and the Sievert integral is established. Switching functions of Landauer *et al.* and of Franklin are computed and discussed.

Temperature dependence of elastic constants of vitreous silica, S. Spinner, *J. Am. Ceram. Soc.* **45,** *No. 8, 394 (Aug. 1962).*
The relation between the elastic moduli and temperature from room temperature to about 1300 °C was determined for a group of vitreous silica specimens by a dynamic resonance method. All the curves were approximately parabolic in shape reaching a maximum near 1050° to 1200° C. At the maximum value, Young's modulus was more than 11% higher and the shear modulus was about 9% higher than their room-temperature values. Poisson's ratio was then computed to rise from about ⅛ at room temperature to about ⅓ at the temperature of maximum elastic modulus. Small but significant differences were observed in the temperature-modulus curves for specimens from different sources. These differences were found to be related to differences in the infrared transmission curves.

On the realistic measurement of precision and accuracy, C. Eisenhart, *ISA Proc. Eighth Natl. Aero-Space Instrumentation Symp., Washington, D.C., pp. 75–83 (May 1962).*
The nature and objectives of measurement. Measurement as a production process. Measurement processes as realizations of methods of measurement. Essential features of the correction of measurements; of the adjustment of measurements. The concepts of limiting mean, true value, bias, precision, and accuracy. The strong law of large numbers and mathematical formulation of the bias and the precision of a measurement process. Importance of being clear on exactly what variations of procedure, apparatus, observers, and environmental conditions are allowable in "repeated" applications of what is to be considered the *same* measurement process (or, the *same* method of measurement) applied to measurement of the *same* quantity under the *same* conditions.

Other NBS Publications

Journal of Research 67A (Phys. and Chem.), No. 3 (May–June 1963) 70 cents.
An absolute calibration of the National Bureau of Standards Thermal Neutron Flux. E. J. Axton. (See above abstract.)
Absorption bands of carbon dioxide from 5.3 to 4.6 microns. A. G. Maki, E. K. Plyer, and R. J. Thibault.
Infrared spectrum of the $\nu_2-\nu_6$ band of $C^{13}C^{12}H_6$. W. J. Lafferty and E. K. Plyler.
Self-broadening of carbon monoxide in the 2ν and 3ν bands. E. K. Plyler and R. J. Thibault.
Thermodynamic properties of polyethylene predicted from paraffin data. M. G. Broadhurst.
Spectrophotometric determination of the thermodynamic pK value of picric acid in water at 25 °C. M. M. Davis and M. Paabo.
Purity analysis of highly purified materials by time-temperature cryometry. G. S. Ross and H. D. Dixon. (See above abstract.)
Synthesis of isomers of eugenol. G. M. Brauer, R. W. Morris, and W. B. Howe. (See above abstract.)
Analysis of families of curves. J. Mandel and F. L. McCrackin. (See above abstract.)
A controlled atmosphere chamber. C. L. Gordon and R. B. Johannsen. (See above abstract.)

Journal of Research, 67B (Math. and Math. Phys.), No. 2 (Apr.–June 1963), 75 cents.
Maximum cellular Boolean functions and perfect Gray codes. A. J. Goldman and B. K. Bender.
The meaning of Betti's reciprocal theorem. C. Truesdell. (See above abstract.)
Effect of molecular weight on viscoelastic properties of polymers as predicted by a molecular theory. H. Oser and R. S. Marvin. (See above abstract.)
Selected bibliography of statistical literature: supplement, 1958–1960. L. S. Deming.

Journal of Research 67D (Radio Prop.), No. 3 (May–June 1963), 70 cents.
Effects of radio wave propagation through mid-latitude 6300 A arcs. J. R. Roach.
Comparison of observed atmospheric radio refraction effects with values predicted through the use of surface weather observations. B. R. Bean and G. D. Thayer.
Ionospheric scattering effects in long-distance propagation. H. A. Whale.
Concerning solutions of the VLF mode problem for an anisotropic curved ionosphere. J. R. Wait.
On the statistical theory of electromagnetic waves in a fluctuating medium (I). K. Furutsu. (See above abstract.)
Reception of skywave signals near a coastline. J. B. Andersen.
Analysis and synthesis of nonuniform transmission lines or stratified layers. G. Latmiral, G. Franceschetti, and R. Vinciguerra. (See above abstract.)
Resonant characteristics of a corrugated sphere. J. R. Wait and C. M. Jackson.
Impedances of long antennas in air and in dissipative media. D. W. Gooch, C. W. Harrison, Jr., R. W. P. King, and T. T. Wu.
Reflection of VLF radio waves from an inhomogeneous ionosphere. Part I. Exponentially varying isotropic model. J. R. Wait and L. C. Walters.

Journal of Research 67D (Radio Prop.), No. 4 (July–Aug. 1963) 70 cents.
Influence of the lower ionosphere on propagation of VLF waves to great distances. J. R. Wait.
Comments on a paper "Auroral Sporadic-*E* Ionization" by Robert D. Hunsucker and Leif Owren. J. M. Bullen and G. A. M. King.
Reply to J. M. Bullen and G. A. M. King's "Comments on a paper 'Auroral Sporadic-*E* Ionization' by R. D. Hunsucker and L. Owren." R. D. Hunsucker and L. Owren.
Optimum reception pattern of the Beverage wave antenna at very low frequencies. E. W. Seeley.

Effect of a dissipative medium of finite size on antenna measurement. K. Iizuka and R. W. P. King.

Some implications of aircraft interference patterns in tropo-scatter reception. J. A. Bradshaw.

Asymptotic behavior of the current on an infinite cylindrical antenna. K. S. Kunz. (See above abstract.)

A dipole approximation of the backscattering from a conductor in a semi-infinite dissipative medium. M. B. Kraichman.

Small electric and magnetic antennas with cores of a lossy dielectric. J. Galejs.

The thermodynamic properties of nitrogen from 114 to 540 °R between 1.0 and 3000 psia, Supplement A (British units), T. R. Strobridge, NBS Tech. Note 129A (Feb. 1963), 50 cents.

Fading correlation bandwidth and short-term frequency stability measurements on a high-frequency transauroral path, J. L. Auterman, NBS Tech. Note 165 (Oct. 1962), 40 cents.

Profiles of electron density over the magnetic equator obtained using the incoherent scatter technique, K. L. Bowles et al., NBS Tech. Note 169 (Mar. 16, 1963), 25 cents.

Lectures on ion-atom collisions, M. R. C. McDowell, NBS Tech. Note 185 (Mar. 15, 1963), 40 cents.

Transmission and reflection of electrons by aluminum foils, M. J. Berger, NBS Tech. Note 187 (April 1, 1963), 15 cents.

The following National Bureau of Standards Technical Note is available by purchase from the Office of Technical Services, U.S. Department of Commerce, Washington 25, D.C. (please order by PB number).

An atlas of whistlers and VLF emissions, A survey of VLF spectra from Boulder, Colo., D. L. Jones, R. M. Gallet, J. M. Watts, and D. N. Frazer, NBS Tech. Note 166 (PB181454) (Jan. 1963), $2.25.

Heats of formation of two isomers of difluorodiazine, G. T. Armstrong and S. Marantz, J. Chem. Phys. **38,** No. 1, 169–172 (Jan. 1963).

Intramolecular rearrangements. V. Formation of ethylene in the photolysis of ethyl acetate from 4 to 500° K, P. Ausloos and R. E. Rebbert, J. Phys. Chem. **67,** No. 1, 163–167 (Jan. 1963).

The evolution of a conference, J. M. Richardson (Intern. Conf. Precision Electromagnetic Measurements, Boulder, Colo., 1962), Trans. IRE Instr. **I–II,** 82 (Dec. 1962).

Infrared absorption spectra of B_2O_3, B_2O_2, and BO_2 in solid argon matrices, A. Sommer, D. White, M. J. Linevsky, and D. E. Mann, J. Chem. Phys. **38,** No. 1, 87–98 (Jan. 1963).

The collaborative test, W. J. Youden, J. Assoc. Offic. Agric. Chem. **46,** 55–62 (Feb. 1963).

Ionic interactions with sugar colorant during char filtration, F. G. Carpenter, D. Larry, and V. R. Dietz, Proc. 7th Tech. Session on Bone Char 1961, p. 259 (Bone Char Research Project Inc., Charlestown, Mass. 1962).

Heat transfer between a cryo-surface and a controlled atmosphere. Part I. Experimental investigation, R. J. Richards, K. Edmonds, and R. B. Jacobs, Intern. Inst. Refrigeration, Suppl. Bull. Inst. Froid, pp. 1–22 (1962).

Microscopy of color phenomena in polymer fracture, S. B. Newman and I. Wolock, Proc. Symp. Adhesion and Cohesion, pp. 218–239 (Elsevier Publ. Co., Amsterdam, The Netherlands, 1963).

Sum rules for vibrational-rotational energy levels including centrifugal distortion, H. C. Allen, Jr., and W. B. Olson, J. Chem. Phys. **37,** No. 2, 212–214 (July 15, 1962).

Studies of within-the-horizon propagation at 9300 Mc, A. P. Barsis, A. F. Barghausen, and R. S. Kirby, IEEE Trans. Ant. Prop. **AP–11,** 24–38 (Jan. 1963).

Dosimetry. Chemical and film media, M. Ehrlich, Book, Technology Needs for Reduction of Patient Dosage from Diagnostic Radiology, Ed., M. L. Janower, pp. 81–100 (Charles C Thomas Publ. Co., Springfield, Ill., 1962).

Some problems in temperature measurements from line spectra, J. T. Jefferies, Book, Temperatures: Its Measurement and Control in Science and Industry **3,** Pt. 1, 703–711 (Reinhold Publ. Corp., New York, N. Y., 1962).

Direct observation of charge storage in the surface states of silicon, G. G. Harman, R. L. Raybold, and O. I. Meyer, J. Appl. Phys. **34,** No. 2, 380–382 (Feb. 1963).

Confidence limits for the reliability of complex systems, J. R. Rosenblatt, Book, Statistical Theory of Reliability, Ed., M. Zelen, pp. 115–148 (Univ. of Wisconsin Press, Madison, Wisc., 1963).

Improved zinc oxide-eugenol type cements, G. M. Brauer, L. Simon, and L. Sangermano, J. Dental Res. **41,** No. 5, 1096–1102 (1962).

Some early results from the ionospheric topside sounder satellite, R. W. Knecht and T. E. VanZandt, Nature **197,** 641–644 (Feb. 16, 1963).

Decibels return loss to magnitude of voltage reflection coefficient, R. W. Beatty, Microwave Eng. Handb. and Buyer s Guide, pp. TD188–TD192 (1961-62).

Dielectric constant of Cr_2O_3 crystals, P. H. Fang and W. S. Brower, Phys. Rev. **129,** No. 4, 1561 (1963).

Curves for ground wave propagation over mixed land and sea paths, J. R. Wait and L. C. Walters, IEEE Trans, Ant. Prop. **AP–11,** 38–45 (Jan. 1963).

Alternation of the muscovite absorption spectrum by KBr pellet preparation, S. Ruthberg, M. W. Barnes, and R. H. Noyce, Appl. Opt. **2,** No. 2, 177 (Feb. 1963).

Method for finding the density expansion of transport coefficients of gases, R. Zwanzig, Phys. Rev. **129,** No. 1, 486–494 (Jan. 1, 1963).

γ-irradiation of small molecules at 4 and 77 °K, R. E. Florin, D. W. Brown, and L. A. Wall, J. Phys. Chem. **66,** 2672–2676 (Dec. 1962).

A survey of some mathematical models in the theory of reliability, G. H. Weiss, Book, Statistical Theory of Reliability, Ed. M. Zelan, p. 3–54 (Univ. of Wisconsin Press, Madison, Wisc., 1963).

Thickness determination, V. A. Lamb, Electroplaters Process Control Handb. Ed., D. G. Foulke and F. E. Crane, Jr., Ch. 12, pp. 327–346 (Reinhold Publ. Corp., New York, N.Y., 1963).

Measuring plasma density of the magnetosphere, K. L. Bowles, Science **139,** No. 3553, 389–391 (Feb. 1, 1963).

Radiation effects on man, L. S. Taylor, Nucleonics **21,** No. 3, 58–60 (Mar. 1963).

Identification of Ga II lines in stellar spectra, W. P. Bidelman and C. H. Corliss, Astrophys. J. **135,** No. 3, 968–969 (1962).

Current trends and prospects, R. B. Stewart, R. V. Smith, and T. R. Strobridge, Cryogenics **2,** No. 6, 321–324 (Dec. 1962).

Hyperfine structure in the spectrum of mercury hydride, T. L. Porter and S. P. Davis, J. Opt. Soc. Am. **53,** No. 3, 338 (Mar. 1963).

Primary processes in the photochemical decomposition of nitroalkanes, R. E. Rebbert and N. Slagg, Bull. Soc. Chim. Belges **71,** 709–721 (1962).

Plating specifications, F. Ogburn, Electroplaters Process Control Handb. Ed. D. G. Foulke and F. E. Crane, Jr., Ch. 17, pp. 406–407 (Reinhold Publ. Corp., New York, N.Y., 1963).

Complex formation between manganese (II), nickel (II), and zinc (II) ions and some symmetrically substituted ethylenediamines: The use of E_r and δH values in assessing inductive and steric effects, D. L. Leussing, Inorganic Chem. **2,** No. 77, 77–82 (1963).

A note on *E*-field and *H*-field losses for ground-based antennas, J. R. Wait, IEEE Trans. Ant. Proc. **51,** 366 (Feb. 1963).

Fluorescence of teeth, A. F. Forziati and M. P. Kumpula, Frontiers of Dental Sci., pp. 106–112 (Natl. Sci. Teachers Assoc., Washington, D.C., Dec. 1962).

A note on diurnal phase changes of very-low-frequency waves for long paths, J. R. Wait, J. Geophys. Res. **68,** No. 1, 338–340 (Jan. 1, 1963).

Helium, V. Arp and R. H. Kropschot, Book, Applied Cryogenic Engineering, Ed., R. W. Vance, Ch. 12, 321–343 (John Wiley & Sons, Inc., New York, N.Y., 1962).

Hartree-Fock approximation of CH_4 and NH_4^+, M. Krauss, J. Chem. Phys. **38,** No. 2, 564–565 (Jan. 15, 1963).

The aurora and trapped electrons. F. E. Roach, J. Geophys. Res. **68,** 1015–1021 (Feb. 15, 1963).

Formation and decay of atoms and small free radicals at low temperatures, D. W. Brown, R. E. Florin, and L. A. Wall, J. Phys. Chem. **66,** 2602–2612 (Dec. 1962).

Behavior of revivified char in storage, J. Redd and F. G. Carpenter, Proc. 7th Tech. Session on Bone Char 1961,

p. 223 (Bone Char Research Project, Inc., Charlestown, Mass., 1962).

A method for determining the height and geographical position of an auroral arc from one observing station, M. H. Rees, J. Geophys. Res. **68,** No. 1, 175–183 (Jan. 1, 1963).

Gas-phase radiolysis of isobutane, R. P. Borkowski and P. J. Ausloos, J. Chem. Phys. **38,** No. 1, 36–44 (Jan. 1, 1963).

A high-latitude investigation of the natural very-low-frequency electromagnetic radiation known as chorus, J. H. Pope, J. Geophys. Res. **68,** No. 1, 83–99 (Jan. 1, 1963).

Comparative measurements on polystyrene with three different equilibrium ultracentrifuges, D. McIntyre, L. C. Williams, P. E. Haxner, H. G. Kim, F. N. Weber, R. F. Bunting, and D. W. Kurke, J. Polymer Sci. **62,** No. 174, S136–S140 (Dec. 1962).

The reactions of methyl radicals with aromatic compounds. I. Toluene, ethylbenzene, and cumene, I. B. Burkley and R. E. Rebbert, J. Phys. Chem. **67,** No. 1, 168–169 (Jan. 1963).

A comparison of direct and servo methods for utilizing cesium beam resonators as frequency standards, R. E. Beehler, W. R. Atkinson, L. E. Heim, and C. S. Snider (Intern. Conf. Precision Electromagnetic Measurements, Boulder, Colo., 1962), IRE Trans. Instr. **I–II,** 231 (Dec. 1962).

Safety levels in military inventory management, F. L. Alt, Operations Res. **10,** No. 6, 786–794 (Dec. 1962).

Size-dependent spin lattice relaxation time, P. H. Fang, Phys. Rev. **129,** No. 4, 1548–1549 (1963).

Mathematical services for standards laboratories, A. T. McPherson, Rev. Math Fisica Teorica, **XIV,** Series A, Publ. 861, Nos. 1 & 2, 277–285 (Univ. Nacional de Tucuman, Argentina, 1962).

Artificial heating of the electrons in the *F* region of the ionosphere, D. T. Farley, Jr., J. Geophys. Res. **68,** No. 2, 401–413 (Jan. 15, 1963).

Some stochastic processes in polymer systems, J. Mazur, J. Chem. Phys. **38,** No. 1, 193–201 (Jan. 1, 1963).

On the three-particle scattering operator in classical gases, J. Weinstock, Physics Letters **3,** No. 6, 260–262 (Feb. 1, 1963).

Cryogenic impurity adsorption from hydrogen, M. J. Hiza, Chem. Eng. Progr. **56,** 68–71 (Oct. 1960).

Rotational vibrational, and electronic energy transfer in the fluorescence of nitric oxide, H. P. Broida and T. Carrington, J. Chem. Phys. **38,** No. 1, 136–147 (Jan. 1, 1963).

Corrosion resistance, G. A. Ellinger, Welding Handbook, 5th Ed. pp. 6.1–6.72 (American Welding Society, New York, N.Y., 1963).

Roger Joseph Boscovich and the combination of observations, C. Eisenhart, Actes du Symp. Intern. R. J. Boskovic 1961, pp. 19–25 (1962).

Observations of sychrotron radio noise at the magnetic equator following the high altitude nuclear explosion of July 9, 1962, G. R. Ochs, D. T. Farley, Jr., K. L. Bowles, and P. Bandyopadhay, J. Geophys. Res. **68,** 701–711 (Feb. 1963).

Tentative U.S. standard for colors of signal lights, F. C. Brechenridge, Illum. Eng. **57,** 575–576 (Sept. 1962).

The sequence selection problem in the crystallization of polymers. I. Homopolymers, F. Gornick and J. L. Jackson, J. Chem. Phys. **38,** No. 5, 1150–1154 (Mar. 1963).

Comment of empirical inference of Doppler widths, R. N. Thomas, Astrophys. J. **137,** No. 1, 38–40 (Jan. 1963).

Reaction of oxygen with unkilned bone char at low temperatures (<300 °C), F. G. Carpenter and V. R. Dietz, Proc. 7th Tech. Session on Bone Char 1961, p. 237 (Bone Char Research Project Inc., Charlestown, Mass., 1962).

Horizons in dentistry, G. C. Paffenbarger, Frontiers of Dental Sci., pp. 122–128 (Natl. Sci. Teachers Assoc., Washington, D.C., Dec. 1962).

The reactions of methyl radicals with aromatic compounds. II. The xylenes, W. A. Saunders and R. E. Rebbert, J. Phys. Chem. **67,** No. 1, 170–171 (Jan. 1963).

Desorption of calcium and sulfate ions from revivified bone char, H. M. Rootare, V. R. Dietz, and F. G. Carpenter, Proc. 7th Tech. Session on Bone Char, 1961, p. 293 (Bone Char Research Project Inc., Charlestown, Mass., 1962).

The conjugacy of magnetic disturbance variations, G. M. Boyd, J. Geophys. Res. **68,** No. 4, 1011–1013 (Feb. 13, 1963).

Infrared spectrum of difluoramine, J. J. Comefore, D. E. Mann, L. J. Schoen, and D. R. Lide, Jr., J. Chem. Phys. **38,** No. 2, 461–463 (Jan. 1963).

Homogeneous anionic polymerization. I. Molecular weights of polystyrene initiated by sodium napthalene, M. Morton, R. Milkovich, D. McIntyre, and J. L. Bradley, J. Polymer Sci. **1,** Pt. A. 443–459 (Jan. 1963).

The giant resonance of the nuclear photoeffect, E. G. Fuller and E. Hayward, Book, Nuclear Reactions II, 113–194, (North-Holland Publ. Co., Amsterdam, The Netherlands 1962).

Microwave studies of butadiene derivatives. I. Spectrum of fluoroprene, D. R. Lide, Jr., J. Chem. Phys. **37,** No. 9, 2074–2079 (Nov. 1962).

Comparison of the rubidium-87 and proton Zeeman transition frequencies in the earth's magnetic field. P. L. Bender, Phys. Rev. **128,** No. 5, 2218–2221 (Dec. 1962.)

Precision millimeter wave interferometry at the U.S. National Bureau of Standards, W. Culshaw, J. M. Richardson, and D. M. Kerns, Interferometry Symp., June 9–11, 1959, paper 4–3, p. 331 (National Physical Laboratory, Teddington, Middlesex, England, 1960).

Relative signs of proton spin-spin coupling constants, E Lustig, J. Chem. Phys. **37,** No. 11, 2725–2726 (Dec. 1962).

Quantitative metallographic evaluations of graphitic microstructures, L. L. Wyman and G. A. Moore, Mod. Castings **43,** No. 1, 7–16 (Jan. 1963).

Critical opalescence of polystyrene solutions, D. McIntyre, A. Wims, and M. S. Green, J. Chem. Phys. **37,** No. 12, 3019–3020 (Dec. 1962).

A possible effect of lower atmospheric divergence on the local electron density in the ionosphere, N. J Macdonald and R. W. Knecht, Inst. Solar Terrestrial Res. Tech. Report 8 (High Altitude Observatory, University of Colorado, Boulder, Colo., 1960).

Interpolation of platinum resistance thermometers, 10° to 273.15° K, R. J. Corruccini, Book, Temperature Its Measurement and Control in Science and Industry **3.** Pt. 1, 329–338 (Reinhold Publ. Corp., New York, N.Y., 1962).

Nuclear magnetic resonance of Ni^{61} in dilute alloys of nickel in cobalt, R. L. Streever, L. H Bennett, R. C. LaForce, and G. F. Day, Phys. Rev. **128,** No. 4, 1632–1633 (Nov. 1962).

The bound-free absorption coefficient of the hydrogen negative ion, S. Geltman, Astrophys. J. **136,** No. 3, 935–945 (Nov. 1962).

Studies of errors in economic statistics, D. Rosenblatt, 1962 Proc. Business and Economic Statistics Section, Am. Stat. Assoc., p. 217 (1962).

The specific heat of saturated liquid parahydrogen from 15 to 32 °K, B. A. Younglove and D. E. Diller, Cryogenics **2,** No. 5, 1–5 (Sept. 1962).

Communications in electronics, J. Stern, Signal **16,** No. 10, 78–79 (June 1962).

Theory of the deep penetration of electrons and charged particles, L. V. Spencer and J. Coyne, Phys. Rev. **128,** No. 5, 2230–2237 (Dec. 1962).

Quantities and units for dosimetry in diagnostic radiology, H. O. Wyckoff (Symp. under the auspices of the Division of Radiological Health, U.S. Public Health Service, Washington, D.C., March 5–6, 1962), Book, Technological Needs for Reduction of Patient Dosage from Diagnostic Radiology, Ed. M. L. Janower, pp. 5–9 (Charles C Thomas, Publ., Springfield, Ill., 1963).

Current trends and prospects in cryogenics, R. W. Stewart, R. V. Smith and T. R. Strobridge, Cryogenics **2,** No. 6, 321–324 (Dec. 1962).

Comments on the Rosen interaction potential of two helium atoms, B. M. Axilrod, J. Chem. Phys. **38,** No. 1, 275–277 (Jan. 1963).

Effective impedance of a wire grid parallel to the earth's surface, J. R. Wait, IRE Trans. Ant. Prop. **AP–10,** No. 5, 538–542 (Sept. 1962).

The intensity and spectral distribution of scattered radiation from Co^{60} sources, B. Petree and J. C. Humphreys, Radiology **80,** No. 1, 120 (Jan. 1963).

Performance characteristics of turbine flowmeters, M. R. Shafer, J. Basic Eng. **84,** Series D, No. 4, 471–485 (Dec. 1962).

Experimental *gf*-values for seventy elements, C. H. Corliss, Astrophys. J. **136,** No. 3, 916–934 (Nov. 1962).

Scientific information activities at the National Bureau of Standards, W. R. Tilley (53d Special Libraries Assoc. Conv., Metals Division, May 29, 1962, Washington, D.C.). Spec. Lib. pp. 29–34 (Jan. 1963).

Current status of the statistical theory of mass spectra, H. M. Rosenstock and M. Krauss, Book, Advances in Mass Spectrometry **2,** 251–284 (Pergamon Press, London, England, 1962).

Available heat sinks for protected underground installations, B. A. Peavy, Proc. Natl. Acad. Sci.-Natl. Res. Council Meeting on Environmental Engineering in Protective Shelters, pp. 237–248 (Feb. 1960).

The sudden ionospheric disturbance, C. S. Warwick, Book, Radio Astronomical and Satellite Studies of the Atmosphere, pp. 457–475 (North-Holland Publ. Co., Amsterdam, The Netherlands, 1963).

Growth rates of potassium crystal from the vapor phase, R. L. Parker, J. Chem. Phys. **37,** No. 8, 1600–1605 (Oct. 1962).

Heat transfer in intensively outgassed powders, R. C. Little, F. G. Carpenter, and V. R. Deitz, J. Chem. Phys. **37,** No. 8, 1896–1898 (Oct. 15, 1962).

Rates of thermal degradation of organic polymers, S. L. Madorsky, SPE J. **18,** No. 12, 1482–1490 (Dec. 1962).

Vacuum ultraviolet photochemistry. V. Photolysis of isobutane, H. Okabe and D. A. Becker, J. Am. Chem. Soc. **84,** No. 21, 4004–4007 (1962).

Traces of products of angular momentum matrices. II. Spherical basis, E. Ambler, J. C. Eisenstein, and J. F. Schooley, J. Math. Phys. **3,** No. 4, 760–771 (July–Aug. 1962).

The present state of atomic spectra, C. M. Moore-Sitterly, Japan, Anal. **11,** No. 11, 1199–1202 (1962).

Correlation factors for impurity diffusion—fcc lattice, J. R. Manning, Phys. Rev. **128,** No. 5, 2169–2174 (Dec. 1962).

Experimental proof of the absence of equilibrium in a helium arc, A. T. Hattenburg and H. J. Kostkowski, Book, Temperature, Its Measurement and Control in Science and Industry **3,** Pt. 1, 587–592 (Reinhold Publ. Corp., New York, N.Y., 1962).

Technical training in the weights and measures program, M. W. Jensen, Scale J. **49,** No. 4, 4–5 (Jan. 1963); Southern Weights and Measures Program **14,** No. 12, 2–5 (Dec. 1962).

Corrosion rates of ferrous alloys (Fe, Cr, and Fe-Cr-Si) measured by polarization techniques, W. J. Schwerdtfeger, Corrosion **19,** No. 1, 17t–25t (Jan. 1963).

Survey of U.S.A. ionospheric research 1957–1959, T. N. Gautier, (Triennium Report of U.S. Natl. Comm. IUGG), Trans. Am. Geophys. Union **41,** No. 2, 232–236 (June 1960).

On the analysis of polarization rotation recordings of satellite radio signals, R. S. Lawrence and C. G. Little, Intern. Sci. Radio Union, IGY Comm. Some Ionospheric Results Obtained During the IGY; Proc. Symp. Organized by URSI/AGI Comm. Brussels, Belgium, pp. 391–399 (Elsevier Publ. Co., Amsterdam, The Netherlands, 1960).

Dissociation constant of *t*-butylammonium ion and related thermodynamic quantities from 5 to 35°, H. B. Hetzer, R. A. Robinson, and R. G. Bates, J. Phys. Chem. **66,** 2696 (1962).

Memorial to Sir Ronald Aylmer Fisher: 1890–1962, W. J. Youden, J. Am. Stat. Assoc. **57,** No. 300, 727–728 (Dec. 1962).

Vapor phase growth kinetics of Hg and K whiskers by field emission, R. L. Parker and S. C. Hardy, J. Chem. Phys. **37,** No. 8, 1606–1609 (Oct. 1962).

Radio properties of aurorae, C. G. Little, U.S.A. Natl. Comm. Intern. Sci. Radio Union Report to Natl. Acad. Sci.-Natl. Res. Council on 13th Gen. Assembly, Sept. 5–15, 1960, London, England, pp. 216–270 (Natl. Acad. Sci.-Natl. Res. Council, Wash., D.C., 1961).

Comments on the use of net rate processes and the equivalent two-level atom in non-LTE computations, R. N. Thomas, Ann. d'Astrophys. **23,** No. 6, 871–878 (1961).

Rate of spherulitic crystallization with chain folds in polychlorotrifluoroethylene, J. D. Hoffman and J. J. Weeks, J. Chem. Phys. **37,** No. 8, 1723–1741 (Oct. 1962).

Energy exchange in the biosphere, D. M. Gates, Book, Harper & Row Publ., New York, N.Y., 1962.

On the propagation of ELF pulses in the earth-ionosphere Waveguide, J. R. Wait, Can. J. Phys. **40,** 1360–1369 (Oct. 1962).

An experimental investigation of over-all heat transfer coefficients for condensing and boiling hydrogen films, K. D. Timmerhaus, D. E. Drayer, and J. W. Dean, Intern Develop. Heat Transfer (ASME) **2,** 270–278 (1961).

The photolysis and radiolysis of $CH_3N_2CH_3$ and $CH_3N_2CH_3$—$CD_3N_2CD_3$ mixtures, R. E. Rebbert and P. Ausloos, J. Phys. Chem. **66,** No. 11, 2253–2258 (Nov. 1962).

A molecular-orbital study of the geometry of HO_2, M. E. Boyd, J. Chem. Phys. **37,** No. 6, 1317–1325 (Sept. 1962).

Isotopes effect in the recrystallization of D-mannose-1-*t* phenylhydrazone, F. Weygand, H. Simon, K. D. Keil, H. S. Isbell, and L. T. Sniegoski, Anal. Chem. **34,** 1753–1755 (Dec. 1962).

Polymorphism in fibrous polypeptides: $\alpha \rightleftarrows \beta$ transformation in naturally occurring keratin, A. F. Diorio, L. Mandelkern, and E. R. Lippincott, J. Phys. Chem. **66,** No. 11, 2096–2100 (Nov. 1962).

Recent radar observations of new forms of ionosphere scatter, K. L. Bowles, U.S.A. Natl. Comm. Intern. Sci. Radio Union Report to Natl. Acad. Sci.-Natl. Res. Council on 13th Gen. Assembly, Sept. 5–15, 1960, London, England, pp. 288–295 (Natl. Acad. Sci.-Natl. Res. Council, Wash., D.C., 1961).

Reaction of methyl-d_2 radicals with isobutane, isobutane-2-*d* and propane, W. M. Jackson, J. R. McNesby, and B. deB. Darwent, J. Chem. Phys. **37,** No. 8, 1610–1615 (Oct. 1962).

Photoionization from outer atomic subshells, A model study, J. W. Cooper, Phys. Rev. **128,** No. 2, 681–693 (Oct. 15, 1962).

Solar flare effects in the *F*-region of the ionosphere, R. W. Knecht and R. E. McDuffie (Proc. Intern. Conf. Cosmic Rays and the Earth Storm), J. Phys. Soc. Japan **17,** Suppl. A, Pt. I, 280–285 (1962).

Low-level low-frequency detection system, N. T. Larson, Rev. Sci. Instr. **33,** 1200–1208 (Nov. 1962).

On the extension of the low-chromosphere model to the region of origin of the UV solar spectrum, R. N. Thomas (Proc. 10th Astrophysical Symp. Liege, Belgium), Mem. Roy. Soc. Belgium **20,** 305 (1961).

The text revision of the International Temperature Scale of 1948, H. F. Stimson, Book, Temperature, Its Measurement and Control in Science and Industry **3,** Pt. 1, 59–66 (Reinhold Publ. Corp., New York, N.Y., 1962).

Analysis of rotation errors of a waveguide theory vane antennuator, W. Larson, IRE Intern. Conv. Record, Pt. **3,** 213–219 (1962).

The structure of lithium dipotassium trimetaphosphate monohydrate, E. D. Eanes and H. M. Ondik, Acta Cryst. **15,** Pt. 12, 1280–1285 (Dec. 1962).

Airglow research in the United States, F. E. Roach (Triennium Report of U.S. Natl. Comm. IUGG) Trans. Am. Geophys. Union **41,** No. 2, 242–243 (1960).

Precursor electrons ahead of cylindrical shock waves, D. I. Jones, Phys. Fluids **5,** No. 9, 1121–1122 (Sept. 1962).

The thermal conductivity of solid nitrogen, H. M. Roder, Letter to Editor Cryogenics, **2,** No. 5, 302–304 (Sept. 1962).

High pressure transition in RbF, G. Piermarini, and C. E. Weir, J. Chem. Phys. **37,** No. 8, 1887–1888 (Oct. 15, 1962).

Thermal reactions of isobutyl radicals, W. M. Jackson, J. R. McNesby, and B. deB. Darwent, J. Chem. Phys. **37,** No. 10, 2256–2260 (Nov. 1962).

**Publications for which a price is indicated are available from the Superintendent of Documents, U.S. Government Printing Office, Washington D.C., 20402 (foreign postage one-fourth additional). Reprints from outside journals and the NBS Journal of Research may often be obtained directly from the authors.*

U.S. GOVERNMENT PRINTING OFFICE:1963

UNIVERSITY MICROFILMS INC
EDITORIAL DEPARTMENT
313 NORTH FIRST ST
ANN ARBOR MICH
S.I.R.-C JUNE

U
GOVERNM
DIVISION
WASHINGTON, D.C. 20402

OFFICIAL BUSINESS

PENALTY FOR PRIVATE USE TO AVOID PAYMENT OF POSTAGE, $300 (GPO)

JOURNAL OF RESEARCH of the National Bureau of Standards Vol. 67C, No. 3 July-September 1963
C. Engineering and Instrumentation

Contents

	Page
Apparatus for the detection of piezoelectric coupling. Lothar Frenkel.	197
Large aperture interferometers with small beam dividers. James B. Saunders.	201
A far-infrared vacuum grating spectrometer. L. R. Blaine.	207
Relation of emittance to other optical properties. J. C. Richmond.	217
Minimization of the arrestment error in one-pan, two-knife balance systems. H. A. Bowman and H. E. Almer.	227
Determination of residual thiosulfate in processed film. Chester I. Pope.	237
Drag compensation and measurement with manned satellites: feasibility study. R. M. Langer and J. P. Vinti.	247
Surface flame propagation on cellulosic materials exposed to thermal radiation. D. Gross and J. J. Loftus.	251
Parallel reversible permeability measurement techniques from 50 kc/s to 3 Gc/s. Cletus A. Hoer and R. D. Harrington.	259
Publications of the National Bureau of Standards.	267

For sale by the Superintendent of Documents, U.S. Government Printing Office, Washington, D.C., 20402. Price 75 cents (single copy). Subscription price: $2.25 a year, 50 cents additional for foreign mailing.

UNITED STATES GOVERNMENT PRINTING OFFICE, WASHINGTON : 1963